Accepted to ApJ
Preprint typeset using LaTeX style emulateapj v. 5/2/11

THE ENERGY-DEPENDENCE OF GRB MINIMUM VARIABILITY TIMESCALES

V. Zach Golkhou[1,2] , Nathaniel R. Butler[1,2] & Owen M. Littlejohns[1,2]

Accepted to ApJ

ABSTRACT

We constrain the minimum variability timescales for 938 GRBs observed by the *Fermi*/GBM instrument prior to July 11, 2012. The tightest constraints on progenitor radii derived from these timescales are obtained from light curves in the hardest energy channel. In the softer bands – or from measurements of the same GRBs in the hard X-rays from *Swift* – we show that variability timescales tend to be a factor 2–3 longer. Applying a survival analysis to account for detections and upper limits, we find median minimum timescale in the rest frame for long-duration and short-duration GRBs of 45 ms and 10 ms, respectively. Fewer than 10% of GRBs show evidence for variability on timescales below 2 ms. These shortest timescales require Lorentz factors $\gtrsim 400$ and imply typical emission radii $R \approx 1{\times}10^{14}$ cm for long-duration GRBs and $R \approx 3{\times}10^{13}$ cm for short-duration GRBs. We discuss implications for the GRB fireball model and investigate whether GRB minimum timescales evolve with cosmic time.

Subject headings: gamma rays: bursts — methods: statistical — Gamma-rays: general

1. INTRODUCTION

Gamma-Ray Bursts (GRBs) are the most luminous explosions in the Universe, originating at cosmological distances and releasing $\sim 10^{51}$ ergs over timescales of seconds to tens of seconds. The gargantuan energy release is accompanied by a very rapid and stochastic temporal variability in the gamma-ray emission. The *Swift* (Gehrels et al. 2004) and *Fermi* Space Telescopes (Meegan et al. 2009) have deepened immensely our understanding of these cosmological beacons (e.g., Gehrels & Razzaque 2013).

The pulses observed in prompt GRB light curves often have a Fast Rising Exponential Decay (FRED) profile (Norris et al. 1996). The time profiles can have a broad morphological diversity in both the number of and duration of these pulses. In the external shock model for GRBs, shells of material produced by the GRB impact material in the circumburst medium (e.g., Rees & Meszaros 1992). Unless the circumburst medium is highly-clumped (Fenimore et al. 1999), this process tends to produce a smooth GRB light curve in contrast to the rapid temporal variability observed in many GRBs. Under the internal shock mechanism (Rees & Meszaros 1994), a variable central engine emits a relativistic outflow comprised of multiple shells with different Lorentz factors, Γ. As faster shells collide with slower shells, kinetic energy is converted to radiation, and multiple shell collisions can lead to a complex GRB light curve (e.g., Rees & Meszaros 1994).

Traditional duration measures such as T_{90} (Kouveliotou et al. 1993), which describes the time during which the central 90% of prompt gamma-ray counts are received, only describe bulk emission properties of the burst. Such a duration does not capture information concerning individual collisions between shells. Instead, detailed temporal analyses that probe variability over a function of timescales are required.

A variety of time series analyses have previously been used to explore the rich properties of prompt GRB light curves. These include structure function (SF) analyses (Trevese et al. 1994; Hook et al. 1994; Cristiani et al. 1996; Aretxaga et al. 1997), autocorrelation function (ACF) analyses (Link et al. 1993; Fenimore et al. 1995; in't Zand & Fenimore 1996; Borgonovo 2004; Chatterjee et al. 2012), and Fourier power spectral density (PSD) analyses (Beloborodov et al. 2000; Chang 2001; Abdo et al. 2010; Guidorzi et al. 2012; Dichiara et al. 2013). Compared to power-spectral analyses, the SF approach is less dependent on the time sampling (Paltani 1999). In, Golkhou & Butler (2014), Paper I hereafter, we developed and applied a fast (i.e. linear) and robust SF estimator, based on non-decimated Haar wavelets, to measure the minimum variability timescale, $\Delta t_{\rm min}$, of *Swift* GRBs. We used the first-order SF of light curves as measured by the *Swift* Burst Alert Telescope (BAT; Barthelmy et al. 2005) to infer the shortest timescale at which a GRB exhibit *uncorrelated temporal variability*.

One limitation of the work presented in Paper I is that we only consider the variability timescale using light curves measured over the narrow 15–350 keV energy band of *Swift*/BAT. A fixed and narrow energy band in the observer frame would probe different regions of the intrinsic GRB spectra, because GRBs are known to occur over a wide range of redshifts (see e.g. Salvaterra et al. 2009; Tanvir et al. 2009; Cucchiara et al. 2011; Jakobsson et al. 2012). Previous studies have shown that GRB pulses vary in duration as a function of energy, with harder energy channels having a lower observed duration (Fenimore et al. 1995; Norris et al. 1996). Working at higher energies – where pulses are narrower – also has the potential to provide tighter limits on variability timescales.

We wish to use the broad *Fermi* Gamma-ray Burst Monitor (GBM;Meegan et al. 2009) energy coverage to overcome this limitation and to effectively standardize a measure of the minimum variability timescale by study-

[1] School of Earth and Space Exploration, Arizona State University, Tempe, AZ 85287, USA
[2] Cosmology Initiative, Arizona State University, Tempe, AZ 85287, USA

ing the energy evolution and/or evaluating the minimum timescale in a fixed rest frame bandpass. Broad energy coverage can potentially also allow us to disentangle the role the ejecta velocity plays in relating radius to minimum timescale and to understand how minimum timescales measured for different instruments should be compared (see, e.g., Sonbas et al. 2014). Also, it is important to note that the GBM provides very fine time resolution (2μs) event mode data for the full GRB and not just the first 1–2 s as was the case for *BATSE* (e.g., Walker et al. 2000).

In the discussion below, we begin with a brief application and summary of the method outlined in detail in Paper I. We then investigate how $\Delta t_{\rm min}$ depends on energy for a large sample of *Fermi*/GBM GRBs (Section 3.1). We compare $\Delta t_{\rm min}$ estimates from *Swift* and *Fermi* for bursts detected in common to demonstrate stability and accuracy of error estimates (Section 3.2). We then use spectral hardness to standardize the $\Delta t_{\rm min}$ estimate (Section 3.4) and conclude by deriving constraints on the sample Lorentz factors and emission radii (Section 3.5) and by investigating potential evolution of $\Delta t_{\rm min}$ with cosmic time (Section 3.6).

2. DATA

We consider 949 GRBs published in the second *Fermi*/GBM GRB catalog (von Kienlin et al. 2014), spanning the first four years of the *Fermi* mission (between 2008 July 14$^{\rm th}$ and 2012 July 11$^{\rm th}$, inclusive). Event lists for 942 of these bursts were downloaded from the online *Fermi*/GBM burst catalog[3].

We analyze the *Fermi*/GBM Time-Tagged Event (TTE) data for each of the 12 sodium iodide scintillators. We only consider those detectors in which each GRB was brightest, as listed in column 2 of Table 7 in von Kienlin et al. (2014). Typically, this entails using event lists for three detectors for each GRB. Following MacLachlan et al. (2013), we extract 200 μs binned light curves in the full (8 keV – 1 MeV) energy range. We also extract light curves in four energy channels of an equal logarithmic width (8–26, 26–89, 89–299 and 299–1000 keV). These channels are referred to as channels 1, 2, 3, and 4 below.

To remove background counts from the *Fermi*/GBM we employ a two-pass procedure. Using the estimates of T_{90} from Table 7 of von Kienlin et al. (2014), we bin each light curve at a resolution of $T_{90}/100$ and fit a linear background model. The background is initially determined considering two regions of each light curve, both T_{90} in length, occurring immediately before and after the identified period of burst emission. Using the background subtracted light curve, we then estimated T_{100} by accumulating a further 5% of the T_{90} interval counts outward from both the beginning and end of T_{90}. The second pass at fitting a linear background is then conducted, masking out all bins included in the total T_{100} region. This second background fit is then scaled to subtract the predicted background counts in the fine-time-resolution light curve. Our analysis – which identifies variations on timescales short compared to the overall burst durations – does not require the fitting of background models more complex than linear.

We analyze the background-subtracted burst counts in the full T_{100} region following the procedure outlined in Paper I. One change is made to the algorithm to optimize for the detection of signal variations on short timescales: instead of re-binning the 200 μs light curve to a fixed S/N per bin, we weight the unbinned light curve by the denoised (following, Kolaczyk 1997) signal. This zeros-out portions of the light curve containing no signal and permits use of the full T_{100} region without adversely affecting our ability to identify variations on much shorter timescales.

For 109 bursts in the second *Fermi*/GBM GRB catalog which also have *Swift* high-energy prompt coverage, the *Swift*/BAT data were obtained from the *Swift* Archive[4]. Using calibration files from the 2008-12-17 BAT data release, we construct 100 μs light curves, in the full 15–350 keV BAT energy range. We use the standard *Swift* software tools: BATECONVERT, BATMASKWTEVT and BATBINEVT. Further details regarding the extraction of the *Swift*/BAT light curves can be found in Paper I.

3. DISCUSSION AND RESULTS

In Paper I, we demonstrate the power of a novel, wavelet-based method – the Haar-Structure Function (denoted $\sigma_{X,\Delta t}$) – to robustly extract the shortest variability timescale of GRBs detected by *Swift*/BAT. In this work, we implement our technique on GRBs detected by the *Fermi*/GBM instrument, which is sensitive to a much broader range of energies. We obtain constraints on the minimum variability timescales for 938 of 949 GRBs reported in the second *Fermi*/GBM GRB catalog (von Kienlin et al. 2014). Of these, we are able to confirm the presence of a linear rise phase (see Section 3.1) in the Haar-Structure Function on short timescales for 528 GRBs. We quote upper-limit values for the remainder. Most (421) of the bursts in this sub-sample are long-duration ($T_{90} > 3$ s) GRBs. In this sub-sample, 24 GRBs have measured redshift, z. The temporal specifications of all 938 GRBs discussed here are determined using fully-automatic software and are presented in Table 2.

3.1. *Studying the Energy-Dependence of* $\Delta t_{\rm min}$

It has been recognized for decades (e.g., Fenimore et al. 1995; Norris et al. 1996) that a defining feature of GRB emission is a narrowing of pulse profiles observed in increasingly higher energy bands. As a result, durations measured by different instruments can be different (e.g., Virgili et al. 2012). Durations also appear to depend on redshift, perhaps as a result of the dependence on bandpass: recently, Zhang et al. (2013) have found evidence that T_{90} duration – when z is known and used to evaluate the GRB duration in a fixed rest frame energy band – may correlate linearly with redshift as is expected from cosmological time dilation. This result is quite sensitive to the particular choice of binning in the analysis (see, Littlejohns & Butler 2014). Here, we seek to understand whether our measure of shortest duration in GRBs is also highly-dependent upon the observed energy band, and on the instrument detecting the GRB, in particular.

[3] http://heasarc.gsfc.nasa.gov/W3Browse/fermi/fermigbrst.html

[4] ftp://legacy.gsfc.nasa.gov/swift/data

The prompt GBM Gamma-ray light curve for GRB 110721A, split in 4 energy bands, and our derived $\sigma_{X,\Delta t}$ curve for each channel are shown in Figure 1. There is a clear evolution in $\Delta t_{\rm min}$ with bandpass, decreasing from the softest to the hardest energy band. To guide the eye, several lines of constant $\sigma_{X,\Delta t} \propto \Delta t$ are also plotted. The expected Poisson level (i.e., measurement error) has been subtracted away, leaving only the flux variation expected for each channel.

Briefly, we review here how our $\Delta t_{\rm min}$ is identified. A general feature observed in our GRB scaleograms, provided there is sufficient signal-to-noise ratio (S/N), is a linear rise phase relative to the Poisson noise. Poisson noise sets a floor on the shortest measurable timescale (denoted $\Delta t_{\rm S/N}$, with $\Delta t_{\rm S/N} \approx 0.1$ s for channels 2 and 3 in Figure 1, bottom). Unlike previous studies by other authors (Bhat 2013; MacLachlan et al. 2013; Walker et al. 2000), we do not implicate the shortest *observable* timescale as $\Delta t_{\rm min}$. Instead, we recognize that pulses can be temporally smooth on short timescales. The departure from this smoothness creates a break in the scaleogram, and this in turn defines our timescale $\Delta t_{\rm min}$ for temporally un-smooth variability. Naturally, this timescale also corresponds to a length-scale, which must be reconciled with GRB progenitor models (Section 3.5).

We now focus on the softest energy band of GRB 110721A, denoting the light curve as $X(t)$. Although there is excess signal present on timescales as short as $\Delta t = 0.4$ s (Figure 1 - channel 1), these timescales correspond to a region of the plot where the first order SF rises linearly timescale, $\sigma_{X,\Delta t} \equiv \left\langle |X(t+\Delta t) - X(t)|^2 \right\rangle_t^{1/2} \propto \Delta t$. (Here, $\langle . \rangle_t$ denotes an average over time t.) We interpret this linear rise as an indication that the GRB exhibits temporally-smooth variations on these timescales (i.e., $X(t+\Delta t) \approx X(t) + X'(t)\Delta t$), while changing to exhibit temporally-unsmooth variations on longer timescales. The $\sigma_{X,\Delta t}$ points deviate significantly from the $\sigma_{X,\Delta t} \propto \Delta t$ curve at $\Delta t_{\rm min} = 0.56 \pm 0.09$ s. This is the timescale of interest, describing the minimum variability time for uncorrelated variations in the GRB. This timescale is associated with the initial rise of the GRB in this channel, as can be seen from the Figure 1 inset.

The value for $\Delta t_{\rm min}$ is found by fitting a broken powerlaw to the $\sigma_{X,\Delta t}$ data points below the peak, assuming that $\sigma_{X,\Delta t}$ initially rises linearly with Δt (see, also, Paper I) until flattening at $\Delta t_{\rm min}$. Uncertainties quoted here and below for $\Delta t_{\rm min}$ are determined by direct propagation of errors and correspond to 1σ confidence. If the lower-limit on $\Delta t_{\rm min}$ falls below the lowest measurable timescale (i.e., $\Delta t_{\rm S/N}$), we report only the 1σ upper limit for $\Delta t_{\rm min}$.

For this particular burst, $\Delta t_{\rm min}$ evolves from the hardest energy band to the softest energy band as one might expect: the softest energy band of a burst has longer minimum variability timescale compared to the hardest energy band of that burst. On timescales longer than $\Delta t_{\rm min}$, $\sigma_{X,\Delta t}$ is flatter than $\sigma_{X,\Delta t} \propto \Delta t$, indicating the presence of temporally-variable structure on these timescales. On a timescale of about 6 s, $\sigma_{X,\Delta t}$ begins turning over as we reach the timescales (tens of seconds) describing the overall emission envelope. We are not concerned here with those longer timescale structures, although we do note that $\sigma_{X,\Delta t}$ provides a rich, aggregate description of this temporal activity.

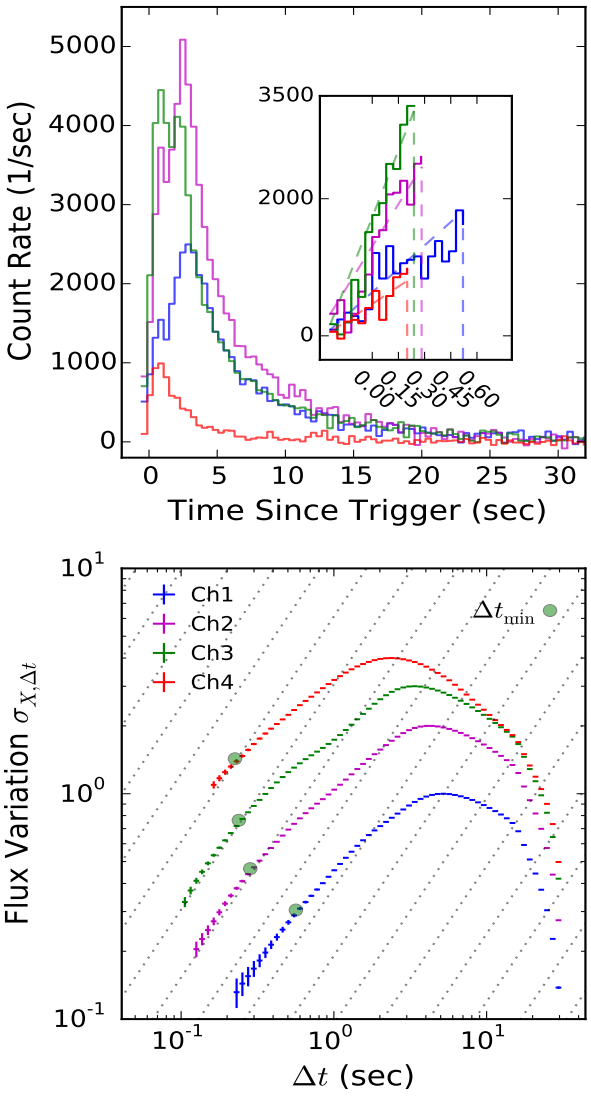

FIG. 1.— Top panel: *Fermi*/GBM light curves of the GRB 110721A split in 4 different energy bands. Bottom panel: The Haar wavelet scaleogram $\sigma_{X,\Delta t}$, rescaled for plotting purposes, corresponding to each channel versus timescale Δt for GRB 110721A. We derive minimum timescales (marked with green circles) – 0.56 ± 0.09 s, 0.28 ± 0.05 s, 0.24 ± 0.04 s, and 0.22 ± 0.04 s for the channels 1, 2, 3, and 4, respectively – which increase in lower energy bands. In the top panel, the inset displays the the pulse rise with finer time binning, with dashed lines dropped onto the x-axis to demark the derived $\Delta t_{\rm min}$ values for each channel.

In order to characterize and measure the average $\Delta t_{\rm min}$ for the *Fermi* sample as a function of spectral energy band, we utilize the Kaplan-Meier (KM; Kaplan & Meier 1958, see also Feigelson & Nelson 1985) survival analysis. This is necessary because many bursts only permit upper limit measurements of $\Delta t_{\rm min}$. Figure 2 summarizes how the minimum variability timescale varies with energy band. The KM cumulative plots – including the shaded 1σ error region – for each bandpass

TABLE 1
THE KAPLAN-MEIER MEDIAN AND $10^{\rm th}$ PERCENTILE TIMESCALES FOR LONG-DURATION GRBS.

Band (keV)	$\Delta t_{\rm min}^{50\%}$ (msec)	$\Delta t_{\rm min}^{10\%}$ (msec)	Number Detected	Number Upper Limit
8–26	540 ± 67	25 ± 8	395	307
26–89	260 ± 26	4^{+4}_{-2}	431	319
89–299	150^{+23}_{-18}	2^{+2}_{-1}	413	335
299–1000	72^{+24}_{-21}	...	156	278
8–1000	130 ± 18	2^{+5}_{-1}	421	334

and the full (all channels combined) *Fermi*/GBM energy range are shown in the top panel. The sample $50^{\rm th}$ percentiles (i.e., medians) and the lowest $10^{\rm th}$ percentiles (shown with the dotted-lines in the top panel of Figure 2) are plotted in the bottom panel. Table 1 summarizes the corresponding values. Since the KM cumulative estimation curve of channel 4 does not cross the 10% limit line, there is no value reported in Table 1 for this case. The reported values clearly show the tendency of increasing $\Delta t_{\rm min}$ with decreasing energy band. Because we tend to find a clear association between $\Delta t_{\rm min}$ and the rise time of the shortest GRB pulse (also, Paper I), this confirms that GRB pulse structures are narrower at higher energy and that understanding this effect is important for understanding any implications drawn from $\Delta t_{\rm min}$.

The KM median values of $\Delta t_{\rm min}$ versus energy band are well-fitted by a line $\Delta t_{min}^{50\%} = 0.20(E/89\,{\rm keV})^{-0.53\pm0.06}$ s (with reduced $\chi^2 = 0.64$). The derived power-law index here is in agreement with the power-law index of the relationship found for the average pulse width of peaks as a function of energy (Fenimore et al. 1995 and also from Norris et al. 1996). The KM estimation of the lowest 10% of $\Delta t_{\rm min}$ values versus the energy band can also be fitted by a power-law, with a steeper index, $\Delta t_{min}^{10\%} = 0.01(E/48\,{\rm keV})^{-0.97\pm0.20}$ s (with reduced $\chi^2 = 1.4$). The steeper index indicates that rare GRBs, which tend to be bright and spectrally hard GRBs, allow for tighter constraints on minimum timescales. This shifts the typical minimum timescales to smaller values as compared to those found for the bulk of the population. We explore the minimum timescale dependence on S/N and spectral hardness below for individual GRBs.

3.2. *Consistency in the Joint Fermi/GBM and Swift/BAT Sample*

In Paper I, we studied the robustness of our minimum timescales extracted for simulated bursts as the S/N is varied. It was demonstrated that the shapes of the $\sigma_{X,\Delta t}$ curves are highly stable as the S/N is strongly decreased (factor of ten), but the determination of the true $\Delta t_{\rm min}$ can be challenging. This is because GRBs tend to show evidence for temporally-smooth variation between timescales of non-smooth variability (e.g., pulse rise times) – which become harder to measure as S/N is decreased – and the longer timescales associated with non-smooth variability (e.g., the full duration of the pulse). The sample of bursts detected jointly by both *Swift*/BAT and *Fermi*/GBM provides a rich dataset to

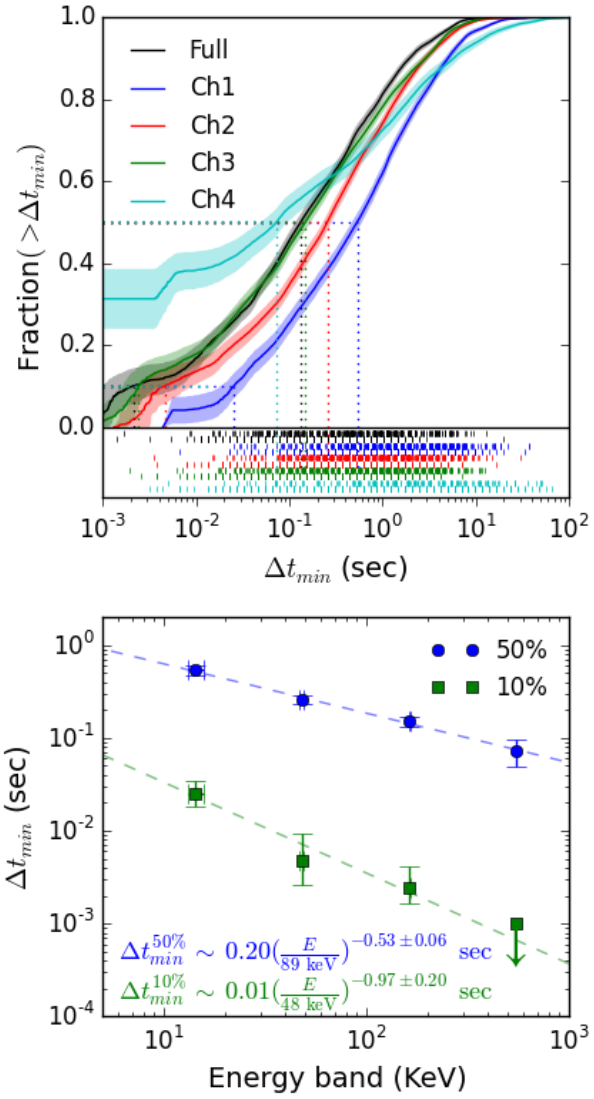

FIG. 2.— Top panel: The KM cumulative estimation curve of all long-duration GRBs in *Fermi* sample for each energy band including shaded 1σ region around each bandpass. The dotted lines show the $50^{\rm th}$ percentile and the lowest $10^{\rm th}$ percentile for each bandpass. The location of the of measured $\Delta t_{\rm min}$ values (top tics) and upper-limits (bottom tics of the same color) are shown in the sub-panel. Bottom panel: The KM median estimation of Δt_{min} versus energy band and the lowest $10^{\rm th}$ percentile of $\Delta t_{\rm min}$ values versus energy band, including error bars. Note: since the KM cumulative estimation curve of channel 4 does not cross the 10% line, we plot an upper-limit.

study this behavior. In addition to allowing us to verify consistency in the $\Delta t_{\rm min}$ estimates for bursts with similar S/N values, we can also directly observe (in many cases) the reliability of $\Delta t_{\rm min}$ for different S/N values.

Figure 3 captures the variety of scaleograms produced for bursts detected by both the *Swift*/BAT and *Fermi*/GBM instruments. Here we utilize the 15–350 keV energy range for both *Swift*/BAT and *Fermi*/GBM, and we align the light curves and extract counts over the same time intervals for each burst. Although the instruments do not have identical effective area curves in these

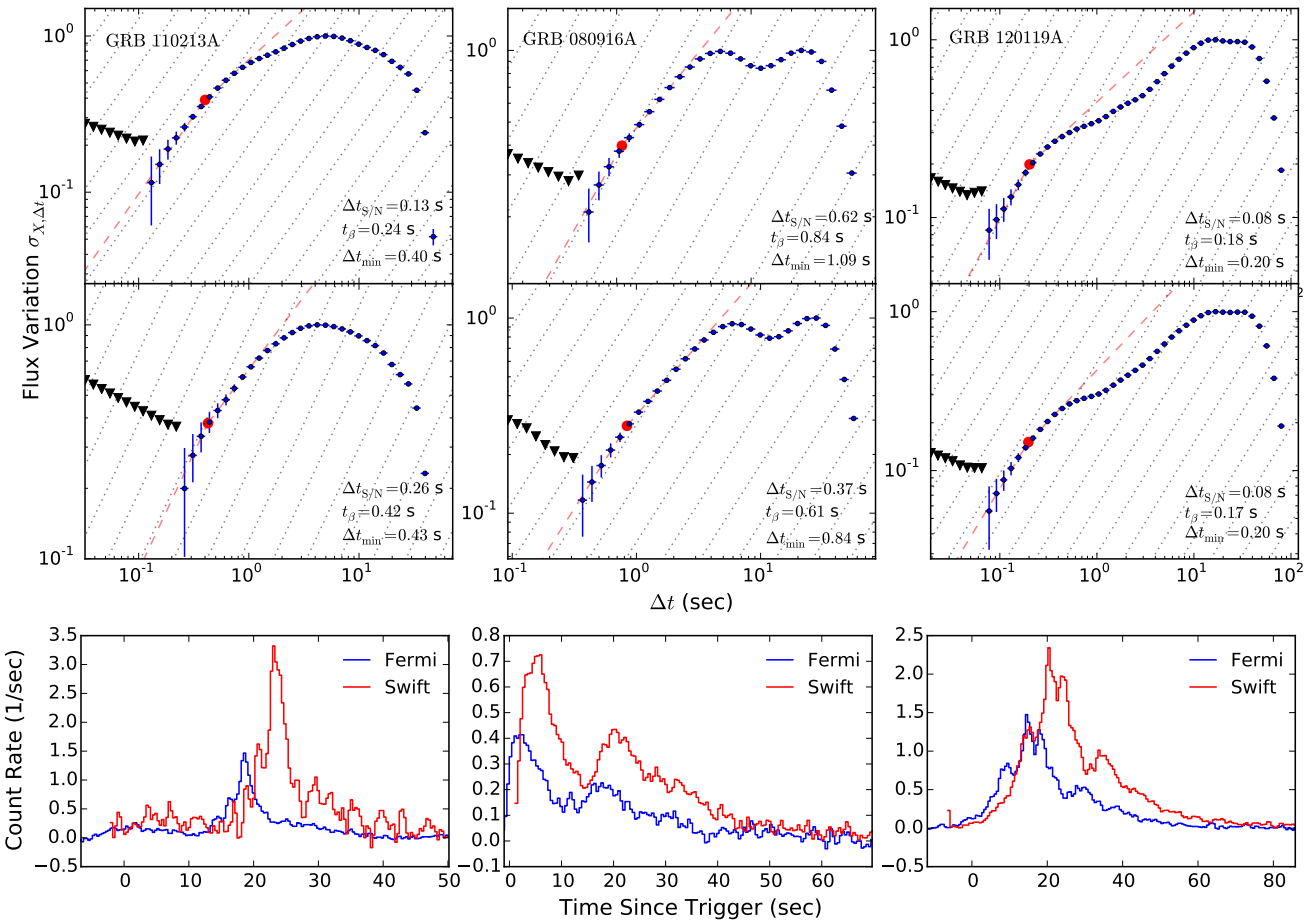

FIG. 3.— A gallery of Haar scaleograms $\sigma_{X,\Delta t}$, representing a variety of possible structure functions calculated for *Fermi*/GBM and *Swift*/BAT (both: 15–350 keV) with different level of sensitivity for detection of various GRBs. The left, middle, and right panels correspond to GRB 110213A, GRB 080916A, and GRB 120119A, respectively. The first and second rows show the structure functions retrieved from the GRBs light curves detected by *Fermi*/GBM and *Swift*/BAT, respectively. The third row shows the light curves in the T_{100} duration region. In each of these, the red dashed-lines represent a passage from the temporally-smooth ($\sigma_{X,\Delta t} \propto \Delta t$) region to a flatter region and the red circle marks the extracted minimum variability timescale, $\Delta t_{\rm min}$, after which the light curves transition to a temporally-unsmooth behavior. Triangles denote 3σ upper limits.

ranges, choosing the same energy range should minimize differences due to energy band (discussed in more detail in Section 3.4 below).

In the case of GRB 110213A (left panels), *Fermi*/GBM captured the higher sensitivity burst light curve. Oppositely in the case of GRB 080916A (middle panels), *Swift*/BAT captured a higher S/N light curve. The S/N level can be gauged from the light curves and taken directly from the $\Delta t_{\rm S/N}$ values, with high S/N translating directly to lower $\Delta t_{\rm S/N}$. There are many bursts (e.g., GRB 120119A, right panels) in the joint *Fermi*/GBM and *Swift*/BAT sample which correspond to closely similar S/N values and for which the resulting scaleograms are almost identical. We note that minimum timescales based simply on $\Delta t_{\rm S/N}$ (e.g., Walker et al. 2000) directly track the noise floor level. This is also the case for t_β, calculated according to the prescription of MacLachlan et al. (2013). In the most extreme examples (i.e., GRBs 090519A and 101011A), the $\Delta t_{\rm S/N}$ values differ by approximately an order of magnitude, the t_β values differ by approximately a factor of five, while the $\Delta t_{\rm min}$ values are consistent (Table 2). Our method distinguishes between the *minimum detectable* timescale and the true minimum timescale in a more robust (although not-perfect, as we discuss more below) fashion.

Figure 4 displays a scatter plot of $\Delta t_{\rm min}$ determined for *Swift*/BAT versus *Fermi*/GBM. A line fit through the data points (blue curve with shaded gray 90% confidence region) is consistent with the dotted-line representing equality. The best-fit line has a normalization $= 1.13 \pm 0.13$ and a slope $= 0.99 \pm 0.02$. For this fit the reduced $\chi^2 = 2.86$ (for 42 degrees of freedom) and is dominated by a small number of outliers. The fraction of bursts not consistent with the fit, both below and above the line are: 12% and 15%, respectively. The close consistency of this line with the unit line demonstrates that our method is robust and that our error bars, calculated by direct error propagation, are likely to be accurate.

We do note, however, that the $\Delta t_{\rm min}$ values calculated for *Swift* versus *Fermi* do exhibit small, systematic differences. On average, bursts detected by *Swift* (in the same energy band) tend to have 13% longer $\Delta t_{\rm min}$ values as compared to *Fermi*. Histograms showing the spread in the overall populations are also drawn along the axes in Figure 4.

To study the origin of the outliers to the fit in Figure 4,

we scale the relative size of the circles with the absolute value of the log of the ratio of flux variation at the shortest observable variability timescale $\Delta t_{\rm S/N}$. This is intended to provide an indication of whether each satellite sampled the same (small circles) or very different (large circles) regions of the scaleogram at the inferred $\Delta t_{\rm min}$. The color bar can be used to identify which instrument generated the higher $\sigma_{X,\Delta t}$.

In general, we find that once the $\log(\Delta t_{\rm S/N})$ ratios exceed 0.5 dex (corresponding to 0.5 dex in log(S/N) or roughly a factor 10 in flux) the more sensitive satellite tends to yield a lower measurement of $\Delta t_{\rm min}$. This is consistent with our findings from Paper I. Given that such variation is not known a-priori in this case (because the light curves are not based on a simulation), the tendency to detect lower $\Delta t_{\rm min}$ when possible suggests a fractal nature of the phenomenon. Care must be taken in interpreting GRB minimum timescales, because the phenomenology suggests these could always be limits on the true minimum timescales. However, we do note the important feature of the scaleograms: hidden (i.e., low S/N) minimum timescales will always correspond to smaller variations in the fractional flux levels. In this sense, a perfect accounting of the minimum timescales may not be necessary, because very short minimum timescales tend to represent fractionally tiny (or alternatively very rare) episodes in the GRB emission.

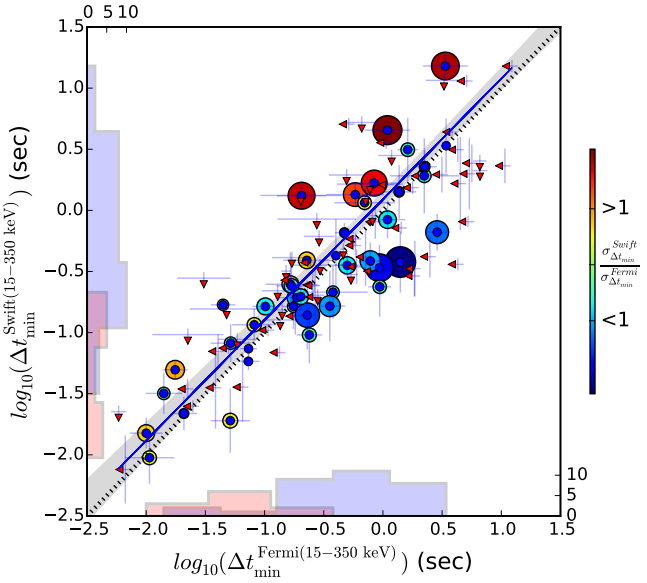

FIG. 4.— $\Delta t_{\rm min}$ for the sample of joint *Fermi*/GBM and *Swift*/BAT bursts. The red and blue histograms correspond to the short and long-duration GRBs, respectively. The arrows show the upper limit burst cases. The black dotted-line represents equality. The relative size of the circles is scaled with the absolute value of the log of the ratio of flux variation at the shortest observable variability timescale $\Delta t_{\rm S/N}$, providing a measure of whether each satellite samples the same (small circles) or very different (large circles) regions of the scaleogram at the inferred $\Delta t_{\rm min}$. The color bar can be used to identify which instrument generated the higher $\sigma_{X,\Delta t}$.

3.3. *Distribution of* $\Delta t_{\rm min}$ *Values for Fermi/GBM*

Figure 5 (left) shows histograms for the *Fermi* GRBs permitting measurement of and also upper limits on $\Delta t_{\rm min}$. The two distributions have consistent mean values. The middle and right panels of Figure 5 show the KM cumulative histograms in the observer and source frames, respectively. The dotted-lines correspond to the minimum timescale of the lowest 10% and 50% (median) of short and long-duration bursts.

We find a median minimum timescale for long-duration (short-duration) GRBs in the observer frame of 134 ms (18 ms). In the source frame, we find a median minimum timescale for long-duration (short-duration) GRBs of 45 ms (10 ms). It is interesting that these numbers are a factor of 3–10 smaller than those we found for *Swift* in Paper I. The largest differences, in the case of short-duration GRBs, are attributable to the increased number of well-detected short-duration GRBs by *Fermi*. As we discuss below (Section 3.4), $\Delta t_{\rm min}$ also appears to vary by a factor of ≈ 3 depending on the burst hardness. The *Fermi* sample is studied using the full energy range, and the sample appears to be spectrally harder than the *Swift* sample, overall.

We also report $\Delta t_{\rm min}$ of the most exotic GRBs in *Fermi* sample – the lowest $10^{\rm th}$ percentile of bursts with the shortest $\Delta t_{\rm min}$. The $10^{\rm th}$ percentile $\Delta t_{\rm min}$ values for long-duration (short-duration) GRBs in the observer frame found to be 2.2 ms (1.9 ms). In the source frame, we find 2.9 ms (2.4 ms). These numbers are consistent with the findings in Paper I that millisecond variability appears to be rare in GRBs.

From Figure 5, we find that the $\Delta t_{\rm min}$ distribution of long-duration GRBs is displaced from that of short-duration GRBs (16σ, t-test 17σ, log-rank test (Mantel 1966)). The log-rank test includes the upper limits, unlike the t-test. This finding is consistent with the presented results in Paper I for *Swift*. This discrepancy is still present in the source frame (2.3σ, t-test and 3.4σ, log-rank test) unlike in Paper I where the distribution centers appeared to be consistent. The *Swift* small sample of short-duration GRBs with known-z is likely the main reason for the observed degeneracy. The significant observer frame discrepancy is likely driven by the fact that short-duration GRBs tend to be detected only at low-redshift, unlike long-duration GRBs which span a broad range of redshifts. Examining the dispersion in $\log(\Delta t_{\rm min})$ values, we see no strong evidence for dissimilar values for the long and short-duration samples ($< 1.3\sigma$, F-test). This finding is also fully consistent with the presented results in Paper I, where it was also found (using a sample of *Swift* GRBs) that the two histograms are quite broad and very similar in dispersion.

Figure 6 displays our minimum variability timescale, $\Delta t_{\rm min}$, versus the GRB duration, T_{90}. The short and long-duration GRBs are shown with diamond and circle symbols, respectively. In this plot the relative size of symbols is proportional to the ratio between minimum variability and S/N timescale ($\Delta t_{\rm min}/\Delta t_{\rm S/N}$). As described above, $\Delta t_{\rm S/N}$ represents the first statistically significant timescale in the Haar wavelet scaleogram. The color of the points in Figure 6 corresponds to the flux variation level, $\sigma_{X,\Delta t}$, at $\Delta t_{\rm min}$. A curved black line is also plotted to show a typical value for the minimum

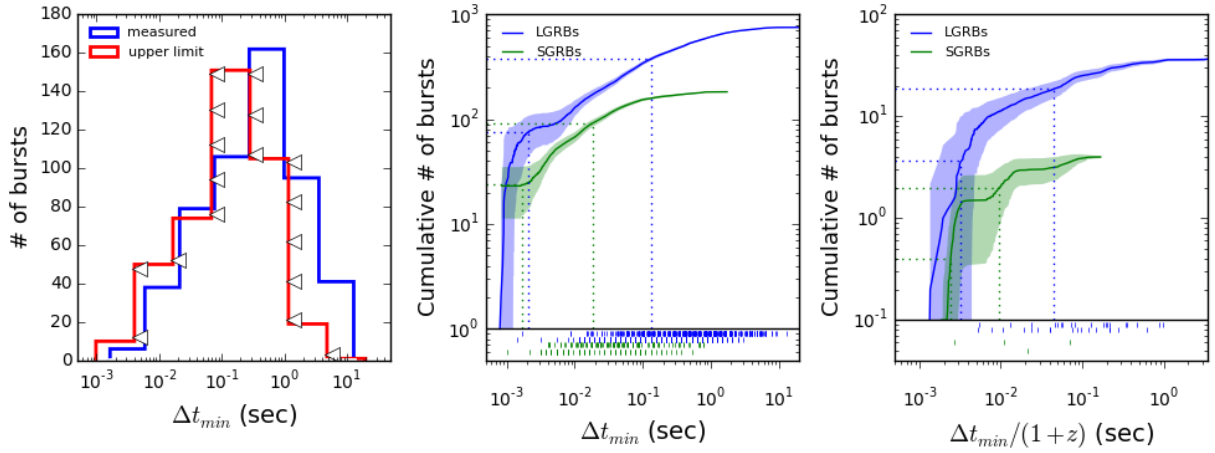

FIG. 5.— Left panel: the histograms of $\Delta t_{\rm min}$ with measurements (blue) and for GRBs allowing for upper limits only (red). Middle and right panels: the cumulative histograms of bursts in the observer and source frames, respectively. The KM estimation curve with 1σ error region around the curve is shown in these panels. The dotted lines correspond to the minimum timescale of the lowest 10% and 50% of bursts, shown for the short and long-duration GRBs, separately. Sub-panels show the locations of detections and upper-limits, as in Figure 2. For long-duration (short-duration) GRBs, we have 421 (107) measurements and 334 (76) upper limits in the observer frame and 24 (3) measurements and 18 (1) upper limits in the source frame.

observable time ($\Delta t_{\rm S/N}$) versus T_{90}. Values for T_{90} are taken from Table 7 of von Kienlin et al. (2014).

We first note from the colors in Figure 6 that GRBs with $\Delta t_{\rm min}$ close to T_{90} tend to have flux variations of order unity. These are bursts with simple, single-pulse time profiles. As can be seen from the range of point sizes in Figure 6, most are not simply low S/N events where fine time structure cannot be observed. Also, we see that there are GRBs with both high and low S/N which have complex time-series ($\Delta t_{\rm min} \ll T_{90}$). Based on the point sizes, the short-timescale variation have higher ratio of $\Delta t_{\rm min}/\Delta t_{\rm S/N}$ for the short-duration GRBs of the similar $\Delta t_{\rm min}$ in comparison with that of the long-duration GRBs. Short-duration GRBs tend to have a higher $\sigma_{X,\Delta t}$ for the similar value of $\Delta t_{\rm min}$ compared with the long-duration GRBs.

These findings are all consistent with the similar results explained in Paper I; although we have a better ratio of short-duration GRBs to long-duration GRBs, here.

From a Kendall's τ-test (Kendall 1938), we find only marginal evidence that $\Delta t_{\rm min}$ and T_{90} are correlated ($\tau_k = 0.33$, 11σ above zero). The $\Delta t_{\rm min}$ values in Figure 6 are bound from above by T_{90}, and they do not strongly correlate with T_{90} within the allowed region of the plot. In Paper I, we studied this relation for the entire sample of *Swift* GRBs and found only a marginal evidence that $\Delta t_{\rm min}$ and T_{90} are correlated ($\tau_k = 0.38$, 1.5σ). Even when we utilized the robust duration estimate $T_{\rm R45}$ (Reichart et al. 2001) in place of T_{90} no significant correlation was found ($\tau_k = 0.6$, 2.4σ). If we perform a truncated Kendall's τ test which only compares GRBs above one-another's threshold (Lloyd-Ronning & Petrosian 2002), the correlation strength drops precipitously ($\tau_k = 0.06$, 1.4σ). We, therefore, believe there is no strong evidence supporting a real correlation between $\Delta t_{\rm min}$ and T_{90}.

3.4. *The Dependence of* $\Delta t_{\rm min}$ *on Spectral Hardness*

We investigate here how a burst's spectral hardness impacts its minimum variability timescale. We define

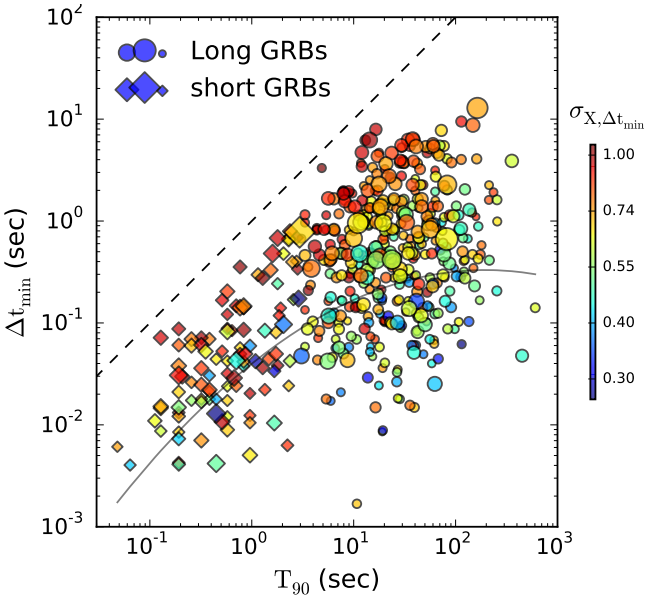

FIG. 6.— The GRB minimum timescale, $\Delta t_{\rm min}$, plotted versus the GRB T_{90} duration. Circles (diamonds) represent long-duration (short-duration) GRBs. The point colors represent the flux variation level ($\sigma_{X,\Delta t_{\rm min}}$) at $\Delta t_{\rm min}$. Also plotted as a curved line is the typical minimum observable timescale, $\Delta t_{\rm S/N}$, as a function of T_{90}. The symbol sizes are proportional to the ratio of $\Delta t_{\rm min}/\Delta t_{\rm S/N}$ for each GRB. The dashed line shows the equality line.

the hardness ratio (HR) as the total counts in the hard composite channel (89–1000 keV, our combined channels 3 and 4) divided by the total counts in the soft composite channel (8–89 keV, our channels 1 and 2). We plot in Figure 7 (top panel) the ratio of $\Delta t_{\rm min}$ for these two composite channels against the HR of the two corresponding bandpasses. GRBs with harder spectra tend to have a lower $\Delta t_{\rm min}$ ratio, by as much as a factor ≈ 3, for

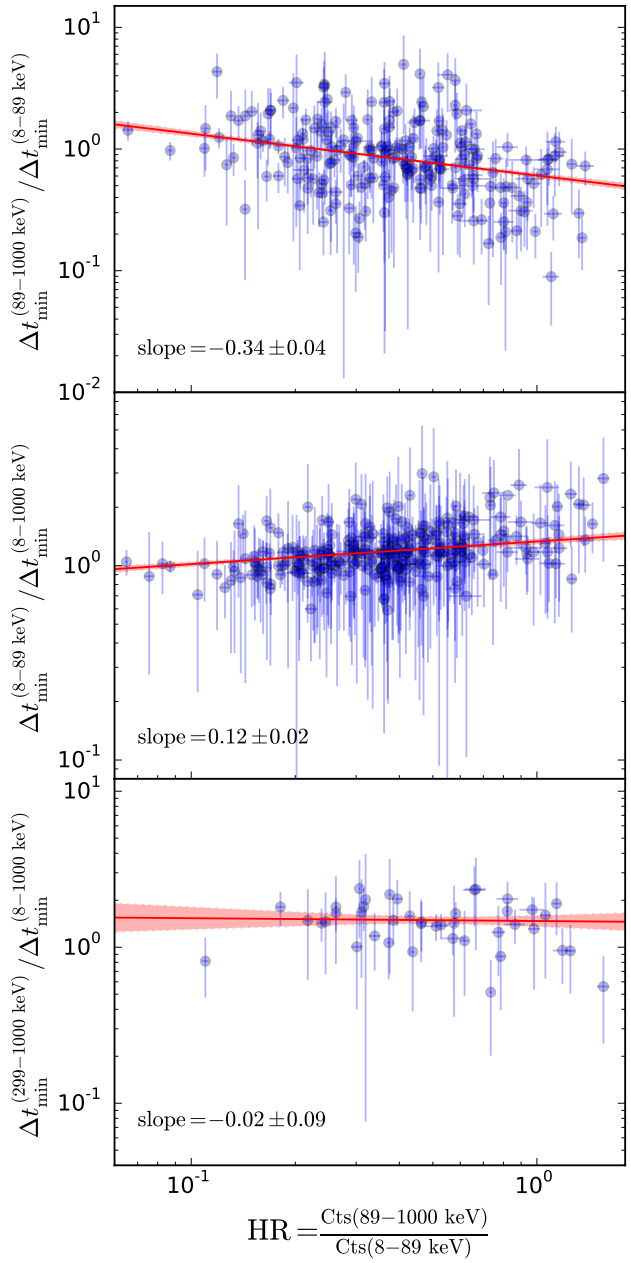

FIG. 7.— Top panel: The ratio of minimum variability timescale for channels 3 + 4 and channels 1 + 2, plotted against hardness ratio for the corresponding composite channels. Middle and bottom panels: The ratio of $\Delta t_{\rm min}$ for channels 1 + 2 and channel 4 over full energy band, separately plotted against hardness ratio. The best fitted linear model through the bursts including shaded 1σ error region is also shown in each panel.

both short and long-duration GRBs. This relationship can be captured using a best-fitted linear model through all the bursts, shown in Figure 7 (top panel), with slope $= -0.34 \pm 0.04$.

The change in minimum timescale with hardness can be understood from the effects of relativistic beaming on emission instantaneously emitted in the rest frame by a moving shell (e.g., Fenimore et al. 1996; Ryde & Petrosian 2002; Kocevski et al. 2003). If the material on the line-of-site has a Doppler factor $\Gamma(1-\beta)$, propagating with a speed $v = \beta c$ and Lorentz factor Γ, material above or below the line of site at angle θ will have a Doppler factor $\Gamma(1-\beta cos(\theta)) \approx (1+(\Gamma\theta)^2)/2\Gamma$, larger by a factor $1 + (\Gamma\theta)^2$. The off-axis emission will also arrive later, at a time $t - t_e = R/c(1 - \cos(\theta))$, where R is the emission radius, after the start of the emission at t_e. If we assume $R = 2\Gamma^2 ct_e$, then the Doppler factor increases in time, in the observer frame, as t/t_e. As a result, the photon flux observed at fixed energy E will decrease as higher and higher rest-frame-energy photons reach the bandpass, as $(t/t_e)^{\alpha-2}$. Here, α is the photon index and the power of 2 arises from relativistic beaming.

Thus, we expect that impulsive releases of energy in the rest frame will be smoothed over – in a fashion that is stronger at low energy ($\alpha \approx -1$) as compared to high energy (above $E_{\rm peak}$, $\alpha \lesssim -2$) – as viewed in the observer frame. The degree of smoothing expected above $E_{\rm peak}$ is a factor 2–3 less than the smoothing expected at observer frame energies below $E_{\rm peak}$. This effect naturally explains the decreasing minimum timescale we observe with increasing spectral bandpass, and it suggests that the tightest constraints on minimum timescale should be obtained from the highest available instrument bandpass. It should also be sufficient to confirm that $E_{\rm pk}$ is below, or perhaps within, a given bandpass.

Figure 7 (middle panel) shows the ratio of $\Delta t_{\rm min}$ for the soft composite channel over the full energy band against the *HR*. This plot shows how $\Delta t_{\rm min}$ is approximately the same in each bandpass until the hardness ratio goes beyond roughly its median value. The bursts in this plot well-fitted by a line with slope $= 0.12 \pm 0.02$.

The ratio of $\Delta t_{\rm min}$ for the hardest channel (#4) over the full energy band against the *HR* is shown in Figure 7 (bottom panel). Here, the best-fit line (slope $= -0.02 \pm 0.09$) is consistent with being flat: the minimum timescales appear to be independent of this hardness ratio for all but perhaps the hardest handful of *Fermi* GRBs. We conclude that utilizing the full *Fermi*/GBM bandpass – which yields $\Delta t_{\rm min}$ constraints consistent with those derived from the soft energy channel for soft GRBs and also $\Delta t_{\rm min}$ constraints consistent with those derived from the hard energy channel for hard GRBs – is an acceptable procedure for determining the tightest constraints on $\Delta t_{\rm min}$.

3.5. *Constraints on the Size of the Central Engine*

The minimum timescale provides an upper limit on the size of the GRB emission region, in turn providing hints on the nature of the GRB progenitor and potentially shedding light on the nature of emission mechanism. In Paper I, we summarized how an association of a minimum timescale with a physical size is not unique, because the observed timescales depend strongly also on the emitting surface velocity.

The minimum Lorentz factor Γ can be estimated from the compactness argument (Lithwick & Sari 2001). If we assume a spectrum with photon index $\alpha = -2$ (see, Ackermann et al. 2013, Figure 25) – typical for GRB spectra above the pair-production limit and also appropriate for the range of energies which dominate the luminosity

(near the νF_ν spectral peak) – we find

$$\Gamma \gtrsim 110 \left(\frac{L}{10^{51}\,\mathrm{erg/s}}\,\frac{1+z}{\Delta t_{\rm min}/0.1\,\mathrm{sec}}\right)^{1/5}, \qquad (1)$$

where L is the gamma-ray luminosity. If we regard $\Delta t_{\rm min}$ as corresponding to the bolometric emission, it is most natural to use the full *Fermi*/GBM bandpass for its estimation rather than a fixed rest frame bandpass. It could be argued that corrections should also be made to account for spectral hardness, based perhaps on the assumption that GRBs have a single, fixed rest frame hardness – an unlikely possibility – modulated only by Lorentz factor. However, based on the analysis in Section 3.4 above, any corrections would be small.

Utilizing our $\Delta t_{\rm min}$ estimates and limits for the full *Fermi*/GBM bandpass, we find that 50% of *Fermi* GRBs must have $\Gamma > 190$. In the case of the most energetic events, 10% of *Fermi* GRBs require $\Gamma > 410$. To calculate these fractions for short-duration bursts without measured redshift, we follow D'Avanzo et al. (2014) in assigning an average $z = 0.85$. For long-duration GRBs lacking redshift, we assign the average $z = 2.18$.

Similarly, for some maximally allowed $\Gamma_{\rm max}$, compactness limits the emission radius to be greater than

$$R_{\rm min} \simeq 2.8{\times}10^{10}\,\frac{L}{10^{51}\,\mathrm{erg/s}}\left(\frac{\Gamma_{\rm max}}{1200}\right)^{-3}\ \mathrm{cm}. \qquad (2)$$

This minimum bound on the radius can be compared to the maximum bound on the radius established by the temporal variability:

$$R_{\rm max} = c\,\frac{\Delta t_{\rm min}}{1+z}\,\Gamma^2_{\rm max},$$
$$\simeq 4.4{\times}10^{15}\,\frac{\Delta t_{\rm min}/0.1\,\mathrm{sec}}{1+z}\left(\frac{\Gamma_{\rm max}}{1200}\right)^{2}\ \mathrm{cm}. \qquad (3)$$

Here, we conservatively take $\Gamma_{\rm max} \sim 1200$ from Racusin et al. (2011).

If emission were to occur at the minimum allowable radius, $R_{\rm min}$, it would correspond to variability timescales as short as $\Delta t = R_{\rm min}/(2c\Gamma^2_{\rm max}) \lesssim 1\mu$s. Because such timescales are not observed, a more realistic bound on the minimum emission radius is $R_c = 2c\Gamma^2_{\rm min}\Delta t_{\rm min}/(1+z)$, or

$$R_c \simeq 7.3{\times}10^{13}\left(\frac{L}{10^{51}\,\mathrm{erg/s}}\right)^{2/5}\left(\frac{\Delta t_{\rm min}/0.1\,\mathrm{sec}}{1+z}\right)^{3/5}\ \mathrm{cm}. \qquad (4)$$

Figure 8 shows the emission radius, R_c, for all the bursts with measured $\Delta t_{\rm min}$ in *Fermi*/GBM sample versus rest-frame T_{90}. The shaded region shows the interval between the $R_{\rm min}$ and $R_{\rm max}$. The interpretation of R_c as a characteristic minimum radius for the emission is motivated further in Section 4.

The short-duration GRBs have a KM mean $R_c = 3.3 \times 10^{13}$ cm. This is about four times smaller than the KM mean $R_c = 1.3 \times 10^{14}$ cm for long-duration GRBs. While this represents a statistically significant separation (18σ, t-test), it is substantially less than the factor of approximately twenty separation between the mean T_{90} durations (Figure 8, also Kouveliotou et al. 1993). In contrast to the findings of Barnacka & Loeb (2014) – where the emission radius was argued to simply scale with the T_{90} duration – we find a broader overlap in the populations.

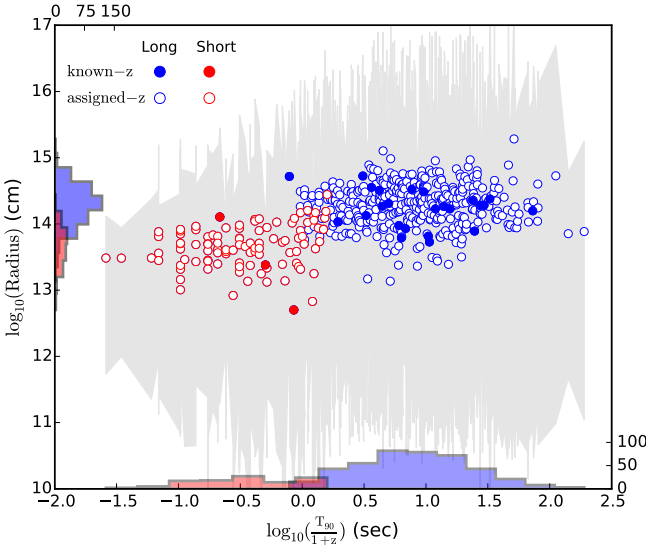

FIG. 8.— The characteristic emission radii R_c (Equation 4) plotted versus rest frame T_{90} for the *Fermi*/GBM bursts. The shaded region shows the interval between the minimum and maximum emission radii allowed. The bursts with known-z and assigned-z are denoted with filled and unfilled circles, respectively. The short and long-duration GRBs are denoted with red and blue colors, respectively.

3.6. *Evolution of* $\Delta t_{\rm min}$ *with* z

Because GRBs are present over a very broad redshift range, the signature of time-dilation – and perhaps of any evolution in GRB time-structure with redshift – should be present in GRB time-series. Finding the signature of time-dilation in GRBs has remained elusive (Norris et al. 1994; Kocevski & Petrosian 2013, but see, e.g., Zhang et al. 2013). In our previous attempt described in Paper I, we utilized *Swift* GRBs and demonstrated a correlation between $\Delta t_{\rm min}$ and redshift, marginally stronger than expected simply from time-dilation. We discussed how this excess correlation strength was possibly due to the utilization of a fixed observer frame bandpass instead of a fixed rest frame bandpass in the analysis. For *Fermi*/GBM, the broad instrument energy range permits analysis in a fixed rest frame bandpass.

We identify 46 *Fermi* GRBs, including 4 short-duration GRBs, with measured redshifts. Light curves are extracted in the rest frame 89–299 keV band and analyzed. In Figure 9 we plot $\Delta t_{\rm min}/(1+z)$ versus $1+z$ for the long-duration GRBs. Redshift values are taken from Butler et al. (2007, 2010, and references therein), Butler (2013), and this webpage[5]. The blue circles in Figure 9 correspond to the KM mean values of $\Delta t_{\rm min}$ for sets of between 7 and 10 bursts, grouped by redshift intervals. The unbinned data are plotted in the background for the entire sample and for those with measured $\Delta t_{\rm min}$ using unfilled and filled circles, respectively.

[5] `http://www.mpe.mpg.de/~jcg/grbgen.html`

We find that the binned data can be well-fitted by a line $\Delta t_{\rm min}/(1+z) \sim 140((1+z)/2.8)^{0.5\pm1.0}$ ms, suggesting possibly increase in timescale with z but also consistent the prediction of simple time-dilation (dotted line).

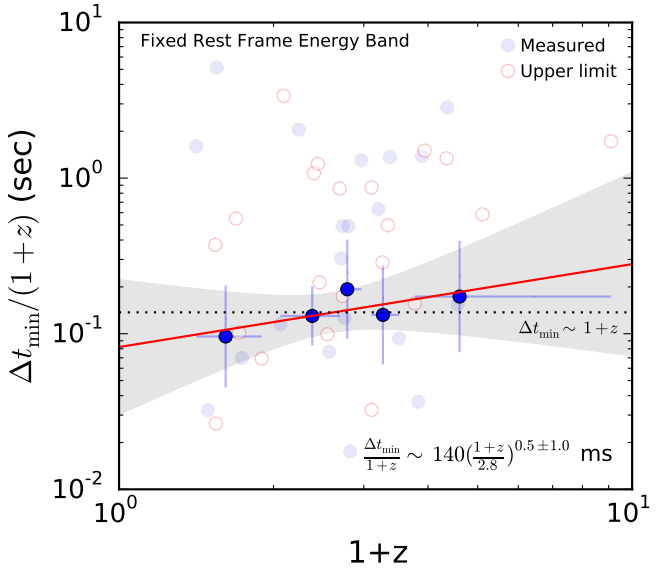

FIG. 9.— Minimum variability timescale in the rest frame 89–299 keV energy band versus redshift, z. The blue circles show the KM mean values of $\Delta t_{\rm min}$ for groups of 7–10 bursts of similar redshift. The shaded region represents the 1σ confidence interval for the fitted red line. The dotted black line shows the expected evolution due to simple cosmological time dilation, namely $\Delta t_{\rm min} \sim 1+z$. The faint blue circles show all GRBs with measured $\Delta t_{\rm min}$ and known-z and the unfilled circles show GRBs with upper limit values for $\Delta t_{\rm min}$.

4. CONCLUSIONS

Using a technique based on Haar wavelets, previously developed in Paper I, we studied the temporal properties of a large sample of GRB gamma-ray prompt-emission light curves captured by the GBM instrument onboard *Fermi* prior to July 11, 2012. We analyzed the time histories in four energy bands. While the derived values for $\Delta t_{\rm min}$ are highly-dependent upon bandpass, we find that the use of the full energy band allows for the tightest constraints on the size of the emission region. In principle, the highest-energy bandpass should yield the tightest constraint (Section 3.4). However, S/N in the highest-energy channels is often low; the full energy bandpass allows for increased S/N while maintaining a consistent $\Delta t_{\rm min}$ estimate.

Applying our technique to the joint *Fermi*/GBM and *Swift*/BAT sample, we find close consistency in the minimum timescales derived for each instrument. However, as suggested by simulations in Paper I – and observed for a handfull of bursts of widely varying S/N in Section 3.2 – $\Delta t_{\rm min}$ values below the measurement limit ($\Delta t_{\rm S/N}$) can be present. It is thus important to consider our $\Delta t_{\rm min}$ values as defined given the observed data, with the possibility of improved limits given better data. We urge caution, in particular, in interpreting minimum timescales determined using hard X-ray data (e.g., *Swift*/BAT). Minimum timescale estimates using the full *Fermi*/GBM bandpass are a factor 2–3 times more constraining than those determined from *Fermi*/GBM data in a *Swift*/BAT bandpass.

Considering measurements and limits, we find a median minimum variability timescale in the observer frame of 134 ms (long-duration; 18 ms for short-duration GRBs). In the source frame, for a smaller sample of 33 GRBs, we find a median timescale of 45 ms (long-duration; 10 ms for short-duration GRBs). This finding validates our previous results in Paper I, confirming that millisecond variability appears to be rare in GRBs. In the most extreme examples, 10% of the long-duration GRB sample yields evidence for 2.2 ms variability (1.9 ms for short-duration GRBs). In the source frame, we find similar numbers, 2.9 ms for long-duration GRBs and 2.4 ms for short-duration GRBs. Even if we restrict to the 67 GRBs within minimum detectable timescales $t_{\rm S/N} < 10$ ms, only 10% of the brightest and/or most impulsive GRBs show evidence for variability on timescales below 4.2 ms in the observer frame.

4.1. *Constraints on the Fireball Model*

In the "external shock" model (e.g., Rees & Meszaros 1992), gamma-rays are produced as the GRB sweeps up and excites clouds in the external medium. The extracted $\Delta t_{\rm min}$ can circumscribe the size scale of the impacted cloud along the line of sight. For a thin shell (e.g., Mészáros 2006), the gamma-ray radiation will start when the relativistic shell hits the inner boundary of the cloud with the peak flux produced as the shell reaches the densest region or center of the cloud. The size scale of the impacted cloud is limited by $2\Gamma^2 c\,\Delta t_{\rm min}$ since the shock is moving near light speed (Fenimore et al. 1996). For the smallest $\Delta t_{\rm min}$ found ~1 ms, and assuming $\Gamma < 1000$, the cloud size must be smaller than 4 AU.

If the angular size of an impacted cloud as viewed from the GRB central engine is Θ, the minimum variability timescales is constrained to be $\delta\Theta\,\Gamma < \Delta t_{\rm min}/2\,T_{\rm rise}$ (Paper I). Here, $T_{\rm rise}$ denotes the overall time to reach the maximum gamma-ray flux. The fraction of the emitting shell that becomes active is expected to be of order $0.1\Delta t_{\rm min}/2\,T_{\rm rise}$ (Fenimore et al. 1999). For the bursts in the *Fermi* sample with typical minimum variability timescale $\Delta t_{\rm min} \sim T_{\rm rise}$, there is no need to consider a highly-clumped external medium and the external shock scenario is viable.

However, there are many bursts (e.g., Figure 6) which do exhibit $\Delta t_{\rm min}/T_{\rm rise} \ll 1$. If this variability results from a clumped external medium, then a significant fraction of the energy from the GRB must escape without interacting and producing gamma-rays. Early X-ray afterglow observations (e.g., Nousek et al. 2006), on the other hand, demonstrate the need for a high (order unity) efficiency in tapping the kinetic energy of the flow to produce gamma-rays. Thus, external shocks likely cannot explain the finest-time-scale variability.

In the "internal shock" scenario (e.g., Rees & Meszaros 1994), the relativistic expanding outflow released from a central engine is assumed to be variable, consisting of multiple shells of different Γ. The dispersion in Γ is related to the observed variability of the light curve, as $\Delta\Gamma/\Gamma \approx 1/2\,(\Delta t_{\rm min}/T_{\rm rise})$ (Paper I), with many of the *Fermi* light curves requiring $\Delta\Gamma \approx \Gamma$. Efficient pro-

duction of gamma-rays also requires $\Delta\Gamma \approx \Gamma$ (Piran 1999; Kobayashi & Sari 2001). It is, therefore, natural to assume that some of the gamma-ray emission is released with the minimum possible Lorentz factor $\Gamma_{\rm min} \approx 200$ (Section 3.5) allowed from compactness considerations. As a result, considering variability at the few millisecond level, some GRBs must emit at radii of order $R_c \approx 2\Gamma^2_{\rm min} c\,\Delta t_{\rm min} \approx 10^{13}$ cm (Equation 4, Figure 8). This is also the extent to which minimum variability timescales can limit the size of the progenitor.

We find that long-duration GRBs appear to have typical emission radii $R_c \approx 1.3{\times}10^{14}$ cm, while short-duration GRBs have four times smaller typical emission radii, $R_c \approx 3.3{\times}10^{13}$ cm. There is large scatter in the inferred radii of each population, and the distributions appear to strongly overlap. It is unclear whether the dichotomy in short and long-duration GRB T_{90} durations maps cleanly to a similar dichotomy in the size of the emission regions.

Finally, we note that our minimum timescales appear to correlate with redshift in fashion consistent with cosmological time-dilation. Correcting for this, we find no significant evidence that $\Delta t_{\rm min}/(1+z)$ evolves with redshift. This may be partly because the number of *Fermi* GRBs with measured redshifts is low (e.g., as compared to *Swift*; Paper I). Future increases in the sample size will surely allow for tighter constraints on minimum emission radii, Lorentz factors, and progenitor dimensions as well as allowing us to better understand whether any of these quantities vary with cosmic time.

REFERENCES

Abdo, A. A., Ackermann, M., Ajello, M., et al. 2010, ApJ, 722, 520
Ackermann, M., Ajello, M., Asano, K., et al. 2013, ApJS, 209, 11
Aretxaga, I., Cid Fernandes, R., & Terlevich, R. J. 1997, MNRAS, 286, 271
Barnacka, A., & Loeb, A. 2014, ApJ, 794, L8
Barthelmy, S. D., Barbier, L. M., Cummings, J. R., et al. 2005, Space Sci. Rev., 120, 143
Beloborodov, A. M., Stern, B. E., & Svensson, R. 2000, ApJ, 535, 158
Bhat, P. N. 2013, ArXiv e-prints, arXiv:1307.7618
Borgonovo, L. 2004, A&A, 418, 487
Butler, N. 2013, The Astronomical Review, 8, 103
Butler, N. R., Bloom, J. S., & Poznanski, D. 2010, ApJ, 711, 495
Butler, N. R., Kocevski, D., Bloom, J. S., & Curtis, J. L. 2007, ApJ, 671, 656
Chang, H.-Y. 2001, ApJ, 557, L85
Chatterjee, R., Bailyn, C. D., Bonning, E. W., et al. 2012, ApJ, 749, 191
Cristiani, S., Trentini, S., La Franca, F., et al. 1996, A&A, 306, 395
Cucchiara, A., Levan, A. J., Fox, D. B., et al. 2011, ApJ, 736, 7
D'Avanzo, P., Salvaterra, R., Bernardini, M. G., et al. 2014, MNRAS, 442, 2342
Dichiara, S., Guidorzi, C., Amati, L., & Frontera, F. 2013, MNRAS, 431, 3608
Feigelson, E. D., & Nelson, P. I. 1985, ApJ, 293, 192
Fenimore, E. E., Cooper, C., Ramirez-Ruiz, E., et al. 1999, ApJ, 512, 683
Fenimore, E. E., in 't Zand, J. J. M., Norris, J. P., Bonnell, J. T., & Nemiroff, R. J. 1995, ApJ, 448, L101
Fenimore, E. E., Madras, C. D., & Nayakshin, S. 1996, ApJ, 473, 998
Gehrels, N., Chincarini, G., & Giommi, et al., P. 2004, ApJ, 611, 1005
Gehrels, N., & Razzaque, S. 2013, Frontiers of Physics, 8, 661
Golkhou, V. Z., & Butler, N. R. 2014, ApJ, 787, 90
Guidorzi, C., Margutti, R., Amati, L., et al. 2012, MNRAS, 422, 1785
Hook, I. M., McMahon, R. G., Boyle, B. J., & Irwin, M. J. 1994, MNRAS, 268, 305
in't Zand, J. J. M., & Fenimore, E. E. 1996, ApJ, 464, 622
Jakobsson, P., Hjorth, J., Malesani, D., et al. 2012, ApJ, 752, 62
Kaplan, E. L., & Meier, P. 1958, Journal of the American Statistical Association, 53, 457
Kendall, M. G. 1938, Biometrika
Kobayashi, S., & Sari, R. 2001, ApJ, 551, 934
Kocevski, D., & Petrosian, V. 2013, ApJ, 765, 116
Kocevski, D., Ryde, F., & Liang, E. 2003, ApJ, 596, 389
Kolaczyk, E. D. 1997, ApJ, 483, 340
Kouveliotou, C., Meegan, C. A., Fishman, G. J., et al. 1993, ApJ, 413, L101
Link, B., Epstein, R. I., & Priedhorsky, W. C. 1993, ApJ, 408, L81
Lithwick, Y., & Sari, R. 2001, ApJ, 555, 540
Littlejohns, O. M., & Butler, N. R. 2014, MNRAS, 444, 3948
Lloyd-Ronning, N. M., & Petrosian, V. 2002, ApJ, 565, 182
MacLachlan, G. A., Shenoy, A., Sonbas, E., et al. 2013, MNRAS, 432, 857
Mantel, N. 1966, Cancer Chemother Rep, 50, 163
Meegan, C., Lichti, G., Bhat, P. N., et al. 2009, ApJ, 702, 791
Mészáros, P. 2006, Reports on Progress in Physics, 69, 2259
Norris, J. P., Nemiroff, R. J., Bonnell, J. T., et al. 1996, ApJ, 459, 393
Norris, J. P., Nemiroff, R. J., Scargle, J. D., et al. 1994, ApJ, 424, 540
Nousek, J. A., Kouveliotou, C., Grupe, D., et al. 2006, ApJ, 642, 389
Paltani, S. 1999, in Astronomical Society of the Pacific Conference Series, Vol. 159, BL Lac Phenomenon, ed. L. O. Takalo & A. Sillanpää, 293
Piran, T. 1999, Phys. Rep., 314, 575
Racusin, J. L., Oates, S. R., Schady, P., et al. 2011, ApJ, 738, 138
Rees, M. J., & Meszaros, P. 1992, MNRAS, 258, 41P
Rees, M. J., & Meszaros, P. 1994, ApJ, 430, L93
Reichart, D. E., Lamb, D. Q., Fenimore, E. E., et al. 2001, ApJ, 552, 57
Ryde, F., & Petrosian, V. 2002, ApJ, 578, 290
Salvaterra, R., Della Valle, M., Campana, S., et al. 2009, Nature, 461, 1258
Sonbas, E., Dhuga, K. S., Veres, P., et al. 2014, ArXiv e-prints, arXiv:1408.3042
Tanvir, N. R., Fox, D. B., Levan, A. J., et al. 2009, Nature, 461, 1254
Trevese, D., Kron, R. G., Majewski, S. R., Bershady, M. A., & Koo, D. C. 1994, ApJ, 433, 494
Virgili, F. J., Qin, Y., Zhang, B., & Liang, E. 2012, MNRAS, 424, 2821
von Kienlin, A., Meegan, C. A., Paciesas, W. S., et al. 2014, ApJS, 211, 13
Walker, K. C., Schaefer, B. E., & Fenimore, E. E. 2000, ApJ, 537, 264
Zhang, F.-W., Fan, Y.-Z., Shao, L., & Wei, D.-M. 2013, ApJ, 778, L11

TABLE 2 GRB Minimum Timescales

Trigger ID	GRB Name	$\Delta t_{\rm min}$ (s)	$\Delta t_{\rm S/N}$ (s)	T_{90} (s)	$T_{100}^{\rm start}$ (s)	$T_{100}^{\rm stop}$ (s)	$\sigma_{X,t_{\rm min}}$	$\sigma_{X,t_{\rm S/N}}$	z
080714086	080714B	0.821 ± 0.223	0.522 ± 0.045	5.376 ± 2.360	-3.437	7.283	0.90	0.57	...
080714425	080714C	1.984 ± 1.040	1.241 ± 0.108	40.192 ± 1.145	-22.987	55.766	0.64	0.40	...
080714745	080714A	1.384 ± 0.143	0.620 ± 0.054	59.649 ± 11.276	-29.747	88.936	0.74	0.33	...
080715950	080715A	< 0.101	0.011 ± 0.001	7.872 ± 0.272	-2.203	11.867	0.90	0.20	...
080717543	080717A	0.568 ± 0.194	0.369 ± 0.032	36.609 ± 2.985	-23.414	49.420	0.53	0.34	...
080719529	080719A	1.990 ± 0.830	1.241 ± 0.108	16.128 ± 17.887	-12.339	19.739	0.64	0.40	...
080723557	080723B	0.040 ± 0.017	0.027 ± 0.002	58.369 ± 1.985	-0.180	89.694	0.22	0.15	...
080723913	080723C	0.013 ± 0.004	0.008 ± 0.001	0.192 ± 0.345	-0.160	0.224	0.96	0.58	...
080723985	080723D	< 0.309	0.065 ± 0.006	42.817 ± 0.659	-4.995	66.909	0.29	0.13	...
080724401	080724A	< 0.129	0.016 ± 0.001	379.397 ± 2.202	-10.638	390.213	0.50	0.13	...
080725435	080725A	< 1.700	0.439 ± 0.038	25.920 ± 1.208	-14.091	35.934	0.28	0.15	...
080725541	080725B	< 0.266	0.065 ± 0.006	0.960 ± 1.292	-0.603	1.230	0.90	0.35	...
080727964	080727C	< 0.883	0.369 ± 0.032	89.089 ± 6.476	-31.416	90.623	0.27	0.20	...
080730520	080730A	< 0.794	0.184 ± 0.016	17.408 ± 6.229	-9.197	25.429	0.28	0.12	...
080730786	080730B	< 0.297	0.046 ± 0.004	13.312 ± 4.222	-7.171	19.295	0.57	0.11	...
080802386	080802A	0.017 ± 0.006	0.011 ± 0.001	0.576 ± 0.091	-0.352	0.796	0.69	0.45	...
080803772	080803A	1.326 ± 0.295	0.738 ± 0.064	26.240 ± 1.691	-13.245	38.973	0.60	0.33	...
080804456	080804B	< 1.538	0.522 ± 0.045	501.830 ± 6.476	-27.198	493.126	0.34	0.32	...
080804972	080804A	0.702 ± 0.338	0.439 ± 0.038	24.704 ± 1.460	-11.880	37.273	0.26	0.16	2.2
080805496	080805B	1.551 ± 0.340	0.620 ± 0.054	29.440 ± 3.566	-6.944	42.221	0.59	0.24	...
080805584	080805C	4.656 ± 1.341	2.087 ± 0.181	65.665 ± 14.676	-25.892	93.609	0.60	0.27	...
080806584	080806A	0.659 ± 0.290	0.310 ± 0.027	2.304 ± 0.453	-3.254	1.138	0.66	0.31	...
080806896	080806B	< 0.538	0.130 ± 0.011	75.777 ± 4.185	-35.328	64.275	0.33	0.14	...
080807993	080807A	0.009 ± 0.003	0.007 ± 0.001	19.072 ± 0.181	-9.447	27.148	0.39	0.30	...
080808451	080808A	0.853 ± 0.267	0.522 ± 0.045	4.352 ± 0.832	-3.696	4.376	0.85	0.52	...
080808565	080808B	2.298 ± 0.106	0.522 ± 0.045	17.728 ± 1.489	-6.343	28.211	0.55	0.12	...
080808772	080808C	1.610 ± 0.709	1.043 ± 0.090	211.970 ± 6.557	-170.562	146.090	0.68	0.44	...
080809808	080809A	< 4.629	1.043 ± 0.090	28.160 ± 2.896	-21.022	32.482	0.61	0.25	...
080810549	080810A	0.102 ± 0.040	0.065 ± 0.006	107.457 ± 15.413	-28.134	114.761	0.43	0.28	3.35
080812889	080812A	0.486 ± 0.311	0.310 ± 0.027	15.040 ± 0.462	-9.237	18.738	0.61	0.39	...
080815917	080815A	< 0.258	0.110 ± 0.010	0.832 ± 0.320	-0.730	0.927	0.62	0.52	...
080816503	080816A	< 0.152	0.033 ± 0.003	64.769 ± 1.810	-1.421	84.710	0.45	0.18	...
080816989	080816B	0.083 ± 0.019	0.039 ± 0.003	4.608 ± 0.453	-0.141	6.805	0.59	0.27	...
080817161	080817A	0.243 ± 0.070	0.110 ± 0.010	60.289 ± 0.466	-23.013	89.108	0.15	0.07	...
080817720	080817B	0.043 ± 0.018	0.023 ± 0.002	4.416 ± 0.363	-2.274	6.526	0.59	0.31	...
080818579	080818A	0.229 ± 0.070	0.078 ± 0.007	59.329 ± 8.749	-28.682	85.806	0.50	0.17	...
080818945	080818B	< 0.493	0.155 ± 0.013	13.376 ± 0.410	-7.141	19.445	0.45	0.30	...
080821332	080821A	0.305 ± 0.118	0.155 ± 0.013	5.888 ± 0.264	-4.199	7.503	0.29	0.15	...
080823363	080823A	0.675 ± 0.207	0.310 ± 0.027	43.457 ± 1.717	-5.181	63.888	0.34	0.15	...
080824909	080824A	0.117 ± 0.019	0.046 ± 0.004	7.424 ± 2.005	-5.754	7.825	0.57	0.22	...
080825593	080825C	< 0.248	0.023 ± 0.002	20.992 ± 0.231	-1.418	32.569	0.50	0.07	...
080828189	080828B	< 0.135	0.078 ± 0.007	3.008 ± 3.329	-1.621	4.379	0.66	0.80	...
080829790	080829A	< 1.534	0.310 ± 0.027	7.680 ± 0.377	-4.122	11.162	0.52	0.19	...
080830368	080830A	0.294 ± 0.220	0.184 ± 0.016	40.896 ± 5.069	-21.972	59.788	0.38	0.24	...
080831053	080831A	< 0.017	0.004 ± 0.001	0.576 ± 1.168	-0.576	0.572	0.88	0.53	...
080831921	080831B	0.797 ± 0.349	0.522 ± 0.045	74.497 ± 1.243	-32.933	106.344	0.41	0.27	...
080904886	080904A	0.193 ± 0.041	0.078 ± 0.007	17.344 ± 1.385	-9.587	23.359	0.31	0.13	...
080905499	080905A	0.012 ± 0.003	0.008 ± 0.001	0.960 ± 0.345	-0.539	1.371	0.87	0.56	0.1218
080905570	080905C	0.447 ± 0.245	0.310 ± 0.027	26.624 ± 2.896	-19.918	32.523	0.36	0.25	...
080905705	080905B	< 3.071	0.738 ± 0.064	105.984 ± 6.802	-23.660	123.652	0.78	0.34	2.374
080906212	080906B	0.173 ± 0.024	0.065 ± 0.006	2.875 ± 0.767	-1.426	4.294	0.27	0.10	...
080912360	080912A	< 4.072	0.620 ± 0.054	16.384 ± 2.896	-11.184	21.412	0.77	0.17	...
080913735	080913B	0.124 ± 0.090	0.065 ± 0.006	41.217 ± 7.281	-20.617	61.371	0.52	0.28	...
080916009	080916C	< 0.160	0.039 ± 0.003	62.977 ± 0.810	-14.295	87.070	0.24	0.11	...
080916406	080916A	1.639 ± 0.197	0.522 ± 0.045	46.337 ± 7.173	-22.503	69.674	0.56	0.18	0.689
080919790	080919B	0.011 ± 0.001	0.004 ± 0.001	0.512 ± 0.405	-0.382	0.637	0.98	0.40	...
080920268	080920A	9.473 ± 1.615	4.174 ± 0.362	113.921 ± 3.125	-33.216	163.865	0.82	0.36	...
080924766	080924A	0.467 ± 0.064	0.219 ± 0.019	39.937 ± 4.222	-27.818	48.429	0.55	0.26	...

Continued on Next Page...

TABLE 2 – Continued

Trigger ID	GRB Name	$\Delta t_{\rm min}$ (s)	$\Delta t_{\rm S/N}$ (s)	T_{90} (s)	$T_{100}^{\rm start}$ (s)	$T_{100}^{\rm stop}$ (s)	$\sigma_{X,t_{\rm min}}$	$\sigma_{X,t_{\rm S/N}}$	z
080925775	080925A	< 0.350	0.078 ± 0.007	31.744 ± 3.167	-16.746	46.099	0.24	0.08	...
080927480	080927A	2.257 ± 0.790	1.043 ± 0.090	45.313 ± 3.083	-22.579	67.568	0.42	0.20	...
080928628	080928A	< 0.344	0.110 ± 0.010	14.336 ± 4.007	-8.896	19.600	0.75	0.41	1.692
081003644	081003C	< 0.546	0.155 ± 0.013	50.177 ± 3.692	-21.521	65.256	0.69	0.46	...
081006604	081006A	< 0.620	0.219 ± 0.019	6.400 ± 0.923	-3.424	9.312	0.69	0.58	...
081006872	081006B	0.134 ± 0.067	0.092 ± 0.008	3.328 ± 1.305	-2.163	4.477	0.75	0.52	...
081008832	081008A	< 1.260	0.261 ± 0.023	150.015 ± 12.892	-29.594	201.406	0.30	0.20	1.9685
081009140	081009A	0.163 ± 0.013	0.039 ± 0.003	41.345 ± 0.264	-3.900	61.004	0.14	0.03	...
081009690	081009B	< 0.601	0.219 ± 0.019	176.191 ± 2.127	-25.547	194.678	0.21	0.18	...
081012045	081012B	< 0.023	0.005 ± 0.001	1.216 ± 1.748	-1.174	1.238	0.93	0.61	...
081012549	081012A	< 2.163	0.522 ± 0.045	30.721 ± 5.615	-20.507	40.626	0.52	0.28	...
081017474	081017B	< 1.446	0.219 ± 0.019	28.416 ± 2.757	-27.044	29.472	0.77	0.38	...
081021398	081021A	< 2.008	0.620 ± 0.054	26.112 ± 3.974	-3.499	29.125	0.43	0.29	...
081022364	081022A	1.982 ± 0.290	0.877 ± 0.076	17.152 ± 3.727	-11.056	23.052	0.74	0.33	...
081024245	081024A	0.086 ± 0.009	0.039 ± 0.003	0.832 ± 1.282	-1.242	0.415	1.02	0.46	...
081024851	081024C	5.151 ± 0.941	2.482 ± 0.215	56.065 ± 2.064	-8.117	82.139	0.32	0.16	...
081024891	081024B	< 0.056	0.016 ± 0.001	0.640 ± 0.264	-0.381	0.893	0.81	0.54	...
081025349	081025A	< 0.196	0.065 ± 0.006	22.528 ± 0.724	-11.667	24.815	0.37	0.32	...
081028538	081028B	< 0.350	0.078 ± 0.007	13.312 ± 1.280	-14.531	11.935	0.41	0.23	...
081101167	081101C	< 4.574	1.043 ± 0.090	9.984 ± 9.051	-8.389	6.980	1.05	0.72	...
081101491	081101A	0.072 ± 0.010	0.033 ± 0.003	0.128 ± 0.091	-0.128	0.128	0.95	0.43	...
081101532	081101B	< 0.158	0.055 ± 0.005	8.256 ± 0.889	-2.456	12.047	0.27	0.25	...
081102365	081102B	0.081 ± 0.015	0.046 ± 0.004	1.728 ± 0.231	-0.923	2.517	0.70	0.40	...
081102739	081102A	< 7.327	0.620 ± 0.054	34.817 ± 2.415	-9.686	51.562	1.36	0.22	...
081105614	081105B	0.036 ± 0.005	0.019 ± 0.002	1.280 ± 1.368	-0.698	1.850	1.01	0.54	...
081107321	081107A	0.034 ± 0.012	0.019 ± 0.002	1.664 ± 0.234	-0.935	2.302	0.30	0.17	...
081109293	081109A	< 5.608	1.476 ± 0.128	58.369 ± 5.221	-25.721	80.494	0.46	0.18	...
081110601	081110A	0.291 ± 0.011	0.078 ± 0.007	11.776 ± 2.573	-5.581	17.821	0.63	0.17	...
081113230	081113A	0.012 ± 0.005	0.008 ± 0.001	0.576 ± 1.350	-0.288	0.860	0.63	0.42	...
081115891	081115A	< 0.158	0.046 ± 0.004	0.320 ± 0.653	-0.350	0.286	0.77	0.52	...
081118876	081118B	< 0.962	0.155 ± 0.013	20.736 ± 1.379	-2.143	31.216	0.31	0.10	...
081119184	081119A	< 0.333	0.078 ± 0.007	0.320 ± 0.680	-0.478	0.158	1.12	0.64	...
081120618	081120A	< 0.467	0.184 ± 0.016	25.344 ± 0.923	-13.827	36.599	0.23	0.22	...
081121858	081121A	0.203 ± 0.030	0.092 ± 0.008	41.985 ± 8.510	-5.898	62.110	0.57	0.26	2.512
081122520	081122A	< 0.102	0.023 ± 0.002	23.296 ± 2.111	-11.796	34.532	0.43	0.18	...
081122614	081122B	0.012 ± 0.002	0.007 ± 0.001	0.192 ± 0.091	-0.160	0.224	0.73	0.40	...
081124060	081124A	0.955 ± 0.040	0.184 ± 0.016	19.456 ± 1.086	-9.127	29.559	0.43	0.08	...
081125496	081125A	< 0.326	0.078 ± 0.007	9.280 ± 0.607	-4.082	14.386	0.19	0.10	...
081126899	081126A	< 0.635	0.110 ± 0.010	54.145 ± 0.923	-29.069	62.968	0.47	0.15	...
081129161	081129A	0.123 ± 0.093	0.065 ± 0.006	62.657 ± 7.318	-28.029	93.493	0.27	0.14	...
081130212	081130A	0.006 ± 0.002	0.004 ± 0.001	2.240 ± 1.002	-1.173	3.285	0.88	0.53	...
081130629	081130B	< 0.685	0.184 ± 0.016	45.569 ± 3.908	-38.657	19.081	0.49	0.20	...
081204004	081204C	< 0.434	0.110 ± 0.010	7.424 ± 1.846	-9.309	5.457	0.57	0.26	...
081204517	081204B	< 0.037	0.008 ± 0.001	0.192 ± 0.286	-0.160	0.224	0.95	0.36	...
081206275	081206A	< 10.133	1.043 ± 0.090	24.576 ± 5.724	-23.623	25.497	0.84	0.21	...
081206604	081206B	1.859 ± 0.239	0.620 ± 0.054	7.936 ± 4.382	-5.984	9.856	0.88	0.29	...
081206987	081206C	< 7.263	1.476 ± 0.128	22.528 ± 2.919	-17.043	27.771	0.99	0.31	...
081207680	081207A	0.346 ± 0.150	0.261 ± 0.023	97.282 ± 2.347	-26.296	131.297	0.17	0.12	...
081209981	081209A	< 0.007	0.004 ± 0.001	0.192 ± 0.143	-0.160	0.224	0.45	0.47	...
081213173	081213A	< 0.020	0.004 ± 0.001	0.256 ± 0.286	-0.384	0.128	0.87	0.52	...
081215784	081215A	0.042 ± 0.004	0.010 ± 0.001	5.568 ± 0.143	-1.544	9.520	0.30	0.07	...
081215880	081215B	0.481 ± 0.082	0.184 ± 0.016	7.680 ± 2.064	-4.058	11.226	0.94	0.36	...
081216531	081216A	< 0.028	0.008 ± 0.001	0.768 ± 0.429	-0.377	1.151	0.39	0.20	...
081217983	081217A	< 0.268	0.065 ± 0.006	29.696 ± 12.892	-12.112	29.737	0.26	0.16	...
081221681	081221A	< 0.600	0.130 ± 0.011	29.697 ± 0.410	-2.773	47.683	0.20	0.06	2.26
081222204	081222A	0.176 ± 0.088	0.092 ± 0.008	18.880 ± 2.318	-8.962	28.043	0.14	0.07	2.77
081223419	081223A	0.082 ± 0.010	0.033 ± 0.003	0.576 ± 0.143	-0.352	0.796	0.61	0.24	...
081224887	081224A	0.544 ± 0.052	0.155 ± 0.013	16.448 ± 1.159	-0.341	25.306	0.25	0.07	...

Continued on Next Page...

TABLE 2 – Continued

Trigger ID	GRB Name	$\Delta t_{\rm min}$ (s)	$\Delta t_{\rm S/N}$ (s)	T_{90} (s)	$T_{100}^{\rm start}$ (s)	$T_{100}^{\rm stop}$ (s)	$\sigma_{X,t_{\rm min}}$	$\sigma_{X,t_{\rm S/N}}$	z
081225257	081225A	< 0.497	0.155 ± 0.013	41.217 ± 5.667	-31.733	42.839	0.41	0.37	...
081226044	081226A	0.143 ± 0.024	0.065 ± 0.006	0.832 ± 1.032	-0.602	1.055	0.87	0.40	...
081226156	081226C	< 0.829	0.261 ± 0.023	65.793 ± 1.619	-55.553	24.607	0.63	0.31	...
081226509	081226B	0.061 ± 0.015	0.033 ± 0.003	0.192 ± 0.143	-0.160	0.224	0.82	0.44	...
081229187	081229A	0.141 ± 0.026	0.055 ± 0.005	0.768 ± 0.724	-0.633	0.895	0.80	0.31	...
081230871	081230B	< 0.620	0.261 ± 0.023	0.512 ± 0.272	-0.382	0.637	0.69	0.99	...
081231140	081231A	0.089 ± 0.057	0.055 ± 0.005	28.736 ± 2.611	-11.869	41.550	0.31	0.19	...
090101758	090101A	0.815 ± 0.278	0.369 ± 0.032	108.802 ± 1.619	-20.076	128.980	0.25	0.11	...
090102122	090102A	0.033 ± 0.013	0.019 ± 0.002	26.624 ± 0.810	-11.645	41.329	0.31	0.18	1.547
090107681	090107B	< 1.404	0.522 ± 0.045	18.432 ± 2.896	-11.178	25.478	0.65	0.59	...
090108020	090108A	0.043 ± 0.008	0.014 ± 0.001	0.704 ± 0.143	-0.414	0.985	0.45	0.14	...
090108322	090108B	0.038 ± 0.006	0.016 ± 0.001	0.192 ± 0.143	-0.160	0.202	0.78	0.33	...
090109332	090109A	< 0.266	0.130 ± 0.011	1.728 ± 0.820	-1.115	2.325	0.91	0.95	...
090112332	090112A	0.480 ± 0.053	0.219 ± 0.019	58.369 ± 4.783	-31.537	72.344	0.76	0.35	...
090112729	090112B	0.101 ± 0.059	0.055 ± 0.005	14.080 ± 5.126	-7.738	20.141	0.18	0.10	...
090113778	090113A	0.136 ± 0.062	0.065 ± 0.006	17.408 ± 3.238	-10.669	23.957	0.53	0.25	1.7493
090117335	090117B	< 0.892	0.130 ± 0.011	27.264 ± 1.286	-13.895	40.352	0.97	0.27	...
090117632	090117C	0.402 ± 0.258	0.261 ± 0.023	75.777 ± 3.238	-50.177	35.008	0.30	0.20	...
090117640	090117A	< 0.138	0.039 ± 0.003	15.552 ± 4.580	-12.020	17.972	0.36	0.19	...
090120627	090120A	0.118 ± 0.027	0.078 ± 0.007	1.856 ± 0.181	-1.439	2.260	0.91	0.60	...
090126227	090126B	1.668 ± 0.140	0.522 ± 0.045	5.632 ± 0.810	-4.586	6.654	0.76	0.24	...
090126245	090126C	0.020 ± 0.009	0.014 ± 0.001	0.960 ± 0.231	-0.859	1.051	0.97	0.65	...
090129880	090129A	0.973 ± 0.054	0.310 ± 0.027	16.640 ± 3.328	-4.998	24.621	0.58	0.19	...
090131090	090131A	0.138 ± 0.005	0.033 ± 0.003	35.073 ± 1.056	-2.175	55.674	0.38	0.09	...
090202347	090202A	< 0.902	0.130 ± 0.011	12.608 ± 0.345	-2.147	19.021	0.69	0.18	...
090206620	090206A	0.017 ± 0.004	0.010 ± 0.001	0.320 ± 0.143	-0.222	0.414	0.58	0.33	...
090207777	090207A	1.651 ± 0.286	0.620 ± 0.054	24.832 ± 3.899	-12.810	35.589	0.55	0.21	...
090213236	090213A	3.244 ± 1.884	2.087 ± 0.181	20.224 ± 6.192	-14.109	26.129	0.80	0.51	...
090217206	090217A	< 0.108	0.019 ± 0.002	33.280 ± 0.724	-15.762	40.481	0.33	0.11	...
090219074	090219A	< 0.282	0.055 ± 0.005	0.448 ± 0.272	-0.233	0.608	1.08	0.64	...
090222179	090222A	< 0.979	0.184 ± 0.016	17.408 ± 3.238	-10.669	23.957	0.70	0.24	...
090225009	090225A	< 0.697	0.184 ± 0.016	2.176 ± 2.833	-2.749	1.355	0.95	0.80	...
090227310	090227A	0.069 ± 0.018	0.046 ± 0.004	16.189 ± 0.831	-8.015	24.183	0.70	0.47	...
090227772	090227B	< 0.005	0.001 ± 0.001	1.280 ± 1.026	-0.698	1.837	0.22	0.20	...
090228204	090228A	0.004 ± 0.001	0.001 ± 0.001	0.448 ± 0.143	-0.221	0.672	0.51	0.17	...
090228976	090228B	< 2.017	0.522 ± 0.045	7.936 ± 1.379	-3.936	11.904	0.68	0.35	...
090301315	090301B	0.425 ± 0.180	0.184 ± 0.016	23.296 ± 2.064	-28.491	17.138	0.40	0.17	...
090304216	090304A	< 0.700	0.310 ± 0.027	2.816 ± 0.923	-1.658	3.942	0.82	0.74	...
090305052	090305B	< 0.029	0.008 ± 0.001	1.856 ± 0.580	-0.991	2.708	0.41	0.39	...
090306245	090306C	< 2.198	0.877 ± 0.076	27.904 ± 14.857	-7.727	38.866	0.59	0.45	...
090307167	090307B	< 5.470	1.476 ± 0.128	29.440 ± 1.810	-8.042	38.768	0.87	0.54	...
090308734	090308B	0.010 ± 0.004	0.004 ± 0.001	1.664 ± 0.286	-1.146	2.174	0.49	0.21	...
090309767	090309B	1.183 ± 0.313	0.620 ± 0.054	56.513 ± 5.146	-2.549	83.896	0.41	0.22	...
090310189	090310A	0.502 ± 0.108	0.219 ± 0.019	116.930 ± 1.056	-11.521	143.982	0.57	0.25	...
090316311	090316A	< 0.099	0.019 ± 0.002	10.240 ± 1.557	-14.797	5.581	0.76	0.50	...
090319622	090319A	< 0.884	0.219 ± 0.019	54.785 ± 2.202	-25.649	69.121	0.59	0.32	...
090320045	090320C	0.794 ± 0.204	0.369 ± 0.032	2.368 ± 0.272	-3.288	1.432	0.86	0.40	...
090320418	090320A	1.924 ± 0.269	0.877 ± 0.076	7.936 ± 1.296	-5.600	10.240	0.94	0.43	...
090320801	090320B	< 0.755	0.155 ± 0.013	29.184 ± 4.536	-14.960	43.108	0.71	0.29	...
090323002	090323A	0.103 ± 0.070	0.055 ± 0.005	135.170 ± 1.448	-6.138	161.460	0.14	0.07	3.57*
090326633	090326A	< 0.313	0.092 ± 0.008	16.128 ± 3.208	-17.203	14.875	0.55	0.36	...
090327404	090327A	0.892 ± 0.612	0.620 ± 0.054	14.080 ± 1.379	-3.014	22.330	0.24	0.16	...
090328401	090328A	< 0.040	0.014 ± 0.001	61.697 ± 1.810	-26.139	91.670	0.20	0.15	0.736*
090328713	090328B	0.004 ± 0.001	0.002 ± 0.001	0.192 ± 1.032	-0.160	0.224	0.49	0.27	...
090330279	090330A	< 0.442	0.155 ± 0.013	73.473 ± 1.717	-51.969	38.580	0.17	0.15	...
090331681	090331A	0.042 ± 0.014	0.023 ± 0.002	0.832 ± 0.143	-0.474	1.183	0.75	0.42	...
090403314	090403A	1.350 ± 0.665	0.738 ± 0.064	14.848 ± 1.846	-9.658	19.874	0.50	0.27	...
090405663	090405A	0.044 ± 0.022	0.027 ± 0.002	0.448 ± 1.498	-0.285	0.608	0.66	0.41	...

Continued on Next Page...

TABLE 2 – Continued

Trigger ID	GRB Name	$\Delta t_{\rm min}$ (s)	$\Delta t_{\rm S/N}$ (s)	T_{90} (s)	$T_{100}^{\rm start}$ (s)	$T_{100}^{\rm stop}$ (s)	$\sigma_{X,t_{\rm min}}$	$\sigma_{X,t_{\rm S/N}}$	z
090409288	090409A	4.008 ± 1.319	2.482 ± 0.215	30.337 ± 2.796	-24.130	10.131	0.80	0.49	...
090411838	090411A	< 0.154	0.033 ± 0.003	21.501 ± 3.237	-4.835	32.144	0.54	0.37	...
090411991	090411B	0.214 ± 0.041	0.130 ± 0.011	14.336 ± 1.086	-4.904	22.160	0.59	0.36	...
090412061	090412A	< 0.741	0.369 ± 0.032	0.896 ± 0.264	-1.275	0.512	0.82	0.98	...
090413122	090413A	0.128 ± 0.070	0.092 ± 0.008	32.513 ± 4.360	-27.634	26.316	0.52	0.38	...
090418816	090418C	0.061 ± 0.009	0.027 ± 0.002	0.320 ± 0.405	-0.222	0.414	0.95	0.43	...
090419997	090419B	0.885 ± 0.705	0.522 ± 0.045	166.915 ± 11.723	-65.793	183.828	0.24	0.14	...
090422150	090422A	0.304 ± 0.114	0.184 ± 0.016	9.216 ± 0.362	-5.082	13.226	0.78	0.47	...
090423330	090423A	1.177 ± 0.592	0.620 ± 0.054	7.168 ± 2.415	-9.440	4.808	0.63	0.33	8.1
090424592	090424A	< 0.036	0.008 ± 0.001	14.144 ± 0.264	-4.512	21.506	0.21	0.06	0.544
090425377	090425A	0.294 ± 0.040	0.110 ± 0.010	75.393 ± 2.450	-3.087	100.937	0.41	0.15	...
090426066	090426B	0.407 ± 0.175	0.261 ± 0.023	16.128 ± 5.152	-9.779	22.299	0.70	0.45	...
090426690	090426C	0.169 ± 0.086	0.130 ± 0.011	7.488 ± 2.496	-4.713	10.023	0.24	0.19	...
090427644	090427B	< 1.669	0.522 ± 0.045	1.024 ± 0.362	-2.301	-0.261	0.75	1.00	...
090427688	090427C	< 1.316	0.261 ± 0.023	12.288 ± 1.280	-7.111	17.327	0.60	0.37	...
090428441	090428A	0.103 ± 0.056	0.046 ± 0.004	3.968 ± 1.506	-2.160	5.760	0.43	0.19	...
090428552	090428B	1.166 ± 0.181	0.439 ± 0.038	31.489 ± 11.846	-24.161	38.484	0.42	0.16	...
090429530	090429C	1.343 ± 0.336	0.620 ± 0.054	14.336 ± 4.007	-9.664	18.832	0.65	0.30	...
090429753	090429D	< 0.077	0.023 ± 0.002	0.640 ± 0.466	-0.509	0.765	0.48	0.34	...
090502777	090502A	0.247 ± 0.065	0.130 ± 0.011	66.048 ± 1.619	-12.712	74.461	0.59	0.31	...
090509215	090509A	< 0.555	0.184 ± 0.016	283.844 ± 2.463	-26.945	296.632	0.67	0.57	...
090510016	090510A	0.005 ± 0.001	0.002 ± 0.001	0.960 ± 0.138	-0.523	1.387	0.66	0.29	0.903
090510325	090510B	< 2.938	0.877 ± 0.076	7.424 ± 1.717	-4.701	10.065	0.91	0.50	...
090511684	090511A	< 0.596	0.219 ± 0.019	7.616 ± 1.605	-5.250	9.950	0.52	0.39	...
090513916	090513A	< 3.891	1.043 ± 0.090	25.280 ± 7.146	-13.438	36.869	0.43	0.32	...
090513941	090513B	3.709 ± 1.682	2.482 ± 0.215	11.776 ± 2.064	-9.677	13.725	0.70	0.47	...
090514006	090514A	0.689 ± 0.131	0.261 ± 0.023	43.521 ± 1.739	-21.364	65.240	0.47	0.18	...
090514726	090514B	< 0.190	0.055 ± 0.005	2.240 ± 0.286	-1.749	2.709	0.45	0.21	...
090514734	090514C	1.021 ± 0.189	0.522 ± 0.045	54.401 ± 4.077	-29.469	68.451	0.37	0.19	...
090516137	090516B	0.683 ± 0.300	0.369 ± 0.032	118.018 ± 4.028	-30.772	141.508	0.28	0.15	...
090516353	090516A	0.415 ± 0.185	0.261 ± 0.023	123.074 ± 2.896	-36.097	123.449	0.41	0.26	4.109
090516853	090516C	0.331 ± 0.099	0.155 ± 0.013	14.464 ± 3.093	-7.258	21.518	0.46	0.22	...
090518080	090518A	0.479 ± 0.158	0.261 ± 0.023	2.048 ± 0.410	-1.658	2.422	0.64	0.35	...
090518244	090518B	0.279 ± 0.064	0.130 ± 0.011	6.784 ± 1.000	-3.744	9.748	0.56	0.26	...
090519462	090519B	< 0.652	0.155 ± 0.013	91.329 ± 3.692	-27.530	117.668	0.73	0.39	...
090519881	090519A	< 0.934	0.369 ± 0.032	74.177 ± 5.177	-21.539	109.724	0.63	0.57	3.85
090520832	090520B	0.354 ± 0.062	0.184 ± 0.016	0.768 ± 0.834	-0.825	0.703	1.03	0.54	...
090520850	090520C	< 0.171	0.039 ± 0.003	3.776 ± 0.923	-2.261	5.259	0.59	0.27	...
090520876	090520D	1.219 ± 0.181	0.369 ± 0.032	30.657 ± 0.859	-22.112	15.269	0.35	0.11	...
090522344	090522A	0.104 ± 0.046	0.065 ± 0.006	20.288 ± 6.262	-14.911	25.447	0.56	0.35	...
090524346	090524A	< 0.383	0.092 ± 0.008	54.337 ± 0.870	-13.415	77.299	0.24	0.10	...
090528173	090528A	< 0.994	0.439 ± 0.038	35.905 ± 2.187	-24.522	46.919	0.17	0.18	...
090528516	090528B	0.163 ± 0.047	0.065 ± 0.006	79.041 ± 1.088	-25.734	116.538	0.22	0.09	...
090529310	090529B	< 0.762	0.219 ± 0.019	3.072 ± 0.362	-2.039	4.081	0.80	0.37	...
090529564	090529C	< 0.049	0.014 ± 0.001	9.853 ± 0.179	-4.389	13.126	0.29	0.13	...
090530760	090530B	< 3.443	0.620 ± 0.054	127.554 ± 1.319	-2.343	159.632	0.45	0.09	...
090531775	090531B	0.049 ± 0.012	0.027 ± 0.002	0.768 ± 0.231	-0.377	1.151	0.94	0.52	...
090602564	090602A	< 0.994	0.261 ± 0.023	20.736 ± 7.209	-11.808	29.010	0.51	0.44	...
090606471	090606A	< 7.550	1.755 ± 0.152	8.064 ± 1.262	-5.274	10.766	0.93	0.79	...
090608052	090608A	< 2.164	0.439 ± 0.038	21.504 ± 2.290	-27.072	15.712	0.70	0.36	...
090610648	090610A	0.422 ± 0.150	0.219 ± 0.019	6.144 ± 8.136	-7.139	5.079	0.53	0.27	...
090610723	090610B	1.210 ± 0.545	0.738 ± 0.064	144.896 ± 3.367	-5.092	213.677	0.61	0.37	...
090610883	090610C	< 2.689	0.620 ± 0.054	7.424 ± 1.639	-6.493	8.273	0.81	0.46	...
090612619	090612A	0.785 ± 0.100	0.261 ± 0.023	42.433 ± 2.888	-36.096	10.313	0.55	0.18	...
090616157	090616A	0.297 ± 0.084	0.155 ± 0.013	1.152 ± 1.168	-0.757	1.534	0.73	0.38	...
090617208	090617A	0.015 ± 0.003	0.007 ± 0.001	0.192 ± 0.143	-0.160	0.224	0.54	0.24	...
090618353	090618A	0.284 ± 0.205	0.155 ± 0.013	112.386 ± 1.086	-2.620	146.845	0.09	0.05	0.54
090620400	090620A	0.279 ± 0.034	0.078 ± 0.007	13.568 ± 0.724	-6.208	20.776	0.23	0.06	...

Continued on Next Page...

TABLE 2 – Continued

Trigger ID	GRB Name	$\Delta t_{\rm min}$ (s)	$\Delta t_{\rm S/N}$ (s)	T_{90} (s)	$T_{100}^{\rm start}$ (s)	$T_{100}^{\rm stop}$ (s)	$\sigma_{X,t_{\rm min}}$	$\sigma_{X,t_{\rm S/N}}$	z
090620901	090620B	< 0.529	0.155 ± 0.013	0.960 ± 0.272	-1.051	0.859	0.80	0.55	...
090621185	090621A	1.144 ± 0.486	0.522 ± 0.045	106.754 ± 14.373	-15.613	157.306	0.23	0.11	...
090621417	090621C	< 0.311	0.078 ± 0.007	27.008 ± 6.136	-17.122	36.608	0.65	0.32	...
090621447	090621D	< 0.344	0.184 ± 0.016	26.112 ± 5.655	-13.187	38.751	0.48	0.52	...
090621922	090621B	0.022 ± 0.004	0.010 ± 0.001	0.384 ± 1.032	-0.316	0.447	0.85	0.37	...
090623107	090623A	< 0.061	0.014 ± 0.001	47.105 ± 2.573	-11.502	69.509	0.54	0.32	...
090623913	090623B	< 0.717	0.130 ± 0.011	7.168 ± 3.114	-3.450	10.440	0.70	0.22	...
090625234	090625A	2.531 ± 1.209	1.755 ± 0.152	14.336 ± 0.923	-10.688	17.808	0.55	0.38	...
090625560	090625B	< 4.831	0.620 ± 0.054	11.776 ± 2.673	-7.373	16.029	1.22	0.23	...
090626189	090626A	< 0.117	0.014 ± 0.001	48.897 ± 2.828	-14.397	74.564	0.44	0.11	...
090629543	090629A	< 1.271	0.522 ± 0.045	20.480 ± 4.762	-19.656	21.099	0.81	0.72	...
090630311	090630A	< 0.415	0.110 ± 0.010	2.880 ± 0.320	-2.066	3.666	0.49	0.21	...
090701225	090701A	0.562 ± 0.079	0.184 ± 0.016	4.160 ± 0.692	-5.579	2.699	0.90	0.30	...
090703329	090703A	0.819 ± 0.473	0.522 ± 0.045	8.960 ± 1.864	-6.739	11.091	0.48	0.31	...
090704242	090704A	5.503 ± 2.061	2.482 ± 0.215	69.889 ± 5.724	-27.225	90.872	0.36	0.16	...
090704783	090704B	1.582 ± 0.496	0.620 ± 0.054	19.456 ± 2.064	-11.431	27.255	0.50	0.19	...
090706283	090706A	0.405 ± 0.164	0.261 ± 0.023	119.810 ± 5.030	-35.841	86.191	0.61	0.39	...
090708152	090708A	< 2.938	0.738 ± 0.064	21.248 ± 3.167	-9.901	27.906	0.60	0.30	...
090709630	090709B	< 1.214	0.310 ± 0.027	22.272 ± 9.230	-1.837	33.779	0.41	0.19	...
090711850	090711A	0.103 ± 0.038	0.078 ± 0.007	51.969 ± 2.560	-26.687	76.714	0.55	0.42	...
090712160	090712A	< 8.746	1.755 ± 0.152	87.041 ± 7.799	-65.537	53.241	0.42	0.23	...
090713020	090713A	2.019 ± 0.648	1.043 ± 0.090	82.817 ± 2.318	-21.558	124.998	0.30	0.16	...
090717034	090717A	< 0.098	0.039 ± 0.003	65.537 ± 1.557	-1.218	98.373	0.12	0.10	...
090717111	090717B	< 0.315	0.092 ± 0.008	0.384 ± 0.181	-0.316	0.383	1.04	0.67	...
090718720	090718A	< 2.821	0.877 ± 0.076	76.481 ± 3.416	-27.975	101.277	0.60	0.47	...
090718762	090718B	0.418 ± 0.028	0.065 ± 0.006	23.744 ± 0.802	-8.363	38.879	0.34	0.05	...
090719063	090719A	0.479 ± 0.037	0.092 ± 0.008	11.392 ± 0.466	-4.749	17.897	0.22	0.04	...
090720276	090720A	< 1.190	0.130 ± 0.011	3.712 ± 0.724	-2.931	4.468	0.82	0.13	...
090720710	090720B	0.002 ± 0.001	0.001 ± 0.001	10.752 ± 1.056	-5.692	15.788	0.50	0.29	...
090725838	090725A	1.985 ± 0.358	0.620 ± 0.054	13.760 ± 1.229	-10.139	17.243	0.68	0.21	...
090726218	090726B	0.165 ± 0.038	0.092 ± 0.008	7.680 ± 0.724	-1.446	9.536	0.25	0.14	...
090730608	090730A	0.143 ± 0.027	0.078 ± 0.007	9.088 ± 1.680	-6.167	11.903	0.71	0.39	...
090802235	090802A	0.015 ± 0.002	0.007 ± 0.001	0.128 ± 0.091	-0.128	0.128	0.72	0.32	...
090802666	090802B	< 1.929	0.877 ± 0.076	27.520 ± 6.192	-14.390	40.374	0.38	0.28	...
090804940	090804A	< 0.406	0.065 ± 0.006	5.568 ± 0.362	-0.619	8.944	0.33	0.07	...
090805622	090805A	0.595 ± 0.235	0.369 ± 0.032	46.592 ± 2.318	-23.769	68.925	0.50	0.31	...
090807832	090807B	0.058 ± 0.021	0.033 ± 0.003	17.920 ± 2.757	-10.150	25.510	0.41	0.23	...
090809978	090809B	0.954 ± 0.016	0.130 ± 0.011	11.008 ± 0.320	-4.365	17.525	0.45	0.06	...
090810659	090810A	2.044 ± 0.777	0.877 ± 0.076	123.458 ± 1.747	-26.686	146.130	0.29	0.12	...
090810781	090810B	1.946 ± 1.098	1.241 ± 0.108	62.977 ± 11.865	-2.990	94.598	0.26	0.17	...
090811696	090811A	< 0.355	0.078 ± 0.007	14.848 ± 1.145	-7.610	21.922	1.10	0.50	...
090813174	090813A	< 0.053	0.011 ± 0.001	7.552 ± 0.362	-3.360	11.644	0.48	0.19	...
090814368	090814C	< 0.010	0.005 ± 0.001	0.192 ± 0.143	-0.160	0.224	0.48	0.54	...
090814950	090814D	< 0.454	0.092 ± 0.008	108.610 ± 8.816	-21.960	111.618	0.56	0.29	...
090815300	090815A	0.049 ± 0.021	0.033 ± 0.003	48.385 ± 1.086	-8.847	70.980	0.16	0.10	...
090815438	090815B	0.829 ± 0.049	0.155 ± 0.013	56.321 ± 18.461	-36.865	47.544	0.53	0.10	...
090815946	090815D	2.252 ± 0.663	1.476 ± 0.128	212.992 ± 1.950	-21.832	257.171	0.51	0.34	...
090817036	090817A	1.108 ± 0.162	0.439 ± 0.038	52.417 ± 10.657	-27.050	65.174	0.60	0.24	...
090819607	090819A	0.004 ± 0.002	0.003 ± 0.001	0.192 ± 0.202	-0.224	0.160	0.90	0.55	...
090820027	090820A	< 0.365	0.065 ± 0.006	12.416 ± 0.181	28.363	49.691	0.15	0.03	...
090820509	090820B	0.047 ± 0.027	0.033 ± 0.003	15.296 ± 4.610	-2.054	22.700	0.34	0.24	...
090823133	090823B	0.639 ± 0.273	0.439 ± 0.038	63.361 ± 4.545	-53.249	36.723	0.55	0.38	...
090824918	090824A	5.731 ± 0.883	2.087 ± 0.181	59.905 ± 10.014	-30.634	84.973	0.65	0.24	...
090826068	090826A	0.105 ± 0.048	0.078 ± 0.007	8.704 ± 2.862	-5.334	11.978	0.45	0.34	...
090828099	090828A	< 0.450	0.092 ± 0.008	68.417 ± 3.167	-30.773	86.191	0.25	0.10	...
090829672	090829A	0.044 ± 0.017	0.023 ± 0.002	67.585 ± 2.896	-5.623	97.098	0.12	0.06	...
090829702	090829B	1.405 ± 0.501	0.738 ± 0.064	101.633 ± 2.290	-16.818	153.903	0.30	0.16	...
090831317	090831A	0.015 ± 0.004	0.008 ± 0.001	39.424 ± 0.572	-0.301	58.829	0.49	0.26	...

Continued on Next Page...

TABLE 2 – Continued

Trigger ID	GRB Name	$\Delta t_{\rm min}$ (s)	$\Delta t_{\rm S/N}$ (s)	T_{90} (s)	$T_{100}^{\rm start}$ (s)	$T_{100}^{\rm stop}$ (s)	$\sigma_{X,t_{\rm min}}$	$\sigma_{X,t_{\rm S/N}}$	z
090902401	090902A	< 0.420	0.078 ± 0.007	3.200 ± 1.797	-3.888	2.128	0.84	0.29	...
090902462	090902B	0.009 ± 0.003	0.005 ± 0.001	19.328 ± 0.286	-0.573	31.691	0.11	0.07	1.822*
090904058	090904B	0.278 ± 0.127	0.155 ± 0.013	56.065 ± 1.846	-21.726	65.727	0.35	0.19	...
090904581	090904C	0.428 ± 0.174	0.261 ± 0.023	38.401 ± 3.093	-21.379	55.037	0.83	0.51	...
090907017	090907A	0.289 ± 0.159	0.219 ± 0.019	39.489 ± 4.443	-32.220	46.345	0.76	0.58	...
090907808	090907B	0.038 ± 0.011	0.023 ± 0.002	0.832 ± 0.320	-0.666	0.991	0.46	0.28	...
090908314	090908A	< 1.285	0.261 ± 0.023	67.329 ± 4.700	-59.137	36.253	0.69	0.34	...
090908341	090908B	< 1.369	0.219 ± 0.019	36.864 ± 0.923	-18.329	55.023	0.76	0.45	...
090909487	090909A	6.245 ± 0.444	1.476 ± 0.128	14.336 ± 2.896	-11.200	17.296	0.97	0.23	...
090909854	090909B	< 0.042	0.011 ± 0.001	1.152 ± 2.244	-1.333	0.525	0.62	0.53	...
090910812	090910A	< 0.333	0.110 ± 0.010	53.441 ± 13.334	-7.771	80.939	0.33	0.29	...
090912660	090912A	8.724 ± 0.682	2.482 ± 0.215	147.651 ± 9.718	-4.926	179.624	0.65	0.18	...
090915650	090915A	< 0.671	0.219 ± 0.019	76.609 ± 1.559	-28.987	113.489	0.41	0.29	...
090917661	090917A	0.438 ± 0.288	0.261 ± 0.023	26.624 ± 1.134	-13.373	39.601	0.52	0.31	...
090920035	090920A	< 1.316	0.261 ± 0.023	26.624 ± 1.056	-20.792	31.383	0.50	0.35	...
090922539	090922A	0.383 ± 0.044	0.130 ± 0.011	87.041 ± 0.810	-2.671	102.648	0.29	0.10	...
090922605	090922B	0.200 ± 0.042	0.110 ± 0.010	52.736 ± 1.810	-26.293	78.620	0.98	0.54	...
090924625	090924A	0.053 ± 0.015	0.023 ± 0.002	0.352 ± 0.101	-0.237	0.463	0.65	0.29	...
090925389	090925A	0.806 ± 0.447	0.522 ± 0.045	25.472 ± 3.525	-3.385	38.115	0.29	0.19	...
090926181	090926A	0.029 ± 0.004	0.014 ± 0.001	13.760 ± 0.286	-0.782	22.747	0.12	0.05	2.1062*
090926914	090926B	< 2.353	0.620 ± 0.054	55.553 ± 7.638	-15.799	84.173	0.24	0.13	1.24
090927422	090927A	0.167 ± 0.063	0.092 ± 0.008	0.512 ± 0.231	-0.446	0.573	0.93	0.52	1.37
090928646	090928A	< 1.026	0.219 ± 0.019	15.616 ± 2.611	-7.994	15.718	0.55	0.23	...
090929190	090929A	0.046 ± 0.021	0.023 ± 0.002	6.174 ± 1.298	-3.060	9.260	0.44	0.22	...
091002685	091002A	0.403 ± 0.109	0.261 ± 0.023	2.752 ± 3.089	-2.712	2.768	0.74	0.48	...
091003191	091003A	0.041 ± 0.011	0.023 ± 0.002	20.224 ± 0.362	-0.688	31.057	0.40	0.23	0.8969*
091005679	091005A	< 1.041	0.310 ± 0.027	6.976 ± 0.572	-8.133	5.787	0.69	0.47	...
091010113	091010A	0.017 ± 0.011	0.011 ± 0.001	5.952 ± 0.143	-1.220	9.056	0.15	0.10	...
091012783	091012A	< 0.019	0.005 ± 0.001	0.704 ± 2.499	-0.350	1.049	0.68	0.43	...
091015129	091015B	< 1.915	0.439 ± 0.038	3.840 ± 0.590	-4.205	3.437	1.12	0.42	...
091017861	091017A	< 1.783	0.219 ± 0.019	2.624 ± 0.462	-2.133	3.081	1.50	0.34	...
091017985	091017B	3.226 ± 0.642	1.476 ± 0.128	44.800 ± 3.367	-23.922	62.094	0.66	0.30	...
091018957	091018B	0.087 ± 0.018	0.046 ± 0.004	0.192 ± 0.286	-0.160	0.224	0.97	0.51	...
091019750	091019A	0.030 ± 0.003	0.014 ± 0.001	0.208 ± 0.172	-0.215	0.199	0.94	0.43	...
091020900	091020A	< 1.339	0.261 ± 0.023	24.256 ± 7.973	-15.599	32.639	0.37	0.12	1.71
091020977	091020B	< 0.029	0.010 ± 0.001	37.505 ± 0.905	-17.457	57.168	0.37	0.34	...
091023021	091023A	0.800 ± 0.085	0.369 ± 0.032	6.528 ± 1.857	-3.683	9.291	0.82	0.38	...
091024372	091024A	< 1.179	0.310 ± 0.027	93.954 ± 5.221	-19.493	137.387	0.41	0.27	1.092
091024380	091024A	< 2.404	0.738 ± 0.064	450.569 ± 2.360	-13.943	452.617	0.31	0.17	...
091026485	091026B	1.152 ± 0.240	0.620 ± 0.054	3.328 ± 0.779	-2.547	4.093	0.78	0.42	...
091026550	091026A	< 1.236	0.439 ± 0.038	8.960 ± 1.379	-9.555	8.275	0.81	0.63	...
091030613	091030B	0.036 ± 0.016	0.023 ± 0.002	19.200 ± 0.871	-8.928	29.280	0.56	0.36	...
091030828	091030A	0.087 ± 0.038	0.055 ± 0.005	98.050 ± 4.128	-30.675	120.306	0.26	0.16	...
091031500	091031A	< 0.034	0.011 ± 0.001	33.921 ± 0.462	-1.857	52.076	0.36	0.30	...
091101143	091101A	0.069 ± 0.024	0.039 ± 0.003	10.688 ± 0.842	-1.578	16.151	0.33	0.19	...
091102607	091102A	< 0.541	0.110 ± 0.010	6.656 ± 3.435	-4.071	9.209	0.74	0.51	...
091103912	091103A	0.329 ± 0.073	0.110 ± 0.010	13.568 ± 6.023	-8.768	18.216	0.36	0.12	...
091106762	091106A	0.059 ± 0.019	0.046 ± 0.004	14.592 ± 16.147	-8.509	20.651	0.19	0.15	...
091107635	091107A	0.485 ± 0.204	0.261 ± 0.023	11.008 ± 10.546	-8.269	13.621	0.48	0.26	...
091109895	091109C	< 0.253	0.039 ± 0.003	30.976 ± 4.580	-20.772	40.838	0.89	0.21	...
091112737	091112A	1.603 ± 0.854	0.738 ± 0.064	24.576 ± 0.923	-12.941	35.933	0.32	0.15	...
091112928	091112B	< 1.100	0.310 ± 0.027	21.184 ± 0.977	-11.256	30.892	0.36	0.27	...
091115177	091115A	< 0.826	0.219 ± 0.019	37.376 ± 2.360	-20.202	54.518	0.74	0.48	...
091117080	091117B	4.017 ± 1.245	2.087 ± 0.181	113.664 ± 2.360	-21.271	118.531	0.60	0.31	...
091120191	091120A	0.096 ± 0.018	0.027 ± 0.002	50.177 ± 2.111	-6.942	67.295	0.28	0.08	...
091122163	091122A	< 0.369	0.092 ± 0.008	1.984 ± 1.925	-2.456	1.504	1.00	0.45	...
091123081	091123B	< 0.851	0.184 ± 0.016	15.552 ± 1.866	-17.688	13.236	0.78	0.34	...
091123298	091123A	0.141 ± 0.038	0.078 ± 0.007	604.491 ± 11.676	-3.840	608.587	0.40	0.22	...

Continued on Next Page...

TABLE 2 – Continued

Trigger ID	GRB Name	$\Delta t_{\rm min}$ (s)	$\Delta t_{\rm S/N}$ (s)	T_{90} (s)	$T_{100}^{\rm start}$ (s)	$T_{100}^{\rm stop}$ (s)	$\sigma_{X,t_{\rm min}}$	$\sigma_{X,t_{\rm S/N}}$	z
091126333	091126A	0.021 ± 0.006	0.011 ± 0.001	0.192 ± 0.091	-0.160	0.224	0.69	0.37	...
091127976	091127A	< 0.103	0.011 ± 0.001	8.701 ± 0.571	-4.304	13.008	0.42	0.07	0.49
091128285	091128A	0.205 ± 0.075	0.110 ± 0.010	87.810 ± 13.662	-25.749	86.635	0.26	0.14	...
091201089	091201A	6.200 ± 0.791	2.951 ± 0.256	12.992 ± 2.010	-14.181	11.649	0.96	0.46	...
091202072	091202B	< 0.898	0.184 ± 0.016	27.648 ± 3.566	-18.704	36.300	0.66	0.47	...
091202219	091202C	< 0.650	0.219 ± 0.019	111.106 ± 3.692	-38.913	116.994	0.42	0.39	...
091207333	091207A	0.035 ± 0.023	0.023 ± 0.002	27.073 ± 0.916	-0.616	40.786	0.49	0.32	...
091208410	091208B	0.151 ± 0.014	0.046 ± 0.004	12.480 ± 5.018	-6.306	18.530	0.46	0.14	1.063
091209001	091209A	< 1.863	0.620 ± 0.054	42.945 ± 8.035	-27.314	48.689	0.25	0.19	...
091215234	091215A	0.825 ± 0.575	0.522 ± 0.045	4.352 ± 0.362	-4.208	4.472	0.53	0.34	...
091219462	091219A	< 0.234	0.092 ± 0.008	8.128 ± 1.866	-4.219	11.939	0.41	0.36	...
091220442	091220A	1.378 ± 0.053	0.310 ± 0.027	18.368 ± 0.590	-2.103	27.824	0.56	0.13	...
091221870	091221A	< 0.437	0.078 ± 0.007	23.040 ± 5.177	-5.261	33.446	0.37	0.15	...
091223191	091223A	0.204 ± 0.034	0.092 ± 0.008	0.576 ± 0.181	-0.544	0.604	0.86	0.39	...
091223511	091223B	< 3.963	1.476 ± 0.128	49.725 ± 1.379	-7.269	74.272	0.32	0.22	...
091224373	091224A	0.057 ± 0.036	0.039 ± 0.003	0.768 ± 0.231	-0.569	0.959	0.68	0.46	...
091227294	091227A	< 0.387	0.078 ± 0.007	21.888 ± 0.889	-9.274	31.423	0.43	0.26	...
091230260	091230B	3.143 ± 1.630	2.087 ± 0.181	62.976 ± 3.874	-26.272	90.204	0.79	0.52	...
091230712	091230C	< 5.208	1.043 ± 0.090	35.137 ± 3.974	-18.021	49.059	0.86	0.29	...
091231206	091231A	1.646 ± 0.328	0.738 ± 0.064	42.561 ± 3.664	-13.320	66.267	0.42	0.19	...
091231540	091231B	< 6.337	1.043 ± 0.090	15.616 ± 2.757	-15.418	15.626	1.27	0.52	...
100101028	100101A	0.338 ± 0.099	0.219 ± 0.019	2.816 ± 0.320	-1.658	3.942	1.01	0.66	...
100101988	100101B	< 0.889	0.184 ± 0.016	1.984 ± 2.049	-1.572	1.952	1.06	0.43	...
100107074	100107A	0.032 ± 0.008	0.019 ± 0.002	0.576 ± 0.465	-0.336	0.812	0.94	0.57	...
100111176	100111A	0.664 ± 0.189	0.310 ± 0.027	19.520 ± 5.367	-20.416	18.428	0.70	0.33	...
100112418	100112A	1.405 ± 0.528	0.877 ± 0.076	23.040 ± 0.572	-15.757	30.093	0.53	0.33	...
100116897	100116A	0.287 ± 0.072	0.130 ± 0.011	102.530 ± 1.485	-11.035	123.266	0.18	0.08	...
100117879	100117A	0.069 ± 0.013	0.033 ± 0.003	0.256 ± 0.834	-0.192	0.320	0.79	0.37	...
100118100	100118A	0.205 ± 0.066	0.110 ± 0.010	9.216 ± 6.720	-5.770	11.434	0.78	0.42	...
100122616	100122A	< 0.171	0.046 ± 0.004	22.528 ± 2.769	-3.783	38.779	0.13	0.06	...
100126460	100126A	0.144 ± 0.062	0.092 ± 0.008	10.624 ± 12.673	-6.541	14.593	0.79	0.50	...
100130729	100130A	< 1.170	0.310 ± 0.027	99.074 ± 3.328	-30.885	105.817	0.32	0.14	...
100130777	100130B	< 1.626	0.310 ± 0.027	86.018 ± 6.988	-30.340	108.120	0.44	0.18	...
100131730	100131A	0.087 ± 0.009	0.033 ± 0.003	3.520 ± 0.453	-1.550	5.454	0.42	0.16	...
100201588	100201A	< 2.151	0.522 ± 0.045	122.114 ± 1.280	-20.185	147.091	0.29	0.15	...
100204024	100204A	1.292 ± 0.273	0.439 ± 0.038	136.195 ± 27.553	-95.234	58.843	0.24	0.08	...
100204566	100204B	< 0.406	0.261 ± 0.023	32.513 ± 2.862	-30.401	18.349	0.67	0.84	...
100204858	100204C	0.140 ± 0.051	0.092 ± 0.008	1.920 ± 2.375	-1.590	2.230	0.91	0.60	...
100205490	100205B	< 1.480	0.261 ± 0.023	14.848 ± 2.290	-8.378	21.154	0.75	0.31	...
100206563	100206A	< 0.017	0.005 ± 0.001	0.128 ± 0.091	-0.128	0.128	0.37	0.25	...
100207665	100207A	< 13.736	2.951 ± 0.256	15.360 ± 3.874	-10.419	20.147	1.11	0.48	...
100207721	100207B	4.675 ± 2.569	2.951 ± 0.256	17.728 ± 6.492	-17.995	17.267	0.72	0.45	...
100208386	100208A	< 0.156	0.092 ± 0.008	0.192 ± 0.264	-0.160	0.224	0.79	1.00	...
100210101	100210A	0.945 ± 0.271	0.522 ± 0.045	29.184 ± 5.655	-19.253	33.271	0.47	0.26	...
100211440	100211A	0.468 ± 0.256	0.219 ± 0.019	21.376 ± 0.923	-9.949	32.557	0.20	0.09	...
100212550	100212B	0.235 ± 0.066	0.130 ± 0.011	3.773 ± 0.270	-1.871	5.649	0.58	0.32	...
100212588	100212A	0.396 ± 0.109	0.219 ± 0.019	2.496 ± 0.202	-1.692	3.293	0.74	0.41	...
100216422	100216A	< 0.045	0.010 ± 0.001	0.192 ± 0.143	-0.160	0.224	0.78	0.57	...
100218194	100218A	3.673 ± 2.832	2.482 ± 0.215	29.185 ± 5.813	-17.989	38.912	0.46	0.31	...
100219026	100219B	< 2.169	0.877 ± 0.076	59.712 ± 4.955	-24.571	76.919	0.46	0.43	...
100221368	100221A	4.651 ± 0.557	1.476 ± 0.128	23.552 ± 1.032	-13.815	31.852	0.72	0.23	...
100223110	100223A	< 0.022	0.007 ± 0.001	0.256 ± 0.091	-0.192	0.320	0.45	0.29	...
100224112	100224B	0.125 ± 0.034	0.065 ± 0.006	67.329 ± 6.988	-30.345	88.812	0.34	0.18	...
100225115	100225A	< 0.277	0.046 ± 0.004	12.992 ± 1.925	-3.059	19.137	0.54	0.30	...
100225249	100225B	< 5.244	2.482 ± 0.215	32.000 ± 20.419	-14.232	47.208	0.75	0.78	...
100225580	100225C	0.125 ± 0.056	0.065 ± 0.006	6.400 ± 1.086	-3.680	9.056	0.19	0.10	...
100225703	100225D	0.071 ± 0.023	0.046 ± 0.004	4.480 ± 1.431	-3.370	5.546	0.74	0.48	...
100228544	100228A	1.399 ± 0.517	0.620 ± 0.054	67.072 ± 4.720	-21.926	98.112	0.65	0.29	...

Continued on Next Page...

TABLE 2 – Continued

Trigger ID	GRB Name	$\Delta t_{\rm min}$ (s)	$\Delta t_{\rm S/N}$ (s)	T_{90} (s)	$T_{100}^{\rm start}$ (s)	$T_{100}^{\rm stop}$ (s)	$\sigma_{X,t_{\rm min}}$	$\sigma_{X,t_{\rm S/N}}$	z
100228873	100228B	< 1.757	0.439 ± 0.038	8.704 ± 2.318	-6.358	10.954	0.90	0.34	...
100301068	100301A	0.010 ± 0.006	0.007 ± 0.001	0.960 ± 1.002	-1.371	0.539	0.75	0.47	...
100301223	100301B	0.163 ± 0.049	0.092 ± 0.008	26.625 ± 1.431	-13.438	39.270	0.61	0.35	...
100304004	100304A	< 1.076	0.310 ± 0.027	181.507 ± 21.682	-30.590	247.104	0.65	0.49	...
100304534	100304B	0.971 ± 0.268	0.522 ± 0.045	19.008 ± 2.782	-18.971	19.029	0.47	0.25	...
100306199	100306A	< 4.089	0.738 ± 0.064	7.168 ± 2.064	-7.904	6.344	1.01	0.61	...
100307928	100307A	1.342 ± 0.669	0.738 ± 0.064	16.128 ± 2.187	-11.059	21.019	0.43	0.23	...
100311518	100311A	< 4.290	0.877 ± 0.076	9.024 ± 1.042	-1.568	11.240	1.11	0.40	...
100313288	100313A	< 1.788	0.184 ± 0.016	12.864 ± 2.099	-9.186	16.406	0.97	0.16	...
100313509	100313B	6.269 ± 0.384	2.087 ± 0.181	34.048 ± 2.996	-15.873	47.782	0.75	0.25	...
100315361	100315A	5.453 ± 1.239	2.482 ± 0.215	35.584 ± 2.290	-22.194	48.610	0.81	0.37	...
100318611	100318A	1.529 ± 0.303	0.877 ± 0.076	18.432 ± 0.923	-10.922	22.050	0.52	0.30	...
100322045	100322A	0.060 ± 0.021	0.033 ± 0.003	37.121 ± 0.231	-14.268	51.435	0.16	0.09	...
100323542	100323A	< 1.659	0.310 ± 0.027	60.673 ± 3.620	-21.511	70.692	0.69	0.25	...
100324172	100324B	< 0.213	0.027 ± 0.002	17.920 ± 2.064	-8.294	27.366	0.39	0.07	...
100325246	100325B	0.582 ± 0.123	0.261 ± 0.023	8.192 ± 1.086	-5.270	10.681	0.67	0.30	...
100325275	100325A	0.100 ± 0.064	0.065 ± 0.006	7.104 ± 1.619	-1.346	10.226	0.42	0.27	...
100326294	100326A	< 0.133	0.046 ± 0.004	5.632 ± 2.064	-8.170	3.070	0.87	0.69	...
100326402	100326B	< 0.451	0.184 ± 0.016	171.011 ± 29.126	-72.705	106.679	0.28	0.26	...
100328141	100328A	< 0.012	0.004 ± 0.001	0.384 ± 0.143	-0.252	0.511	0.80	0.51	...
100330309	100330A	< 0.202	0.078 ± 0.007	10.048 ± 0.318	-3.207	15.066	0.28	0.22	...
100330856	100330B	0.830 ± 0.165	0.310 ± 0.027	5.120 ± 0.453	-3.686	6.502	0.82	0.31	...
100401297	100401A	< 0.575	0.092 ± 0.008	92.416 ± 4.291	-28.449	102.759	0.84	0.29	...
100406758	100406A	0.589 ± 0.112	0.310 ± 0.027	5.888 ± 2.919	-4.199	7.503	0.84	0.44	...
100410356	100410A	1.862 ± 0.586	1.241 ± 0.108	9.728 ± 2.202	-10.707	8.635	0.78	0.52	...
100410740	100410B	< 0.274	0.046 ± 0.004	22.016 ± 4.700	-11.930	31.850	0.92	0.41	...
100411516	100411A	0.053 ± 0.019	0.033 ± 0.003	0.512 ± 0.231	-0.318	0.701	0.89	0.55	...
100413732	100413A	0.579 ± 0.169	0.369 ± 0.032	179.651 ± 2.817	-18.053	193.922	0.62	0.40	...
100414097	100414A	0.026 ± 0.007	0.014 ± 0.001	26.497 ± 2.073	-11.269	41.427	0.18	0.09	...
100417166	100417A	0.008 ± 0.004	0.005 ± 0.001	0.192 ± 0.091	-0.160	0.224	0.69	0.44	...
100417789	100417B	4.668 ± 0.775	2.482 ± 0.215	52.545 ± 1.856	-14.351	76.018	0.92	0.49	...
100420008	100420B	0.796 ± 0.222	0.369 ± 0.032	20.288 ± 0.405	-9.855	29.691	0.39	0.18	...
100421917	100421A	< 1.544	0.369 ± 0.032	47.489 ± 10.849	-30.454	30.321	0.55	0.28	...
100423244	100423B	< 0.310	0.046 ± 0.004	16.512 ± 2.226	-6.579	25.100	0.65	0.24	...
100424729	100424B	0.470 ± 0.127	0.261 ± 0.023	175.107 ± 1.493	-29.411	163.199	0.66	0.36	...
100424876	100424C	< 0.361	0.078 ± 0.007	169.987 ± 3.557	-15.379	208.994	0.50	0.21	...
100427356	100427A	< 0.500	0.130 ± 0.011	12.544 ± 7.389	-11.075	11.246	0.52	0.26	...
100429999	100429A	< 5.330	0.620 ± 0.054	25.024 ± 6.582	-25.154	24.635	0.90	0.16	...
100502356	100502A	< 0.255	0.078 ± 0.007	95.810 ± 2.382	-14.519	124.391	0.42	0.31	...
100503554	100503A	< 0.093	0.023 ± 0.002	129.602 ± 10.230	-14.648	169.384	0.36	0.26	...
100504806	100504A	7.929 ± 0.893	2.951 ± 0.256	16.512 ± 1.810	-6.963	25.871	0.90	0.34	...
100506653	100506A	< 2.295	0.522 ± 0.045	21.376 ± 1.891	-18.525	23.768	0.42	0.21	...
100507577	100507A	0.578 ± 0.222	0.369 ± 0.032	44.033 ± 5.221	-17.746	65.012	0.26	0.17	...
100510810	100510A	< 5.659	0.877 ± 0.076	31.169 ± 4.017	-18.725	43.284	0.86	0.19	...
100511035	100511A	0.082 ± 0.017	0.027 ± 0.002	42.433 ± 1.478	-19.539	64.452	0.34	0.12	...
100513879	100513B	0.376 ± 0.150	0.219 ± 0.019	11.136 ± 1.145	-6.288	15.840	0.23	0.14	...
100515467	100515A	< 0.193	0.055 ± 0.005	10.624 ± 1.431	-5.901	15.233	0.19	0.09	...
100516369	100516A	< 0.061	0.016 ± 0.001	2.112 ± 1.134	-2.971	1.228	0.94	0.69	...
100516396	100516B	0.084 ± 0.046	0.055 ± 0.005	0.640 ± 0.487	-0.893	0.381	0.86	0.56	...
100517072	100517B	0.069 ± 0.036	0.039 ± 0.003	55.808 ± 1.810	-4.270	81.104	0.22	0.12	...
100517132	100517C	0.693 ± 0.393	0.522 ± 0.045	19.840 ± 3.620	-10.333	29.149	0.52	0.39	...
100517154	100517D	< 0.186	0.039 ± 0.003	30.464 ± 0.810	-15.333	45.282	0.46	0.20	...
100517243	100517E	< 1.080	0.184 ± 0.016	29.632 ± 4.482	-28.161	30.782	0.85	0.24	...
100517639	100517F	< 0.219	0.039 ± 0.003	5.440 ± 0.604	-3.461	7.365	0.56	0.23	...
100519204	100519A	0.961 ± 0.465	0.522 ± 0.045	62.913 ± 3.929	-21.585	89.748	0.18	0.10	...
100522157	100522A	< 0.090	0.019 ± 0.002	35.326 ± 0.715	-2.547	52.905	0.58	0.22	...
100525744	100525A	0.045 ± 0.011	0.023 ± 0.002	1.472 ± 1.974	-1.119	1.816	0.85	0.44	...
100527795	100527A	< 0.230	0.065 ± 0.006	184.579 ± 3.238	-92.674	120.498	0.49	0.30	...

Continued on Next Page...

TABLE 2 – Continued

Trigger ID	GRB Name	$\Delta t_{\rm min}$ (s)	$\Delta t_{\rm S/N}$ (s)	T_{90} (s)	$T_{100}^{\rm start}$ (s)	$T_{100}^{\rm stop}$ (s)	$\sigma_{X,t_{\rm min}}$	$\sigma_{X,t_{\rm S/N}}$	z
100528075	100528A	< 0.428	0.078 ± 0.007	22.464 ± 0.749	-11.378	33.318	0.19	0.07	...
100530737	100530A	0.965 ± 0.403	0.620 ± 0.054	3.328 ± 0.810	-2.675	3.965	0.81	0.52	...
100604287	100604A	0.416 ± 0.223	0.261 ± 0.023	13.440 ± 0.871	-8.957	17.654	0.29	0.18	...
100605774	100605A	1.562 ± 0.310	0.522 ± 0.045	8.192 ± 2.862	-5.085	11.193	0.78	0.26	...
100608382	100608A	0.545 ± 0.173	0.369 ± 0.032	30.208 ± 1.619	-22.606	35.982	0.51	0.34	...
100609783	100609A	< 2.015	0.522 ± 0.045	230.404 ± 8.689	-9.593	236.935	0.25	0.17	...
100612545	100612A	0.024 ± 0.007	0.016 ± 0.001	0.576 ± 0.181	-0.288	0.860	0.64	0.43	...
100612726	100612B	< 0.394	0.065 ± 0.006	8.576 ± 3.210	-3.549	13.485	0.20	0.05	...
100614498	100614B	0.167 ± 0.091	0.110 ± 0.010	172.291 ± 12.447	-149.763	22.975	0.33	0.22	...
100615083	100615A	0.487 ± 0.092	0.184 ± 0.016	37.377 ± 0.979	-2.627	51.172	0.38	0.14	1.398
100619015	100619A	< 0.473	0.130 ± 0.011	96.002 ± 1.319	-29.359	113.681	0.42	0.22	...
100620119	100620A	< 0.944	0.261 ± 0.023	51.841 ± 8.518	-20.497	75.407	0.55	0.36	...
100621452	100621B	< 1.532	0.310 ± 0.027	123.906 ± 5.515	-29.098	141.884	0.60	0.24	...
100621529	100621C	< 0.120	0.033 ± 0.003	1.024 ± 0.202	-0.957	1.083	1.02	0.66	...
100625773	100625A	0.031 ± 0.005	0.010 ± 0.001	0.192 ± 0.143	-0.160	0.224	0.92	0.29	...
100625891	100625B	1.123 ± 0.321	0.738 ± 0.064	29.184 ± 1.086	-16.459	36.065	0.54	0.36	...
100629801	100629A	0.146 ± 0.014	0.055 ± 0.005	0.832 ± 0.373	-0.538	1.119	0.76	0.29	...
100701490	100701B	< 0.004	0.001 ± 0.001	22.016 ± 5.568	-1.790	32.090	0.39	0.33	...
100704149	100704A	0.413 ± 0.105	0.219 ± 0.019	214.404 ± 5.917	-38.145	275.680	0.29	0.15	...
100706693	100706A	< 0.295	0.065 ± 0.006	0.128 ± 0.143	-0.192	0.064	0.76	0.99	...
100707032	100707A	0.665 ± 0.012	0.078 ± 0.007	81.793 ± 1.218	-2.742	113.386	0.44	0.05	...
100709602	100709A	< 1.297	0.261 ± 0.023	100.098 ± 1.527	-23.050	138.079	0.52	0.21	...
100713980	100713B	0.293 ± 0.080	0.130 ± 0.011	7.616 ± 0.529	-4.162	11.038	0.45	0.20	...
100714672	100714A	< 0.387	0.110 ± 0.010	35.584 ± 5.126	-17.988	52.816	1.06	0.75	...
100714686	100714B	0.101 ± 0.015	0.039 ± 0.003	5.632 ± 2.064	-6.122	5.118	0.68	0.26	...
100715477	100715A	1.559 ± 0.529	0.738 ± 0.064	14.848 ± 3.665	-8.378	21.154	0.42	0.20	...
100717372	100717A	< 0.053	0.016 ± 0.001	5.952 ± 1.507	-3.588	8.352	0.85	0.52	...
100717446	100717B	< 0.035	0.011 ± 0.001	2.432 ± 1.356	-1.338	3.502	0.71	0.71	...
100718160	100718B	< 0.093	0.033 ± 0.003	32.640 ± 1.864	-30.925	17.055	0.47	0.41	...
100718796	100718A	6.240 ± 0.521	2.087 ± 0.181	38.656 ± 8.002	-14.291	54.875	0.85	0.28	...
100719311	100719B	0.480 ± 0.069	0.155 ± 0.013	1.600 ± 0.854	-2.120	0.856	0.95	0.31	...
100719825	100719C	0.672 ± 0.303	0.439 ± 0.038	3.072 ± 3.114	-3.861	0.912	0.71	0.46	...
100719989	100719D	< 0.039	0.014 ± 0.001	21.824 ± 1.305	-8.396	34.153	0.12	0.10	...
100722096	100722A	0.057 ± 0.013	0.019 ± 0.002	7.165 ± 1.055	-3.546	10.702	0.30	0.10	...
100722291	100722B	< 0.159	0.092 ± 0.008	1.280 ± 0.905	-1.850	0.698	0.80	0.97	...
100724029	100724A	0.062 ± 0.029	0.039 ± 0.003	114.690 ± 3.238	-11.967	145.144	0.08	0.05	...
100725475	100725B	0.471 ± 0.123	0.261 ± 0.023	146.434 ± 4.971	-23.608	160.881	0.49	0.27	...
100727238	100727A	< 5.037	1.043 ± 0.090	23.808 ± 2.769	-13.678	28.924	0.99	0.36	...
100728095	100728A	< 0.090	0.027 ± 0.002	165.378 ± 2.896	-7.363	207.605	0.17	0.11	1.567
100728439	100728B	0.174 ± 0.105	0.110 ± 0.010	10.240 ± 1.846	-7.117	13.261	0.23	0.14	2.106
100730463	100730A	2.726 ± 0.989	1.241 ± 0.108	63.873 ± 8.776	-25.030	93.749	0.44	0.20	...
100802240	100802A	3.948 ± 0.414	1.476 ± 0.128	28.672 ± 3.167	-16.056	40.977	0.77	0.29	...
100804104	100804A	0.057 ± 0.031	0.039 ± 0.003	6.592 ± 0.771	-2.812	9.953	0.16	0.11	...
100805300	100805B	< 0.042	0.011 ± 0.001	0.064 ± 0.072	-0.128	-0.001	0.88	0.57	...
100805845	100805C	0.928 ± 0.076	0.310 ± 0.027	58.430 ± 6.426	-1.567	87.231	0.60	0.20	...
100810049	100810A	0.169 ± 0.069	0.110 ± 0.010	2.560 ± 1.741	-3.123	1.971	0.59	0.38	...
100811108	100811A	< 0.019	0.004 ± 0.001	0.384 ± 0.091	-0.252	0.511	0.53	0.27	...
100811781	100811B	0.278 ± 0.168	0.184 ± 0.016	78.080 ± 3.840	-91.642	63.738	0.49	0.33	...
100814160	100814A	< 3.299	0.522 ± 0.045	150.530 ± 1.619	-23.817	180.890	0.60	0.14	1.44
100814351	100814B	0.482 ± 0.072	0.184 ± 0.016	7.424 ± 0.923	-4.445	10.321	0.31	0.12	...
100816009	100816B	< 1.320	0.522 ± 0.045	62.401 ± 5.278	-22.266	71.334	0.17	0.16	...
100816026	100816A	< 0.333	0.039 ± 0.003	2.045 ± 0.229	-1.012	3.068	0.42	0.10	0.8049
100819498	100819A	< 3.737	0.738 ± 0.064	12.544 ± 1.810	-11.075	13.879	0.65	0.28	...
100820373	100820A	< 0.056	0.016 ± 0.001	8.960 ± 2.187	-5.203	12.627	0.28	0.17	...
100825287	100825A	0.460 ± 0.055	0.184 ± 0.016	3.328 ± 1.846	-2.931	3.709	0.51	0.20	...
100826957	100826A	< 0.106	0.027 ± 0.002	84.993 ± 0.724	-3.774	120.297	0.14	0.06	...
100827455	100827A	< 0.010	0.004 ± 0.001	0.576 ± 0.389	-0.416	0.732	0.41	0.37	...
100829374	100829B	1.116 ± 0.186	0.369 ± 0.032	94.977 ± 2.767	-11.729	116.467	0.41	0.14	...

Continued on Next Page...

TABLE 2 – Continued

Trigger ID	GRB Name	$\Delta t_{\rm min}$ (s)	$\Delta t_{\rm S/N}$ (s)	T_{90} (s)	$T_{100}^{\rm start}$ (s)	$T_{100}^{\rm stop}$ (s)	$\sigma_{X,t_{\rm min}}$	$\sigma_{X,t_{\rm S/N}}$	z
100829876	100829A	0.043 ± 0.003	0.011 ± 0.001	8.704 ± 0.389	-4.214	13.098	0.51	0.14	...
100831651	100831A	< 2.380	1.476 ± 0.128	40.193 ± 11.986	-23.296	37.078	0.65	0.81	...
100902990	100902B	2.756 ± 0.302	0.738 ± 0.064	22.272 ± 3.338	-15.127	29.171	0.63	0.17	...
100905907	100905B	< 1.443	0.369 ± 0.032	11.520 ± 1.145	-10.310	11.578	0.49	0.23	...
100906576	100906A	< 0.303	0.065 ± 0.006	110.594 ± 2.828	-4.127	134.098	0.17	0.11	1.727
100907751	100907A	< 3.082	0.219 ± 0.019	5.376 ± 2.187	-4.205	6.515	1.84	0.29	...
100910818	100910A	< 0.064	0.011 ± 0.001	13.824 ± 0.724	-5.224	22.001	0.47	0.12	...
100911816	100911A	0.164 ± 0.060	0.110 ± 0.010	5.632 ± 1.999	-3.562	7.678	0.70	0.47	...
100915243	100915B	1.982 ± 0.354	1.043 ± 0.090	7.936 ± 3.367	-11.360	4.480	0.96	0.51	...
100916779	100916A	0.088 ± 0.008	0.039 ± 0.003	12.800 ± 2.111	-4.288	18.880	0.88	0.39	...
100918863	100918A	< 2.057	0.310 ± 0.027	86.017 ± 8.689	-4.822	134.498	0.34	0.08	...
100919884	100919A	0.692 ± 0.429	0.439 ± 0.038	49.601 ± 2.975	-38.401	21.044	0.27	0.17	...
100922625	100922A	0.817 ± 0.190	0.439 ± 0.038	4.352 ± 0.923	-3.184	5.496	0.91	0.49	...
100923844	100923A	< 1.057	0.155 ± 0.013	51.713 ± 5.838	-17.127	72.830	0.62	0.18	...
100924165	100924A	< 0.343	0.078 ± 0.007	9.024 ± 0.362	-5.109	12.841	0.52	0.17	...
100926595	100926A	< 0.582	0.155 ± 0.013	32.256 ± 0.572	-30.222	14.914	0.28	0.19	...
100926694	100926B	2.261 ± 0.423	0.738 ± 0.064	37.888 ± 2.611	-21.894	47.805	0.69	0.23	...
100929235	100929A	1.612 ± 0.282	0.738 ± 0.064	8.192 ± 2.360	-6.365	9.913	0.80	0.37	...
100929315	100929B	0.466 ± 0.084	0.184 ± 0.016	4.608 ± 1.305	-2.797	6.357	0.87	0.35	...
100929916	100929C	0.036 ± 0.006	0.016 ± 0.001	0.320 ± 0.143	-0.286	0.350	0.87	0.39	...
101002279	101002A	< 0.874	0.261 ± 0.023	7.168 ± 2.290	-7.904	6.344	0.82	0.56	...
101003244	101003A	< 0.453	0.092 ± 0.008	9.984 ± 1.448	-6.736	13.124	0.36	0.16	...
101004426	101004A	4.074 ± 1.692	2.087 ± 0.181	161.027 ± 7.836	-141.058	27.355	0.54	0.28	...
101008697	101008A	0.280 ± 0.048	0.130 ± 0.011	8.960 ± 1.846	-6.995	10.835	0.96	0.45	...
101010190	101010A	0.857 ± 0.410	0.522 ± 0.045	65.025 ± 6.165	-31.985	74.648	0.63	0.38	...
101011707	101011A	< 1.419	0.261 ± 0.023	36.352 ± 2.318	-19.047	53.269	1.15	0.64	...
101013412	101013A	< 0.084	0.016 ± 0.001	15.360 ± 0.572	-7.027	20.314	0.51	0.29	...
101014175	101014A	0.048 ± 0.003	0.016 ± 0.001	449.415 ± 1.410	-13.188	450.823	0.23	0.08	...
101015558	101015A	< 0.574	0.130 ± 0.011	500.552 ± 7.408	-18.252	498.504	0.42	0.23	...
101016243	101016A	0.343 ± 0.011	0.065 ± 0.006	3.840 ± 0.362	-1.786	4.205	0.62	0.12	...
101017619	101017B	2.264 ± 0.373	1.241 ± 0.108	47.872 ± 1.950	-24.945	70.775	0.86	0.47	...
101021009	101021A	0.318 ± 0.123	0.184 ± 0.016	120.770 ± 12.237	-51.457	89.321	0.32	0.18	...
101021063	101021B	< 0.108	0.046 ± 0.004	1.536 ± 2.360	-1.235	1.790	0.63	0.55	...
101023951	101023A	0.468 ± 0.025	0.130 ± 0.011	76.801 ± 8.256	-14.464	114.560	0.29	0.08	...
101024486	101024A	0.102 ± 0.040	0.065 ± 0.006	20.224 ± 2.828	-13.908	26.329	0.65	0.42	...
101025146	101025A	0.503 ± 0.184	0.369 ± 0.032	14.336 ± 1.846	-8.896	19.600	0.93	0.69	...
101026034	101026A	0.017 ± 0.010	0.011 ± 0.001	0.256 ± 0.091	-0.256	0.256	0.56	0.36	...
101027230	101027A	0.022 ± 0.007	0.014 ± 0.001	1.344 ± 1.802	-1.947	0.733	0.88	0.54	...
101030664	101030A	< 9.810	2.087 ± 0.181	95.746 ± 4.375	-69.633	54.959	0.79	0.25	...
101031625	101031A	< 0.014	0.007 ± 0.001	0.384 ± 0.462	-0.252	0.511	0.54	0.52	...
101101744	101101A	0.059 ± 0.021	0.039 ± 0.003	3.328 ± 2.862	-3.955	2.685	0.38	0.25	...
101101899	101101B	3.682 ± 1.935	1.755 ± 0.152	31.232 ± 1.619	-20.063	37.382	0.42	0.20	...
101102840	101102A	< 3.802	0.738 ± 0.064	43.520 ± 6.676	-23.251	63.354	0.55	0.33	...
101104810	101104A	< 0.148	0.055 ± 0.005	1.280 ± 0.572	-1.146	1.402	0.54	0.41	...
101107011	101107A	< 0.849	0.310 ± 0.027	375.814 ± 8.444	-31.567	378.118	0.38	0.36	...
101112924	101112A	0.390 ± 0.086	0.155 ± 0.013	9.472 ± 2.996	-8.691	8.243	0.47	0.19	...
101112984	101112B	< 5.121	1.476 ± 0.128	82.944 ± 1.717	-28.320	91.114	0.66	0.28	...
101113483	101113A	< 1.198	0.261 ± 0.023	12.288 ± 0.572	-4.501	18.095	0.66	0.22	...
101116481	101116A	0.088 ± 0.034	0.055 ± 0.005	0.576 ± 0.820	-0.416	0.732	0.97	0.60	...
101117496	101117C	0.470 ± 0.093	0.261 ± 0.023	50.177 ± 1.639	-5.184	73.065	0.45	0.25	...
101119685	101119A	< 0.404	0.078 ± 0.007	0.640 ± 0.607	-0.637	0.637	1.14	0.62	...
101123952	101123A	< 0.077	0.014 ± 0.001	103.938 ± 0.724	-4.124	163.187	0.22	0.07	...
101126198	101126A	< 0.177	0.039 ± 0.003	43.837 ± 1.747	-11.444	65.679	0.14	0.06	...
101127093	101127A	2.765 ± 1.240	1.476 ± 0.128	29.440 ± 4.471	-17.812	40.774	0.83	0.44	...
101127102	101127B	5.416 ± 0.520	1.755 ± 0.152	60.672 ± 7.322	-30.731	85.736	0.65	0.21	...
101128322	101128A	< 1.624	0.310 ± 0.027	8.192 ± 1.493	-6.877	9.401	0.61	0.28	...
101129652	101129A	0.018 ± 0.005	0.011 ± 0.001	0.384 ± 0.143	-0.252	0.511	0.53	0.34	...
101129726	101129B	< 0.024	0.005 ± 0.001	0.576 ± 0.143	-0.346	0.796	0.57	0.35	...

Continued on Next Page...

TABLE 2 – Continued

Trigger ID	GRB Name	$\Delta t_{\rm min}$ (s)	$\Delta t_{\rm S/N}$ (s)	T_{90} (s)	$T_{100}^{\rm start}$ (s)	$T_{100}^{\rm stop}$ (s)	$\sigma_{X,t_{\rm min}}$	$\sigma_{X,t_{\rm S/N}}$	z
101130074	101130B	3.312 ± 0.561	2.087 ± 0.181	4.864 ± 2.769	-4.714	4.958	1.05	0.66	...
101201418	101201A	0.844 ± 0.329	0.261 ± 0.023	112.639 ± 7.455	-33.282	139.026	0.24	0.07	...
101202154	101202A	< 1.458	0.877 ± 0.076	18.432 ± 3.665	-9.130	27.526	0.83	0.95	...
101204343	101204B	0.015 ± 0.003	0.007 ± 0.001	0.128 ± 0.091	-0.128	0.128	0.71	0.32	...
101205309	101205A	< 3.249	0.738 ± 0.064	7.936 ± 5.938	-7.776	8.064	1.06	0.51	...
101206036	101206A	< 0.813	0.130 ± 0.011	34.813 ± 5.837	-17.091	52.161	0.66	0.22	...
101207536	101207A	0.068 ± 0.028	0.046 ± 0.004	61.441 ± 3.727	-6.013	94.134	0.50	0.34	...
101208498	101208B	0.097 ± 0.010	0.033 ± 0.003	2.048 ± 0.951	-1.658	2.422	0.37	0.13	...
101211485	101211A	1.092 ± 0.435	0.522 ± 0.045	13.568 ± 7.030	-9.536	17.448	0.42	0.20	...
101213451	101213A	< 5.901	0.877 ± 0.076	45.057 ± 1.950	-22.252	67.828	0.90	0.19	0.414
101213849	101213B	0.069 ± 0.022	0.046 ± 0.004	6.656 ± 1.145	-5.095	8.185	0.39	0.26	...
101214748	101214A	< 0.038	0.007 ± 0.001	2.240 ± 2.084	-2.517	1.941	0.92	0.58	...
101216721	101216A	< 0.105	0.027 ± 0.002	1.917 ± 0.551	-0.954	2.864	0.20	0.12	...
101219686	101219B	5.386 ± 0.868	2.087 ± 0.181	51.009 ± 1.775	-8.423	72.157	0.56	0.22	0.55
101220576	101220A	7.748 ± 0.937	2.951 ± 0.256	72.449 ± 4.048	-21.684	93.495	0.47	0.18	...
101223834	101223A	< 20.645	2.482 ± 0.215	56.065 ± 5.497	-41.217	42.437	1.44	0.28	...
101224227	101224A	0.050 ± 0.008	0.023 ± 0.002	1.728 ± 1.680	-0.923	2.517	0.88	0.41	...
101224578	101224B	< 0.145	0.039 ± 0.003	44.737 ± 0.889	-2.649	66.667	0.28	0.21	...
101224614	101224C	< 3.617	0.620 ± 0.054	25.601 ± 3.416	-15.233	35.711	0.62	0.19	...
101224998	101224D	0.212 ± 0.073	0.130 ± 0.011	18.688 ± 8.719	-19.044	18.130	0.90	0.55	...
101225377	101225B	0.557 ± 0.141	0.310 ± 0.027	81.217 ± 35.377	-7.910	125.258	0.18	0.10	...
101227195	101227A	< 0.535	0.092 ± 0.008	95.488 ± 1.639	-16.013	141.529	0.90	0.44	...
101227406	101227B	0.231 ± 0.109	0.092 ± 0.008	153.347 ± 2.573	-27.564	185.578	0.28	0.11	...
101227536	101227C	< 0.075	0.023 ± 0.002	28.865 ± 3.088	-14.500	42.931	0.61	0.32	...
101231067	101231A	0.098 ± 0.011	0.039 ± 0.003	23.614 ± 0.572	-6.265	27.955	0.46	0.18	...
110101202	110101A	0.208 ± 0.031	0.110 ± 0.010	3.584 ± 1.493	-4.080	3.044	1.02	0.54	...
110101506	110101B	1.915 ± 0.614	1.241 ± 0.108	235.523 ± 8.256	-103.425	141.832	0.72	0.47	...
110102788	110102A	0.206 ± 0.039	0.110 ± 0.010	253.956 ± 2.049	-119.426	184.990	0.22	0.12	...
110105877	110105A	0.276 ± 0.074	0.110 ± 0.010	123.394 ± 6.476	-17.725	127.863	0.37	0.15	...
110106893	110106B	0.671 ± 0.287	0.439 ± 0.038	35.521 ± 3.612	-23.837	33.350	0.63	0.41	...
110107886	110107A	< 0.330	0.078 ± 0.007	183.555 ± 24.406	-61.185	122.967	0.58	0.35	...
110108977	110108A	1.001 ± 0.542	0.738 ± 0.064	51.456 ± 6.955	-19.677	76.516	0.63	0.47	...
110112934	110112B	0.024 ± 0.012	0.016 ± 0.001	2.304 ± 2.538	-2.102	2.474	0.70	0.47	...
110117364	110117A	< 32.263	19.855 ± 1.720	72.448 ± 9.051	-28.161	89.192	0.89	0.91	...
110117626	110117B	< 0.441	0.110 ± 0.010	43.264 ± 1.639	-23.640	62.447	0.69	0.36	...
110118857	110118A	0.334 ± 0.063	0.155 ± 0.013	34.561 ± 2.360	-23.346	45.428	0.41	0.19	...
110119931	110119A	< 0.280	0.130 ± 0.011	205.828 ± 1.864	-26.362	298.834	0.39	0.39	...
110120666	110120A	0.018 ± 0.007	0.011 ± 0.001	28.417 ± 9.793	-13.821	42.695	0.31	0.19	...
110123804	110123A	< 0.358	0.092 ± 0.008	17.856 ± 0.810	-7.608	27.359	0.14	0.08	...
110124784	110124A	1.141 ± 0.401	0.738 ± 0.064	5.376 ± 2.202	-5.997	4.723	0.86	0.56	...
110125894	110125A	< 0.753	0.184 ± 0.016	4.800 ± 0.923	-2.520	6.264	0.56	0.22	...
110128073	110128A	1.594 ± 0.248	0.738 ± 0.064	12.160 ± 4.971	-11.843	12.355	0.88	0.41	2.339
110130230	110130A	< 1.525	0.620 ± 0.054	47.360 ± 2.187	-16.863	70.753	0.59	0.47	...
110131780	110131A	< 0.252	0.092 ± 0.008	0.384 ± 1.478	-0.380	0.383	0.87	0.79	...
110201399	110201A	< 1.426	0.522 ± 0.045	8.192 ± 0.870	-5.853	10.425	0.67	0.65	...
110204179	110204A	0.279 ± 0.177	0.184 ± 0.016	28.673 ± 6.720	-17.968	39.066	0.28	0.19	...
110205027	110205B	0.841 ± 0.132	0.522 ± 0.045	6.400 ± 3.238	-5.984	6.752	1.01	0.63	...
110205588	110205C	1.100 ± 0.469	0.877 ± 0.076	158.720 ± 2.290	-29.430	170.557	0.76	0.60	...
110206202	110206B	0.464 ± 0.166	0.310 ± 0.027	12.288 ± 1.639	-12.487	11.951	0.86	0.57	...
110207470	110207A	< 0.035	0.005 ± 0.001	37.888 ± 2.290	-19.642	45.133	0.87	0.42	...
110207959	110207B	0.662 ± 0.189	0.369 ± 0.032	7.680 ± 4.944	-4.570	10.714	0.87	0.48	...
110209165	110209A	< 1.042	0.310 ± 0.027	5.632 ± 0.916	-6.570	4.670	0.78	0.68	...
110212550	110212B	0.004 ± 0.001	0.003 ± 0.001	0.064 ± 0.036	-0.080	0.048	0.42	0.27	...
110213220	110213A	0.481 ± 0.046	0.155 ± 0.013	34.305 ± 1.639	-17.759	50.155	0.45	0.14	1.46
110213876	110213C	0.072 ± 0.013	0.039 ± 0.003	0.320 ± 0.810	-0.286	0.350	1.01	0.55	...
110217591	110217A	< 8.528	2.087 ± 0.181	60.672 ± 11.611	-17.766	87.176	0.89	0.44	...
110220761	110220A	0.968 ± 0.099	0.219 ± 0.019	33.024 ± 8.738	-18.091	47.619	0.67	0.15	...
110221244	110221A	< 2.216	0.439 ± 0.038	13.056 ± 1.846	-8.007	17.943	0.64	0.19	...

Continued on Next Page...

TABLE 2 – Continued

Trigger ID	GRB Name	$\Delta t_{\rm min}$ (s)	$\Delta t_{\rm S/N}$ (s)	T_{90} (s)	$T_{100}^{\rm start}$ (s)	$T_{100}^{\rm stop}$ (s)	$\sigma_{X,t_{\rm min}}$	$\sigma_{X,t_{\rm S/N}}$	z
110226989	110226A	0.935 ± 0.213	0.522 ± 0.045	14.080 ± 0.923	-6.035	18.746	0.49	0.27	...
110227009	110227A	< 0.204	0.039 ± 0.003	1.728 ± 0.653	-1.051	2.389	0.80	0.54	...
110227229	110227B	1.162 ± 0.657	0.620 ± 0.054	18.432 ± 2.187	-10.154	26.502	0.38	0.20	...
110227420	110227C	0.834 ± 0.341	0.522 ± 0.045	25.600 ± 6.869	-23.936	27.008	0.36	0.23	...
110228011	110228A	< 2.126	0.439 ± 0.038	44.481 ± 2.834	-30.721	20.031	0.34	0.15	...
110228792	110228B	4.334 ± 0.930	1.476 ± 0.128	17.152 ± 2.360	-12.336	21.772	0.67	0.23	...
110301214	110301A	0.117 ± 0.007	0.027 ± 0.002	5.693 ± 0.362	-2.822	8.538	0.23	0.05	...
110302043	110302A	< 1.905	0.369 ± 0.032	38.336 ± 2.509	-25.192	46.083	0.70	0.18	...
110304071	110304A	< 0.791	0.184 ± 0.016	19.520 ± 1.498	-9.333	28.926	0.63	0.25	...
110307972	110307A	< 0.101	0.016 ± 0.001	2.304 ± 3.444	-2.888	1.642	1.09	0.41	...
110311812	110311A	1.653 ± 0.372	0.620 ± 0.054	6.400 ± 1.639	-4.960	7.776	0.61	0.23	...
110316139	110316A	< 0.075	0.019 ± 0.002	2.944 ± 2.199	-4.467	1.383	0.94	0.58	...
110318552	110318A	0.052 ± 0.024	0.033 ± 0.003	14.464 ± 1.094	-9.722	17.752	0.19	0.12	...
110319628	110319C	3.353 ± 1.320	1.755 ± 0.152	15.336 ± 1.446	-9.899	20.587	0.55	0.29	...
110319815	110319B	1.184 ± 0.382	0.738 ± 0.064	31.232 ± 5.049	-17.977	44.151	0.65	0.40	...
110321346	110321A	3.755 ± 0.563	1.476 ± 0.128	30.720 ± 10.764	-13.964	41.947	0.76	0.30	...
110322558	110322A	< 0.443	0.155 ± 0.013	36.097 ± 1.846	-21.973	49.827	0.57	0.49	...
110328520	110328B	< 1.131	0.219 ± 0.019	141.315 ± 29.767	-32.705	211.743	0.21	0.13	...
110331604	110331A	< 0.411	0.155 ± 0.013	3.200 ± 0.951	-1.648	4.720	0.52	0.38	...
110401920	110401A	0.042 ± 0.013	0.023 ± 0.002	2.368 ± 1.270	-1.840	2.904	0.59	0.32	...
110402009	110402A	0.016 ± 0.004	0.008 ± 0.001	35.649 ± 1.461	-16.437	54.487	0.63	0.33	...
110409179	110409A	0.009 ± 0.002	0.005 ± 0.001	0.128 ± 0.143	-0.192	0.064	0.61	0.38	...
110410133	110410A	< 1.210	0.184 ± 0.016	61.952 ± 1.379	-22.963	64.373	0.72	0.27	...
110410772	110410B	< 0.282	0.155 ± 0.013	8.064 ± 1.368	-8.730	7.310	0.50	0.55	...
110411629	110411B	< 4.331	0.439 ± 0.038	23.552 ± 1.950	-15.504	31.340	1.11	0.25	...
110412315	110412A	3.645 ± 0.307	1.043 ± 0.090	20.733 ± 4.636	-3.014	30.966	0.54	0.15	...
110413938	110413A	< 0.844	0.184 ± 0.016	54.272 ± 2.172	-24.129	70.283	1.02	0.76	...
110415541	110415A	0.426 ± 0.186	0.219 ± 0.019	166.146 ± 0.810	-81.989	248.629	0.44	0.23	...
110420946	110420B	< 0.012	0.003 ± 0.001	0.128 ± 0.516	-0.128	0.128	0.97	0.52	...
110421757	110421A	< 0.197	0.039 ± 0.003	40.449 ± 0.923	-16.443	47.857	0.25	0.17	...
110422029	110422B	0.025 ± 0.005	0.011 ± 0.001	0.320 ± 0.453	-0.267	0.286	0.83	0.38	...
110424758	110424A	0.029 ± 0.004	0.011 ± 0.001	0.672 ± 1.120	-0.356	0.944	1.01	0.40	...
110426629	110426A	3.890 ± 0.476	1.241 ± 0.108	356.357 ± 4.345	-5.933	370.949	0.38	0.12	...
110428338	110428B	< 0.207	0.065 ± 0.006	101.634 ± 2.919	-53.761	54.151	0.35	0.20	...
110430375	110430A	1.158 ± 0.154	0.310 ± 0.027	32.513 ± 1.717	-3.376	49.598	0.29	0.08	...
110503145	110503B	< 0.577	0.219 ± 0.019	7.936 ± 1.145	-4.192	11.648	0.26	0.20	...
110505203	110505A	< 0.209	0.078 ± 0.007	4.096 ± 0.545	-2.420	5.740	0.26	0.21	...
110509142	110509A	4.423 ± 0.997	1.755 ± 0.152	68.864 ± 2.757	-25.701	78.966	0.51	0.20	...
110509475	110509B	< 0.031	0.008 ± 0.001	0.640 ± 0.779	-0.637	0.637	0.87	0.45	...
110511616	110511A	< 0.665	0.369 ± 0.032	5.888 ± 1.639	-5.479	6.223	0.48	0.54	...
110517453	110517A	0.042 ± 0.021	0.027 ± 0.002	0.576 ± 1.810	-0.352	0.796	0.67	0.43	...
110517573	110517A	< 0.068	0.014 ± 0.001	23.040 ± 0.362	-11.661	34.189	0.34	0.21	...
110520302	110520B	1.089 ± 0.434	0.738 ± 0.064	12.288 ± 11.337	-16.583	7.855	0.64	0.43	...
110521478	110521B	0.482 ± 0.038	0.130 ± 0.011	6.141 ± 0.809	-3.037	9.181	0.60	0.16	...
110522256	110522A	< 4.687	1.476 ± 0.128	28.160 ± 2.673	-22.654	33.384	0.44	0.24	...
110522296	110522B	< 1.063	0.261 ± 0.023	27.136 ± 1.950	-18.502	35.467	0.85	0.41	...
110522633	110522C	< 0.365	0.078 ± 0.007	58.112 ± 2.828	-13.153	86.779	0.57	0.24	...
110523344	110523A	< 0.525	0.130 ± 0.011	44.544 ± 2.611	-23.437	65.197	0.51	0.24	...
110526715	110526A	0.018 ± 0.011	0.011 ± 0.001	0.448 ± 0.528	-0.349	0.544	0.41	0.26	...
110528624	110528A	< 0.739	0.261 ± 0.023	69.633 ± 5.526	-16.318	103.428	0.40	0.33	...
110529034	110529A	< 0.014	0.003 ± 0.001	0.512 ± 0.091	-0.382	0.637	0.45	0.20	...
110529262	110529B	0.118 ± 0.023	0.033 ± 0.003	45.825 ± 1.810	-22.591	53.012	0.41	0.11	...
110529811	110529C	< 4.650	1.043 ± 0.090	34.817 ± 4.636	-19.803	49.449	0.52	0.19	...
110531448	110531A	< 3.878	1.043 ± 0.090	38.656 ± 2.360	-15.335	53.058	0.54	0.20	...
110601681	110601A	< 0.162	0.033 ± 0.003	52.206 ± 13.350	-25.910	77.968	0.87	0.47	...
110605183	110605A	2.272 ± 0.075	0.369 ± 0.032	82.689 ± 3.083	-19.503	114.439	0.52	0.08	...
110605780	110605B	0.330 ± 0.072	0.155 ± 0.013	1.536 ± 1.056	-1.009	2.046	0.80	0.38	...
110609185	110609A	0.791 ± 0.375	0.522 ± 0.045	9.984 ± 4.471	-8.272	9.792	0.70	0.46	...

Continued on Next Page...

TABLE 2 – Continued

Trigger ID	GRB Name	$\Delta t_{\rm min}$ (s)	$\Delta t_{\rm S/N}$ (s)	T_{90} (s)	$T_{100}^{\rm start}$ (s)	$T_{100}^{\rm stop}$ (s)	$\sigma_{X,t_{\rm min}}$	$\sigma_{X,t_{\rm S/N}}$	z
110609425	110609B	< 0.785	0.310 ± 0.027	33.024 ± 2.896	-23.015	28.166	0.49	0.44	...
110610640	110610A	< 0.136	0.055 ± 0.005	43.521 ± 2.862	-15.860	59.429	0.24	0.22	...
110613631	110613A	2.594 ± 1.358	1.755 ± 0.152	40.193 ± 3.874	-20.249	59.709	0.41	0.28	...
110616648	110616A	2.209 ± 0.932	1.476 ± 0.128	12.544 ± 2.611	-10.819	12.254	0.55	0.37	...
110618366	110618A	12.874 ± 0.363	1.755 ± 0.152	163.843 ± 11.406	-59.600	241.866	0.54	0.07	...
110622158	110622A	0.522 ± 0.600	0.261 ± 0.023	70.401 ± 0.773	-8.228	106.524	0.10	0.05	...
110624906	110624A	< 1.128	0.310 ± 0.027	3.520 ± 4.948	-3.022	3.982	0.87	0.56	...
110625579	110625B	< 4.195	0.620 ± 0.054	35.584 ± 1.846	-18.128	52.676	0.58	0.14	...
110625881	110625A	0.101 ± 0.012	0.027 ± 0.002	26.881 ± 0.572	-0.865	43.756	0.19	0.05	...
110626448	110626A	0.827 ± 0.111	0.310 ± 0.027	6.400 ± 1.145	-3.936	8.800	0.55	0.21	...
110629174	110629A	0.062 ± 0.034	0.039 ± 0.003	61.694 ± 18.690	-0.319	92.201	0.51	0.32	...
110702187	110702A	0.165 ± 0.064	0.110 ± 0.010	34.369 ± 5.736	-27.769	40.607	0.42	0.28	...
110703557	110703A	< 0.296	0.092 ± 0.008	6.720 ± 1.619	-7.550	5.822	0.41	0.20	...
110705151	110705A	0.007 ± 0.004	0.004 ± 0.001	0.192 ± 0.036	-0.112	0.272	0.43	0.22	...
110705364	110705B	< 0.233	0.055 ± 0.005	19.200 ± 0.923	-3.872	28.960	0.54	0.23	...
110706202	110706A	< 0.372	0.130 ± 0.011	12.032 ± 4.382	-7.498	16.422	0.40	0.33	...
110706477	110706B	0.968 ± 0.523	0.620 ± 0.054	73.217 ± 14.612	-27.027	106.197	0.21	0.13	...
110706728	110706C	< 0.104	0.046 ± 0.004	16.896 ± 6.339	-8.244	25.348	0.36	0.32	...
110706977	110706D	0.272 ± 0.171	0.184 ± 0.016	33.216 ± 4.007	-20.431	31.693	0.18	0.12	...
110709463	110709C	0.406 ± 0.023	0.092 ± 0.008	24.061 ± 0.722	-11.908	35.972	0.50	0.11	...
110709642	110709A	0.113 ± 0.043	0.055 ± 0.005	43.201 ± 0.405	-11.473	64.127	0.31	0.15	...
110709862	110709D	< 0.903	0.310 ± 0.027	5.376 ± 1.493	-4.461	6.259	0.48	0.30	...
110710954	110710A	0.101 ± 0.031	0.046 ± 0.004	22.720 ± 1.604	-11.265	24.405	0.41	0.18	...
110716018	110716A	0.087 ± 0.034	0.039 ± 0.003	7.168 ± 1.747	-6.624	7.624	0.43	0.19	...
110717180	110717A	0.011 ± 0.003	0.005 ± 0.001	0.112 ± 0.072	-0.071	0.151	0.64	0.32	...
110717319	110717B	0.143 ± 0.066	0.065 ± 0.006	90.369 ± 0.810	-19.022	112.904	0.17	0.08	...
110720177	110720A	< 1.198	0.261 ± 0.023	11.200 ± 0.602	-5.672	16.616	0.41	0.11	...
110721200	110721A	0.116 ± 0.065	0.055 ± 0.005	21.822 ± 0.572	-0.326	32.622	0.11	0.05	...
110722694	110722A	< 2.514	0.439 ± 0.038	73.473 ± 11.404	-21.936	109.558	0.31	0.10	...
110722710	110722B	< 1.041	0.310 ± 0.027	14.336 ± 2.721	-11.712	16.784	0.49	0.28	...
110725236	110725A	< 0.335	0.078 ± 0.007	20.224 ± 1.056	-11.037	29.201	0.52	0.28	...
110726211	110726B	0.297 ± 0.068	0.155 ± 0.013	29.952 ± 10.608	-16.674	40.811	0.47	0.24	...
110728056	110728A	< 0.047	0.033 ± 0.003	0.704 ± 0.231	-0.177	0.921	0.76	0.99	...
110729142	110729A	< 0.267	0.110 ± 0.010	408.582 ± 2.290	-69.423	410.662	0.19	0.17	...
110730008	110730A	3.726 ± 1.291	1.755 ± 0.152	28.416 ± 2.919	-22.074	34.442	0.61	0.29	...
110730660	110730B	0.557 ± 0.189	0.310 ± 0.027	33.856 ± 1.811	-23.117	37.457	0.39	0.22	...
110731465	110731A	0.021 ± 0.015	0.014 ± 0.001	7.485 ± 0.572	-3.705	11.181	0.16	0.10	2.83
110801335	110801B	0.070 ± 0.024	0.039 ± 0.003	0.384 ± 0.326	-0.316	0.447	0.79	0.44	...
110803783	110803A	< 2.303	0.522 ± 0.045	186.883 ± 2.986	-156.675	123.457	0.68	0.31	...
110806934	110806A	< 0.404	0.130 ± 0.011	28.416 ± 0.923	-5.014	42.698	0.24	0.16	...
110809461	110809A	0.245 ± 0.086	0.130 ± 0.011	12.544 ± 4.615	-10.563	14.391	0.32	0.17	...
110812899	110812B	0.280 ± 0.052	0.155 ± 0.013	11.264 ± 3.727	-7.882	14.526	0.57	0.32	...
110813237	110813A	0.497 ± 0.164	0.184 ± 0.016	22.784 ± 3.114	-13.001	32.331	0.30	0.11	...
110817191	110817A	0.179 ± 0.041	0.078 ± 0.007	5.949 ± 0.572	-1.580	8.874	0.22	0.10	...
110818860	110818A	< 2.791	0.522 ± 0.045	67.073 ± 3.916	-43.192	90.258	0.64	0.27	3.36
110819665	110819A	0.249 ± 0.063	0.130 ± 0.011	16.384 ± 6.149	-8.624	23.972	0.57	0.30	...
110820476	110820C	1.134 ± 0.172	0.522 ± 0.045	11.264 ± 7.331	-9.674	12.734	0.70	0.32	...
110824009	110824A	< 0.011	0.003 ± 0.001	76.607 ± 9.220	-2.685	114.513	0.26	0.18	...
110825102	110825A	0.025 ± 0.004	0.007 ± 0.001	62.465 ± 0.231	-0.447	91.993	0.19	0.05	...
110825265	110825B	< 3.304	0.877 ± 0.076	51.073 ± 3.389	-29.971	59.894	0.54	0.32	...
110831282	110831A	< 0.987	0.155 ± 0.013	98.881 ± 3.138	-28.680	127.551	0.94	0.26	...
110901230	110901A	0.384 ± 0.267	0.261 ± 0.023	22.528 ± 5.620	-13.205	25.979	0.42	0.29	...
110903009	110903B	0.288 ± 0.014	0.078 ± 0.007	28.672 ± 2.429	-15.223	41.811	0.41	0.11	...
110903111	110903A	< 0.210	0.055 ± 0.005	341.254 ± 2.288	-27.997	340.998	0.27	0.16	...
110904124	110904A	< 0.233	0.078 ± 0.007	83.905 ± 3.853	-24.368	123.296	0.28	0.22	...
110904163	110904B	< 0.327	0.110 ± 0.010	51.457 ± 4.128	-26.841	75.525	0.48	0.29	...
110904531	110904C	1.471 ± 0.708	0.738 ± 0.064	20.480 ± 5.479	-12.698	28.058	0.27	0.13	...
110906302	110906B	0.832 ± 0.155	0.310 ± 0.027	23.936 ± 2.550	-17.232	30.368	0.49	0.18	...

Continued on Next Page...

TABLE 2 – Continued

Trigger ID	GRB Name	$\Delta t_{\rm min}$ (s)	$\Delta t_{\rm S/N}$ (s)	T_{90} (s)	$T_{100}^{\rm start}$ (s)	$T_{100}^{\rm stop}$ (s)	$\sigma_{X,t_{\rm min}}$	$\sigma_{X,t_{\rm S/N}}$	z
110909116	110909A	0.279 ± 0.067	0.130 ± 0.011	20.736 ± 1.639	-22.560	18.672	0.66	0.31	...
110911071	110911A	1.894 ± 0.458	1.241 ± 0.108	8.960 ± 4.352	-9.043	8.787	1.05	0.69	...
110916016	110916A	0.681 ± 0.123	0.261 ± 0.023	1.792 ± 1.993	-2.301	1.277	0.96	0.37	...
110919634	110919A	0.251 ± 0.072	0.130 ± 0.011	35.073 ± 3.974	-6.170	62.898	0.17	0.09	...
110920338	110920A	0.337 ± 0.188	0.184 ± 0.016	9.728 ± 0.810	-5.331	11.095	0.38	0.21	...
110920546	110920A	< 2.096	0.369 ± 0.032	160.771 ± 5.221	-2.659	191.860	0.14	0.04	...
110921444	110921C	0.345 ± 0.109	0.219 ± 0.019	149.507 ± 10.691	-68.609	86.150	0.64	0.41	...
110921577	110921A	< 1.497	0.877 ± 0.076	40.705 ± 1.810	-30.209	30.615	0.31	0.31	...
110921912	110921B	0.024 ± 0.010	0.016 ± 0.001	17.664 ± 0.345	-7.850	27.294	0.21	0.14	...
110923835	110923A	1.388 ± 0.170	0.439 ± 0.038	46.398 ± 11.279	-22.509	69.323	0.63	0.20	...
110926107	110926A	0.605 ± 0.253	0.310 ± 0.027	75.265 ± 1.280	-18.385	89.990	0.27	0.14	...
110928180	110928B	< 0.203	0.110 ± 0.010	148.226 ± 1.925	-192.673	91.909	0.20	0.23	...
110929187	110929A	0.416 ± 0.097	0.184 ± 0.016	5.120 ± 0.572	-3.046	7.142	0.47	0.21	...
110930564	110930A	6.368 ± 0.798	1.755 ± 0.152	37.889 ± 5.431	-25.519	49.862	0.71	0.20	...
111001804	111001A	0.021 ± 0.012	0.014 ± 0.001	0.384 ± 1.361	-0.444	0.319	0.85	0.55	...
111003465	111003A	0.415 ± 0.027	0.078 ± 0.007	16.640 ± 1.056	-7.725	25.389	0.31	0.06	...
111005398	111005B	0.721 ± 0.160	0.439 ± 0.038	30.720 ± 3.093	-15.718	34.662	0.51	0.31	...
111008992	111008B	< 12.204	2.087 ± 0.181	42.496 ± 4.128	-11.671	57.996	0.71	0.20	...
111009282	111009A	< 1.073	0.184 ± 0.016	20.736 ± 4.221	-1.826	24.281	0.31	0.07	...
111010237	111010A	4.084 ± 1.659	2.087 ± 0.181	82.433 ± 8.444	-29.758	119.422	0.40	0.21	...
111010660	111010B	0.466 ± 0.078	0.155 ± 0.013	8.704 ± 2.111	-5.334	11.978	0.72	0.24	...
111010709	111010C	0.918 ± 0.299	0.369 ± 0.032	52.993 ± 0.923	-12.740	75.736	0.34	0.14	...
111010899	111010D	< 0.789	0.439 ± 0.038	18.560 ± 2.988	-23.919	10.417	0.44	0.46	...
111011094	111011A	< 0.007	0.002 ± 0.001	1.472 ± 0.771	-0.799	2.136	0.67	0.43	...
111012456	111012A	0.463 ± 0.108	0.184 ± 0.016	20.736 ± 0.724	-9.248	31.984	0.31	0.13	...
111012811	111012B	0.050 ± 0.012	0.023 ± 0.002	7.936 ± 1.145	-4.448	11.392	0.29	0.13	...
111015427	111015A	< 0.550	0.110 ± 0.010	92.737 ± 3.319	-21.640	137.838	0.63	0.21	...
111017657	111017A	< 1.527	0.110 ± 0.010	11.072 ± 0.410	-5.231	16.779	0.68	0.06	...
111018595	111018B	< 1.584	0.439 ± 0.038	8.192 ± 1.864	-4.829	11.449	0.90	0.37	...
111018785	111018C	5.258 ± 1.211	2.951 ± 0.256	29.697 ± 1.810	-21.047	33.268	0.65	0.37	...
111022854	111022C	< 0.035	0.008 ± 0.001	0.192 ± 0.707	-0.224	0.160	0.79	0.42	...
111024722	111024B	< 0.250	0.039 ± 0.003	68.609 ± 2.896	-40.110	96.404	0.52	0.16	...
111024896	111024C	0.038 ± 0.010	0.023 ± 0.002	1.792 ± 1.846	-0.490	2.429	0.99	0.60	...
111025078	111025A	< 5.390	1.241 ± 0.108	51.712 ± 2.202	-20.322	76.874	0.76	0.39	...
111103441	111103A	0.138 ± 0.037	0.078 ± 0.007	11.968 ± 6.426	-6.056	17.744	0.44	0.25	...
111103948	111103C	0.018 ± 0.006	0.011 ± 0.001	0.320 ± 0.181	-0.222	0.414	0.71	0.45	...
111105457	111105A	0.241 ± 0.060	0.092 ± 0.008	43.520 ± 0.572	-19.655	35.180	0.78	0.30	...
111107035	111107A	3.425 ± 0.439	1.476 ± 0.128	12.032 ± 0.923	-7.498	16.422	0.89	0.38	2.893
111107076	111107B	1.089 ± 0.282	0.620 ± 0.054	77.185 ± 0.810	-29.068	93.648	0.43	0.24	...
111109453	111109B	< 0.981	0.310 ± 0.027	4.864 ± 2.757	-4.581	4.702	0.57	0.47	...
111109873	111109C	< 3.936	0.620 ± 0.054	9.664 ± 6.457	-9.394	9.830	1.09	0.28	...
111112908	111112A	< 0.023	0.005 ± 0.001	0.192 ± 0.091	-0.160	0.224	0.65	0.26	...
111113410	111113B	0.395 ± 0.093	0.155 ± 0.013	15.360 ± 1.639	-8.627	21.478	0.39	0.15	...
111114233	111114A	0.801 ± 0.398	0.522 ± 0.045	22.016 ± 2.673	-7.378	28.702	0.58	0.38	...
111117510	111117A	0.009 ± 0.003	0.004 ± 0.001	0.576 ± 0.143	-0.416	0.732	0.70	0.34	...
111117526	111117B	< 2.730	1.043 ± 0.090	23.808 ± 1.717	-13.069	34.293	0.49	0.34	...
111120556	111120A	< 2.860	0.369 ± 0.032	98.626 ± 2.970	-27.729	84.697	0.50	0.14	...
111124308	111124A	1.964 ± 0.185	0.877 ± 0.076	8.960 ± 3.114	-5.203	12.538	0.89	0.40	...
111127810	111127A	0.166 ± 0.130	0.110 ± 0.010	19.008 ± 2.548	-10.181	27.249	0.15	0.10	...
111201599	111201A	2.912 ± 0.897	1.476 ± 0.128	16.896 ± 3.974	-6.956	23.428	0.59	0.30	...
111203054	111203A	0.143 ± 0.060	0.092 ± 0.008	55.553 ± 5.684	-44.545	16.940	0.28	0.18	...
111203609	111203B	1.124 ± 0.622	0.738 ± 0.064	22.016 ± 6.734	-13.722	30.058	0.51	0.34	...
111208353	111208A	5.394 ± 0.408	1.476 ± 0.128	40.961 ± 4.345	-24.415	53.819	0.60	0.16	...
111216389	111216A	0.087 ± 0.027	0.046 ± 0.004	83.777 ± 0.500	-18.851	105.951	0.37	0.19	...
111220486	111220A	0.051 ± 0.008	0.016 ± 0.001	39.041 ± 5.101	-6.318	49.900	0.23	0.07	...
111221739	111221A	0.018 ± 0.006	0.011 ± 0.001	27.136 ± 7.186	-13.952	40.016	0.42	0.27	...
111222619	111222A	0.007 ± 0.001	0.003 ± 0.001	0.320 ± 0.143	-0.222	0.414	0.76	0.34	...
111226795	111226A	< 4.661	0.877 ± 0.076	74.753 ± 8.749	-25.023	93.066	0.33	0.10	...

Continued on Next Page...

TABLE 2 – Continued

Trigger ID	GRB Name	$\Delta t_{\rm min}$ (s)	$\Delta t_{\rm S/N}$ (s)	T_{90} (s)	$T_{100}^{\rm start}$ (s)	$T_{100}^{\rm stop}$ (s)	$\sigma_{X,t_{\rm min}}$	$\sigma_{X,t_{\rm S/N}}$	z
111228453	111228B	0.775 ± 0.011	0.092 ± 0.008	2.944 ± 0.979	-1.363	4.487	0.68	0.08	...
111228657	111228A	< 0.085	0.033 ± 0.003	99.842 ± 2.111	-49.409	78.603	0.18	0.12	0.714
111230683	111230A	< 0.246	0.065 ± 0.006	28.160 ± 1.557	-26.692	29.347	0.52	0.41	...
111230819	111230B	< 0.108	0.033 ± 0.003	12.736 ± 1.145	-6.952	18.360	0.56	0.32	...
120101354	120101A	< 0.103	0.016 ± 0.001	0.128 ± 0.072	-0.160	0.096	1.44	0.45	...
120102095	120102A	0.338 ± 0.023	0.092 ± 0.008	28.417 ± 8.204	-25.674	29.990	0.47	0.13	...
120102416	120102B	0.597 ± 0.272	0.369 ± 0.032	20.224 ± 2.769	-20.335	19.903	0.40	0.25	...
120105584	120105A	< 1.909	0.439 ± 0.038	22.528 ± 2.202	-19.408	25.407	0.53	0.24	...
120107384	120107A	< 0.060	0.027 ± 0.002	23.040 ± 0.143	-11.341	34.509	0.25	0.24	...
120109824	120109A	3.875 ± 1.183	1.476 ± 0.128	38.656 ± 3.114	-21.079	55.815	0.69	0.26	...
120111051	120111A	5.451 ± 2.729	2.482 ± 0.215	76.801 ± 5.515	-26.410	104.150	0.45	0.20	...
120114433	120114B	0.688 ± 0.159	0.369 ± 0.032	2.752 ± 1.569	-0.263	3.984	1.06	0.57	...
120114681	120114A	1.346 ± 1.016	0.877 ± 0.076	43.264 ± 5.804	-29.369	56.718	0.37	0.24	...
120118709	120118B	1.410 ± 0.482	0.738 ± 0.064	37.825 ± 12.586	-22.152	53.109	0.33	0.17	2.943
120118898	120118C	< 0.168	0.027 ± 0.002	17.152 ± 2.111	-9.180	25.100	0.58	0.17	...
120119170	120119A	< 0.463	0.078 ± 0.007	55.297 ± 6.229	-15.904	85.811	0.33	0.09	1.728
120119229	120119B	0.083 ± 0.030	0.055 ± 0.005	41.728 ± 1.557	-20.692	62.330	0.44	0.29	...
120119354	120119C	0.464 ± 0.057	0.219 ± 0.019	16.384 ± 1.493	-16.048	16.548	0.61	0.29	...
120120432	120120A	< 8.745	1.241 ± 0.108	32.256 ± 6.481	-15.893	48.265	1.09	0.28	...
120121101	120121B	< 1.305	0.439 ± 0.038	18.432 ± 3.727	-12.458	24.198	0.38	0.22	...
120121251	120121C	< 1.648	0.310 ± 0.027	37.121 ± 11.876	-23.877	49.992	0.28	0.09	...
120122300	120122A	0.576 ± 0.147	0.310 ± 0.027	16.701 ± 1.881	-8.264	24.968	0.48	0.26	...
120129312	120129B	0.276 ± 0.030	0.130 ± 0.011	1.280 ± 0.689	-1.274	1.274	1.05	0.49	...
120129580	120129A	0.047 ± 0.015	0.011 ± 0.001	3.072 ± 0.362	-0.870	4.913	0.15	0.04	...
120130699	120130A	0.168 ± 0.027	0.092 ± 0.008	27.777 ± 0.694	-7.181	40.844	0.44	0.24	...
120130906	120130B	0.354 ± 0.135	0.219 ± 0.019	3.584 ± 1.379	-3.056	3.961	0.51	0.32	...
120130938	120130C	< 1.482	0.369 ± 0.032	38.913 ± 7.455	-24.417	52.994	0.30	0.15	...
120203812	120203A	1.382 ± 0.211	0.439 ± 0.038	10.240 ± 2.429	-9.933	10.445	0.80	0.25	...
120204054	120204A	< 0.213	0.078 ± 0.007	49.089 ± 0.429	-14.128	83.542	0.05	0.04	...
120205285	120205A	0.121 ± 0.055	0.078 ± 0.007	0.576 ± 0.272	-0.864	0.284	0.96	0.61	...
120206949	120206A	0.074 ± 0.015	0.039 ± 0.003	9.472 ± 3.338	-4.951	13.875	0.33	0.17	...
120210650	120210A	0.084 ± 0.024	0.039 ± 0.003	1.344 ± 0.264	-0.731	1.949	0.48	0.22	...
120212353	120212B	0.050 ± 0.015	0.023 ± 0.002	0.864 ± 0.577	-1.262	0.458	0.93	0.43	...
120212383	120212A	1.378 ± 0.169	0.522 ± 0.045	9.216 ± 0.724	-6.618	11.690	0.66	0.25	...
120213606	120213B	0.116 ± 0.025	0.065 ± 0.006	13.824 ± 3.328	-9.917	17.585	0.53	0.30	...
120217808	120217A	0.415 ± 0.060	0.155 ± 0.013	5.888 ± 2.862	-3.431	8.271	0.59	0.22	...
120217904	120217B	< 0.050	0.011 ± 0.001	2.624 ± 0.300	-1.525	3.689	0.29	0.12	...
120218276	120218B	0.991 ± 0.330	0.620 ± 0.054	256.260 ± 5.221	-212.996	61.708	0.45	0.28	...
120219563	120219B	< 0.690	0.439 ± 0.038	8.128 ± 0.429	-5.179	10.979	0.61	0.69	...
120220210	120220A	< 2.436	1.043 ± 0.090	21.248 ± 1.639	-15.898	26.370	0.40	0.39	...
120222021	120222A	0.042 ± 0.014	0.019 ± 0.002	1.088 ± 0.143	-0.607	1.359	0.29	0.13	...
120222119	120222A	5.529 ± 0.464	1.755 ± 0.152	29.440 ± 5.382	-19.576	39.009	0.78	0.25	...
120223933	120223A	< 1.565	0.184 ± 0.016	14.336 ± 2.360	-7.616	20.880	0.85	0.19	...
120224282	120224B	< 0.957	0.261 ± 0.023	60.929 ± 3.093	-28.461	79.976	0.34	0.22	...
120224898	120224C	< 0.207	0.078 ± 0.007	29.184 ± 4.222	-14.192	43.876	0.65	0.55	...
120226447	120226B	0.074 ± 0.016	0.046 ± 0.004	14.592 ± 3.916	-10.493	18.521	0.70	0.44	...
120226871	120226A	0.147 ± 0.055	0.078 ± 0.007	52.993 ± 0.572	-15.347	83.726	0.17	0.09	...
120227391	120227A	0.106 ± 0.036	0.065 ± 0.006	19.712 ± 1.717	-10.531	28.671	0.93	0.57	...
120227725	120227B	0.175 ± 0.061	0.092 ± 0.008	17.408 ± 0.810	-8.365	26.261	0.27	0.14	...
120302080	120302A	< 1.418	0.261 ± 0.023	80.384 ± 16.927	-29.100	120.406	1.18	0.69	...
120302722	120302B	< 0.134	0.046 ± 0.004	1.600 ± 0.779	-0.856	2.264	0.86	0.74	...
120304061	120304A	0.677 ± 0.014	0.130 ± 0.011	9.984 ± 1.055	-5.200	14.660	0.50	0.10	...
120304248	120304B	0.018 ± 0.005	0.010 ± 0.001	5.376 ± 0.572	-2.925	7.795	0.62	0.33	...
120308588	120308B	< 0.311	0.078 ± 0.007	25.600 ± 1.557	-27.529	16.759	0.56	0.20	...
120312671	120312A	1.314 ± 0.587	0.738 ± 0.064	13.312 ± 3.167	-8.643	17.823	0.55	0.31	...
120314412	120314A	< 0.201	0.078 ± 0.007	1.280 ± 1.086	-1.914	0.634	0.65	0.51	...
120316008	120316A	< 0.155	0.027 ± 0.002	26.624 ± 0.362	-11.645	41.329	0.73	0.25	...
120319983	120319A	< 0.741	0.219 ± 0.019	72.448 ± 7.832	-9.467	91.224	0.66	0.49	...

Continued on Next Page...

TABLE 2 – Continued

Trigger ID	GRB Name	$\Delta t_{\rm min}$ (s)	$\Delta t_{\rm S/N}$ (s)	T_{90} (s)	$T_{100}^{\rm start}$ (s)	$T_{100}^{\rm stop}$ (s)	$\sigma_{X,t_{\rm min}}$	$\sigma_{X,t_{\rm S/N}}$	z
120323162	120323B	< 0.275	0.065 ± 0.006	4.352 ± 0.724	-2.928	5.752	0.53	0.24	...
120323507	120323A	0.013 ± 0.001	0.004 ± 0.001	0.448 ± 0.091	-0.285	0.608	0.27	0.08	...
120326056	120326A	0.974 ± 0.140	0.219 ± 0.019	11.776 ± 1.810	-6.176	16.285	0.38	0.08	1.798
120327418	120327B	0.026 ± 0.012	0.016 ± 0.001	0.256 ± 1.319	-0.320	0.192	0.77	0.48	...
120328268	120328B	0.094 ± 0.045	0.055 ± 0.005	29.697 ± 1.056	-2.055	48.104	0.09	0.05	...
120331055	120331A	0.015 ± 0.005	0.007 ± 0.001	16.384 ± 10.367	-5.031	21.668	0.62	0.28	...
120402669	120402B	< 0.624	0.110 ± 0.010	20.224 ± 0.810	-12.093	28.145	0.45	0.11	...
120403857	120403B	< 1.345	0.261 ± 0.023	4.288 ± 1.935	-6.095	2.423	1.30	0.42	...
120410585	120410A	< 0.059	0.014 ± 0.001	1.088 ± 1.180	-1.567	0.604	0.87	0.37	...
120411925	120411A	0.060 ± 0.018	0.033 ± 0.003	38.912 ± 1.493	-19.133	58.278	0.81	0.44	...
120412055	120412A	< 2.242	0.522 ± 0.045	9.728 ± 3.566	-8.915	10.427	0.85	0.42	...
120412920	120412B	< 0.476	0.130 ± 0.011	101.182 ± 4.871	-0.743	151.027	0.39	0.18	...
120415076	120415A	0.978 ± 0.116	0.369 ± 0.032	12.544 ± 4.128	-6.723	18.231	0.57	0.21	...
120415891	120415B	< 0.046	0.014 ± 0.001	0.960 ± 0.264	-0.731	1.179	0.52	0.44	...
120415958	120415C	1.156 ± 0.777	0.620 ± 0.054	12.544 ± 1.717	-10.563	14.391	0.41	0.22	...
120420249	120420A	2.318 ± 0.291	0.738 ± 0.064	25.600 ± 4.419	-3.712	37.504	0.57	0.18	...
120420858	120420B	1.615 ± 0.698	0.877 ± 0.076	254.913 ± 4.222	-21.676	296.948	0.38	0.21	...
120426090	120426A	< 0.192	0.027 ± 0.002	2.880 ± 0.181	-1.202	4.530	0.27	0.05	...
120426585	120426B	1.620 ± 0.878	0.738 ± 0.064	30.973 ± 3.620	-15.423	46.187	0.35	0.16	...
120427054	120427A	< 0.894	0.110 ± 0.010	5.632 ± 0.572	-0.964	8.702	0.54	0.09	...
120427153	120427B	2.693 ± 0.710	1.476 ± 0.128	22.784 ± 1.999	-9.939	31.748	1.01	0.55	...
120429003	120429A	< 0.182	0.092 ± 0.008	1.664 ± 0.968	-1.018	2.302	0.49	0.53	...
120429484	120429B	< 0.773	0.130 ± 0.011	15.360 ± 1.619	-5.555	21.939	0.52	0.27	...
120430980	120430A	< 1.624	0.439 ± 0.038	14.592 ± 2.172	-9.533	19.481	0.85	0.46	...
120504468	120504A	3.667 ± 0.553	1.755 ± 0.152	41.985 ± 2.673	-12.406	62.318	0.53	0.25	...
120504945	120504B	0.120 ± 0.026	0.065 ± 0.006	5.760 ± 0.779	-5.155	6.307	1.06	0.58	...
120506128	120506A	0.675 ± 0.175	0.369 ± 0.032	2.304 ± 1.379	-1.933	2.666	0.76	0.41	...
120509619	120509A	< 0.027	0.014 ± 0.001	0.704 ± 1.404	-0.542	0.766	0.75	0.79	...
120510900	120510B	< 7.403	1.241 ± 0.108	62.465 ± 3.908	-29.160	82.643	0.65	0.23	...
120511638	120511A	< 0.528	0.130 ± 0.011	45.249 ± 2.940	-22.414	67.613	0.75	0.43	...
120512112	120512A	0.123 ± 0.048	0.078 ± 0.007	18.176 ± 1.350	-2.265	27.517	0.18	0.12	...
120513531	120513A	0.348 ± 0.121	0.219 ± 0.019	23.808 ± 0.923	-12.301	35.061	0.67	0.42	...
120519721	120519A	0.060 ± 0.026	0.033 ± 0.003	0.960 ± 0.202	-0.603	1.307	0.39	0.21	...
120520949	120520A	0.398 ± 0.090	0.184 ± 0.016	5.760 ± 1.356	-7.587	3.875	0.70	0.32	...
120521380	120521B	3.757 ± 1.182	1.755 ± 0.152	91.134 ± 4.222	-26.803	136.302	0.62	0.29	...
120522361	120522B	0.239 ± 0.090	0.130 ± 0.011	28.160 ± 8.039	-12.922	30.445	0.26	0.14	...
120524134	120524A	0.024 ± 0.004	0.014 ± 0.001	0.704 ± 0.466	-0.478	0.921	0.81	0.46	...
120526303	120526A	< 0.327	0.055 ± 0.005	43.649 ± 1.002	-2.392	68.305	0.44	0.23	...
120528442	120528A	< 0.682	0.219 ± 0.019	16.384 ± 5.177	-8.880	23.716	0.26	0.19	...
120530121	120530A	< 1.136	0.219 ± 0.019	77.054 ± 1.810	-2.763	115.108	0.36	0.15	...
120531393	120531A	< 6.901	1.241 ± 0.108	25.344 ± 7.186	-15.363	35.063	0.98	0.36	...
120603439	120603A	0.030 ± 0.021	0.019 ± 0.002	0.384 ± 0.345	-0.252	0.511	0.40	0.26	...
120604220	120604A	0.143 ± 0.017	0.065 ± 0.006	10.496 ± 5.615	-3.094	12.836	0.92	0.42	...
120604343	120604B	4.706 ± 0.283	1.476 ± 0.128	12.032 ± 3.278	-8.522	15.398	0.89	0.28	...
120605453	120605A	0.461 ± 0.029	0.130 ± 0.011	18.112 ± 1.086	-1.466	26.407	0.69	0.19	...
120608489	120608A	< 0.066	0.039 ± 0.003	0.960 ± 1.611	-0.667	1.243	0.53	0.53	...
120608777	120608B	0.278 ± 0.088	0.184 ± 0.016	24.832 ± 3.840	-24.250	22.907	0.47	0.32	...
120609580	120609A	0.243 ± 0.152	0.155 ± 0.013	1.792 ± 0.810	-1.661	1.917	0.50	0.32	...
120611108	120611A	< 0.444	0.046 ± 0.004	49.921 ± 1.639	-21.305	54.573	1.11	0.27	...
120612680	120612B	1.587 ± 0.654	1.043 ± 0.090	63.232 ± 7.886	-27.128	67.702	0.54	0.35	...
120612687	120612C	0.060 ± 0.012	0.027 ± 0.002	0.256 ± 0.453	-0.320	0.192	0.70	0.32	...
120616630	120616A	0.006 ± 0.003	0.004 ± 0.001	0.048 ± 0.484	-0.072	0.024	0.74	0.53	...
120618128	120618A	1.323 ± 0.146	0.439 ± 0.038	17.600 ± 1.820	-8.840	26.184	0.44	0.15	...
120618919	120618B	0.142 ± 0.061	0.078 ± 0.007	47.616 ± 12.299	-33.467	42.693	0.65	0.36	...
120619884	120619A	< 0.454	0.092 ± 0.008	0.960 ± 0.960	-0.731	1.179	1.18	0.40	...
120624309	120624A	< 0.016	0.003 ± 0.001	0.640 ± 0.160	-0.381	0.893	0.27	0.13	...
120624933	120624B	< 0.129	0.033 ± 0.003	271.364 ± 4.580	-257.028	148.171	0.19	0.10	...
120625119	120625A	< 0.149	0.039 ± 0.003	7.424 ± 0.571	-3.933	10.833	0.21	0.12	...

Continued on Next Page...

TABLE 2 – Continued

Trigger ID	GRB Name	$\Delta t_{\rm min}$ (s)	$\Delta t_{\rm S/N}$ (s)	T_{90} (s)	$T_{100}^{\rm start}$ (s)	$T_{100}^{\rm stop}$ (s)	$\sigma_{X,t_{\rm min}}$	$\sigma_{X,t_{\rm S/N}}$	z
120629565	120629A	0.147 ± 0.027	0.078 ± 0.007	0.704 ± 1.026	-0.734	0.665	0.94	0.50	...
120701654	120701B	< 0.224	0.130 ± 0.011	1.024 ± 1.451	-1.469	0.571	0.83	0.97	...
120703417	120703B	< 1.189	0.219 ± 0.019	64.513 ± 3.083	-24.555	85.095	0.28	0.09	...
120703498	120703C	2.220 ± 0.413	1.043 ± 0.090	77.568 ± 2.187	-30.871	96.327	0.65	0.30	...
120703726	120703A	0.058 ± 0.043	0.033 ± 0.003	8.960 ± 1.379	-3.667	14.163	0.16	0.09	...
120707800	120707A	0.061 ± 0.025	0.039 ± 0.003	40.960 ± 4.238	-18.276	62.825	0.17	0.11	...
120709883	120709A	< 0.069	0.014 ± 0.001	27.328 ± 0.958	-13.933	40.707	0.55	0.17	...
120710100	120710A	0.670 ± 0.517	0.439 ± 0.038	131.840 ± 1.056	-7.875	155.607	0.22	0.15	...
120711115	120711A	< 0.075	0.011 ± 0.001	44.033 ± 0.724	57.830	128.262	0.50	0.13	...
120711446	120711C	1.139 ± 0.260	0.522 ± 0.045	87.552 ± 3.874	-32.427	123.394	0.90	0.41	...

NOTE. — Redshift values marked with $\star$ are taken from `http://www.mpe.mpg.de/~jcg/grbgen.html`.